Cover Page

Universiteit Leiden

The handle http://hdl.handle.net/1887/44146 holds various files of this Leiden University dissertation.

Author: Thomas, B.
Title: Towards artificial photosynthesis : resolving supramolecular packing of artificial antennae chromophores through a hybrid approach
Issue Date: 2016-11-10

Towards Artificial Photosynthesis

Resolving supramolecular packing of artificial antennae chromophores
through a hybrid approach

Towards Artificial Photosynthesis

Resolving supramolecular packing of artificial antennae chromophores
through a hybrid approach

PROEFSCHRIFT

Ter verkrijging van de graad van Doctor

aan de Universiteit Leiden,

op gezag van de Rector Magnificus Prof. Mr C. J. J. M. Stolker,

volgens besluit van het College voor Promoties

te verdedigen op donderdag 10 november 2016

klokke 15:00 uur

door

Brijith Thomas

Geboren te Kallooppara, India in1988

Promotiecommissie

Promoter: Prof. dr. H. J. M. de Groot

Referent: Prof. dr. W. J. de Grip

Overige Leden: Prof. dr. A. P. M. Kentgens, Radboud University, Nijmegen

                     Prof. dr. J. Brouwer

                     Prof. dr. K. Lammertsma

                     Dr. A. Pandit

                     Dr. N. S. Pannu

For my parents

& Aunt Sara

Table of contents

Chapter 3   60

De novo structure determination of an artificial bichromophoric light-harvesting antenna system by integrating MAS NMR and Electron Nano Crystallography

Chapter 4   84

Structural analysis of DATZnS(4H) using homology modelling

Abbreviations

1D	one-dimensional
2D	two-dimensional
APT	attached proton test
A2	1,7-perylene-3,4,9,10-tetracarboxylic monoimide dibutylester
BChl	bacteriochlorophyll
COSY	correlation spectroscopy
CP	cross polarization
cNDI	core expanded naphthalene diimide
CRAMPS	combined rotation and multiple pulse spectroscopy
D1	4-(isopentylthio)naphthalene monoimide
DATZnS	fused NDI-zinc-salphen based chromophore
DFT	density functional theory
DMF	dimethylformamide
DNP	dynamic nuclear polarization
EET	excited energy transfer
EM	electron microscopy
ENC	electron nano crystallography
FRET	froster resonance energy transfer
FSLG	frequency-switched Lee-Goldburg
HETCOR	heteronuclear correlation
HMBC	heteronuclear multiple bond correlation
HOMO	highest occupied molecular orbitals
HSQC	heteronuclear single quantum correlation
IR	infrared
LGCP	lee-goldburg cross polarisation
LUMO	lowest unoccupied molecular orbitals
MAS	magic angle spinning
Me	methyl
MR	molecular replacement
MW	molecular weight

NDI	naphthalene diimide
NICS	nucleus-independent chemical shift
NMI	napthalene monoimide
NMR	nuclear magnetic resonance
OTP	ortho-terphenyl
PCET	proton coupled electron transfer
ppm	parts per million
rf	radio frequency
SQDQ	single quantum double quantum
SSNMR	solid state nuclear magnetic resonance
TEM	transmission electron microscopy
TEMPO	2,2,6,6-tetramethylpiperydin-l-oxyl
TPPM	two pulse-phase modulation
XDS	x-ray detector software

Introduction and Methodology

1.1 Introduction

Spurred by worries over climate change and looming energy crisis, there is an increasing interest in mimicking natural photosynthesis for the conversion of solar energy into fuel.[1-4] Natural photosynthesis achieves solar to fuel conversion with photosynthetic antennae and reaction centers.[5-7] Biological systems are robust against random environmental fluctuations and can adapt to long-term evolutionary changes as well.[9] Their successful operation is based on a very limited set of functionally independent subsystems: protein complexes, subunits, and motifs dedicated to light harvesting,[4,10] charge separation and catalysis for extracting protons and electrons from water and for CO_2 reduction.[12] The most proficient light-harvesting antennae found in nature are chlorosomes, which are composed of a remarkably small set of interacting moderately sized organic dye molecules, mainly chlorophylls (MW~800).[4] Self-assembled bacteriochlorophyll (BChl) *c*, *d* or *e* organic dye pigments are preprogrammed for different tasks by adaptation of their structure, their interactions with the surrounding "responsive" matrix for the proper matching of time scales and length scales in the supramolecular biological organization.[13-17] Chlorophylls are sterically crowded in their side chains, and this makes for a flat energy landscape and molecules that can be easily distorted by packing effects to adapt the functional properties. These systems are frustrated by steric hindrance in the side chains. This leads to a flat energy landscape with respect to distortion of the molecule, where static and dynamic heterogeneity induced by the surrounding can have a very pronounced effect on the HOMO-LUMO gap and the redox potentials. As a result, one class of dye molecules can be used for different tasks, light harvesting, charge separation, water oxidation or proton reduction.

In the chlorosomes quantum delocalization is combined with symmetry breaking of the lowest exciton state to gain polaronic charge transfer character. Chlorophylls are spatially arranged in such a way to facilitate polaronic charge transfer character through the alignment of electric dipoles for a high dielectric susceptibility and charge transfer bias. This kind of chemical design is necessary to achieve oxidation of H_2O, which is a multielectron process. Moreover, the chlorophylls form two-dimensional sheets that allow for strong exciton overlap, enabling triplet exciton formation for photoprotection. Organic dyes in chlorosomes self-assemble in nanotubes and nanorods with coaxial cylinders and this serves as an inspiration for the design of nanodevices like modular tandem cells, or "artificial leaves" that perform light harvesting (at a time scale of ns), charge separation (ms) and multi-electron catalysis (ms).[18,19] Extensive studies have been performed in recent years on self-assembled chlorophylls in chlorosomes antennae, and have found that charge transfer states can be mixed effectively into exciton states when the building blocks have their dipole moments arranged in a parallel manner. Under ideal conditions, they can perform multi-electron photochemistry close to the thermodynamic limit for energy conversion and with nearly quantitative chemical yield, much better than any chemically engineered artificial system to date. Ultrafast, long-distance transmission of excitation energy in chlorophylls is achieved through the helical H-bonding chains and tight packing of BChls arising from π–π stacking in coaxial nanotubes. An induced misfit in the structural framework is achieved through chemical heterogeneity in the alkyl chains for optimization of the light-harvesting functionality. The various studies about the connection between the atomistic level and supramolecular organization of photosynthesis shows remarkable similarity in molecular nano architecture of the reaction center. To build a scaffold that replicates these nano architectures with biological functions like light harvesting, charge separation and catalysis, the challenge is to tune the different modules, which perform these functions in a controlled way. Since we know the functional entities involved in photosynthesis, it is possible to apply the well-known axiomatic design approach in the engineering world, which involves finding similar counterparts in organic and inorganic molecules.[9] The essence of axiomatic design in a solar fuel cell device is to build an artificial reaction center, which satisfies the

needs of light harvesting and charge separation. Functional requirements of artificial reaction centers are, absorption of photons to harvest light energy followed by transfer of the energy to the reaction center and then separation of charge to feed the catalyst.

Design parameters to achieve the functional requirements are matching the band gap of HOMO-LUMO with a wavelength of photons, suitable distance and energy gap for FRET, finely tuned reduction potential of the domain with a catalyst. Conformational entropy to mediate the conversions could be achieved through induced misfits. The morphology of the responsive matrix encodes the functional requirement and design parameters to achieve the system needs. As a first strategy to meet the system requirements, there has been much work on semi-synthetic dye molecules, where natural chlorophylls were chemically modified to reduce their chemical complexity and increase their stability.[20,21] The recent studies on chlorophylls and semi-synthetic dye molecules has provided us with a set of common characteristics for the programming and scaffolding of synthetic dye molecules for the design of nanodevices for artificial photosynthesis. Robustness of the synthetic antenna molecules can be used to match the design parameters with functional requirements.[22,23] In this thesis fused NDI-zinc salphen with a rigid supramolecular recognition motif formed out of salphen and a bichromophoric NMI functionalized perylene derivative with phenoxy spacers with the overlap of donors emission and acceptors absorption for FRET can be functionalized further for rationally designing the device. These molecules have remarkable chemical, thermal and photostability.

Insight into the packing obtained by the computational integration of two different bioimaging techniques, solid-state NMR and cryo-EM shows that chlorosomes contain well-ordered microdomains of self-assembled chlorophyll with *syn-anti* stacking mode. In the pursuit for nanodevices for solar to fuel conversion, a clear understanding about the packing serves to guide the design of new nanosized materials to meet the functional requirements for the design of a device compatible module for efficient light harvesting for the organic solar fuel cell. Recent advances in understanding about the chemical programming of chlorophyll cofactors for light harvesting, charge separation and driving catalysis at high redox potential in natural photosynthetic systems using MAS NMR

techniques provides a set of common denominators for the programming of artificial antenna complexes. The key point of this work is to transfer the body of knowledge acquired on chlorophyll tuning in photo biological systems to the artificial light harvesting component as a first step for the rational design of the device. Nature achieves functional complexity using a limited set of molecules, while the synthetic world has a lot of chemical diversity. The challenge that is addressed in this thesis is to take a set of molecules - perylene derivatives and DATZnS derivatives, and work towards the rational design of artificial light harvesting component and discover new concepts.

A cognizance about the packing will enable to steer the morphology in the desired direction. Moderately sized molecules like DATZnS derivatives and D1A2
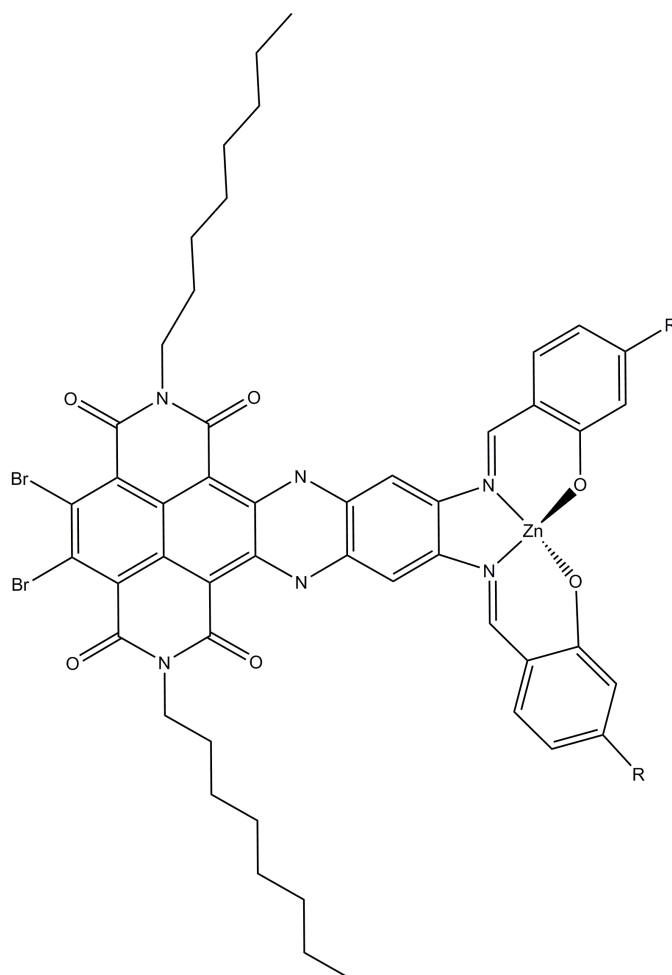

Figure 1.1 The structure of the DATZnS (R = 3′-NMe or 4H) derivative, a bichromophoric light harvesting antenna complex. The dipole moment is aligned along the principal axis of the molecule.

self-assemble to form supramolecular scaffolds with well-defined packing motifs that are planar aromatic. Chirality and asymmetry present in the molecules with protons on the conjugated aromatic molecules makes it suitable for the methodology that is discussed in this thesis. While asymmetry contributes to resolve the proton peaks in the spectrum, chirality leads to unique packing.

1.1.1 DATZnS derivatives

Core-expanded naphthalene diimide (cNDI) fused with a zinc bis-salicylimide phenylene (salphen) moiety is an alternative to porphyrin-based components used in supramolecular light-harvesting architectures (Figure 1.1).[5,24,25] Strategically incorporating metal-based supramolecular recognition motifs inside a chromophoric structure suggest the family of DATZnS derivatives as a new component for rationally designed light-harvesting assemblies.[26] The fused cNDI-zinc–salphen dyad behaves as one pigment and absorbs light between 600 and 750 nm with a modest Stokes shift.[26] Studies that were done on a homologue with orthogonal coordination of pyridine ligands to the rigid supramolecular scaffold of the DATZnS compound show that it does not undergo any change in its redox potentials or any internal excited state quenching and does not appreciably alter its excited state lifetime. Therefore it is expected that attachment of a catalyst as a ligand to the supramolecular scaffold limits the electronic influence of supramolecular interactions on the molecular orbitals involved in light absorption. This will give the flexibility to design it as a light-harvesting antenna complex for a solar fuel cell device.

1.1.2 Perylene derivative D1-A2

In the molecule D1A2, the energy donor naphthalene monoimide (NMI) has been attached to the 1, 7-bay-positions of the perylene derivative, thus leaving the peri positions free for further modification to design it as a device (Figure 1.2). The physical properties of perylene diimide dyes can be controlled by functionalization of the bay positions. Phenoxy spacers help to prevent π-π aggregation usually observed with perylene motifs and quenches the electron transfer from the naphthalene donor chromophores to the acceptor perylenes. Electrochemical properties and absorption spectra of D1 and A2 chromophores are independent of

17
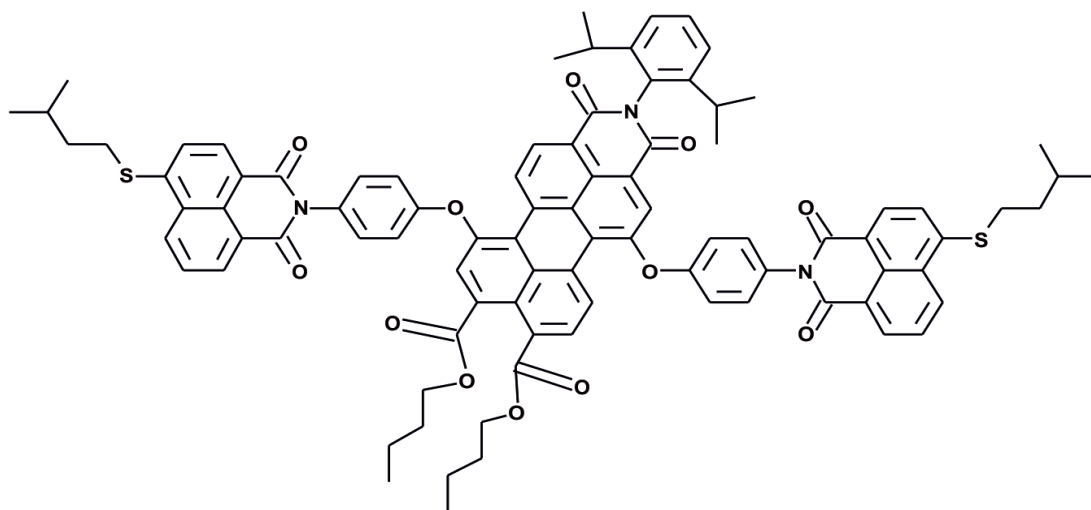
Figure 1.2 Structure of the perylene derivative with naphthalene monoimide (NMI) as bay substituents with phenoxy spacers. Overlap between the emission of NMI and absorption of perylene derivatives leads to transfer of energy through a FRET mechanism, which makes it an interesting antenna complex.

the coupling using the phenoxy spacer. Recent studies by Rajeev *et al.* show that the excited-state dynamics of D1A2, in toluene, has quantitative and ultrafast (ca. 1 ps) intramolecular excited energy transfer (EET) by the Forster mechanism. This arises due to the overlap of NMI's emission with absorption of perylene derivatives. Phenoxy coupling will impart high chemical stability and rigidity for the well-defined scaffold of the antenna molecules. The combination of an effective and fast energy transfer along with broad absorption in the visible region suggest that D1A2 or similarly designed dyes may fulfill a major role in the future development of organic supramolecular antenna systems.

1.2 Methodology

1.2. 1 NMR

NMR is a technology that has wide application in materials chemistry and biological chemistry to study the structure, dynamics and mechanisms of functions.

The NMR spin Hamiltonian is expressed as

$$\hat{H} = \hat{H}_z + \hat{H}_D + \hat{H}_{CS}. \tag{1.1}$$

Here $\widehat{H}_z$ is the Zeeman interaction, $\widehat{H}_{CS}$ is the chemical shielding term and $\widehat{H}_D$ represents the dipolar coupling. The Zeeman interaction is the interaction between the nuclear spins and the applied magnetic field. The Zeeman Hamiltonian is often represented as

$$\widehat{H}_Z = -\hat{\mu}B_0, \qquad (1.2)$$

where $\hat{\mu} = \gamma\hbar\hat{I}$ indicates the nuclear magnetic momentum operator and B_0 is the applied magnetic field. Even though the Zeeman interaction is the predominant term in the spin Hamiltonian it contains little information about structure. The chemical shielding Hamiltonian, which is anisotropic, can be described by

$$\widehat{H}_{CS} = \gamma\hat{I}\sigma B_0 , \qquad (1.3)$$

where B_0 is the applied magnetic field, σ is the second rank chemical shielding tensor, and $\hat{I}$ is the nuclear spin operator.[27] The $\widehat{H}_{CS}$ depends on the orientation of the molecule with respect to the applied magnetic field, which makes it a rich source of information about the structure. The anisotropy is due to the fact that in a molecule the charge distribution is rarely spherically symmetric. Three principal values of chemical shielding tensor are described as isotropic value, anisotropy and, asymmetry of interaction. The isotropic average of the tensor is given by

$$\sigma_{iso} = \frac{1}{3}\left(\sigma_{xx}^{PAF} + \sigma_{yy}^{PAF} + \sigma_{zz}^{PAF}\right), \qquad (1.4)$$

where σ^{PAF} indicates the principal values of the shielding tensor along the respective principal axis. The reduced anisotropy is given by

$$\delta = \sigma_{zz}^{PAF} - \sigma_{iso}, \qquad (1.5)$$

and the shielding asymmetry is defined as

$$\eta = \left(\sigma_{yy}^{PAF} - \sigma_{xx}^{PAF}\right)\Big/\sigma_{zz}^{PAF} , \qquad (1.6)$$

where σ_{iso} is the isotropic value, δ is the anisotropy and η is the asymmetry parameter.[28]

The dipolar coupling is based on the interaction of small local fields of the nuclear magnetic moments of different nuclei, and it is of two types, the homonuclear dipolar Hamiltonian between protons and the heteronuclear dipolar Hamiltonian between proton and carbon spins. The homonuclear dipolar Hamiltonian is represented as

$$\hat{H}_{dd}^{homo} = -\sum_{i>j}\left[\left(\frac{\mu_0}{4\pi}\right)\frac{\gamma^2\hbar}{r_{ij}^3}\right]\cdot\frac{1}{2}\left(3cos^2\theta_{ij}-1\right)\left[3\hat{I}_z^i\hat{S}_z^j - \hat{I}^i.\hat{I}^j\right], \qquad (1.7)$$

while the heteronuclear dipolar Hamiltonian is given by

$$\hat{H}_{dd}^{hetero} = -\sum_{i>j}\left[\left(\frac{\mu_0}{4\pi}\right)\frac{\gamma^I\gamma^S\hbar}{r_{ij}^3}\right]\cdot\frac{1}{2}\left(3cos^2\theta_{ij}-1\right)2\hat{I}_z^i\hat{S}_z^j. \qquad (1.8)$$

Here i and j label the spins, r_{ij} indicates the internuclear distance between the spins i and j, and θ_{ij} indicates the angle between the i-j internuclear vector. The strength of the dipolar coupling depends on γ, the distance between the nucleus and the orientation of the spin pairs with respect to the magnetic field.

The Larmor frequency refers to the rate of precession of the magnetic moment of the nuclei around the external magnetic field B_o according to

$$\omega_0 = \gamma B_0. \qquad (1.9)$$

The chemical shift anisotropy arises due to the fact that in a molecule, the charge distribution is rarely spherically symmetrical. In solution NMR, a single isotropic chemical shift is observed due to fast molecular tumbling. In solids no such motion prevails, resulting in spectral broadening. High resolution in the spectra can be achieved through combined rotation and multiple-pulse spectroscopy (CRAMPS).[29,30] This involves a combination of multiple pulse techniques and magic angle spinning to suppress homonuclear dipolar interactions between the abundant spins and the chemical shift anisotropy. The dipolar coupling between nuclei depends on the geometric factor $(3cos^2\theta - 1)$ as shown
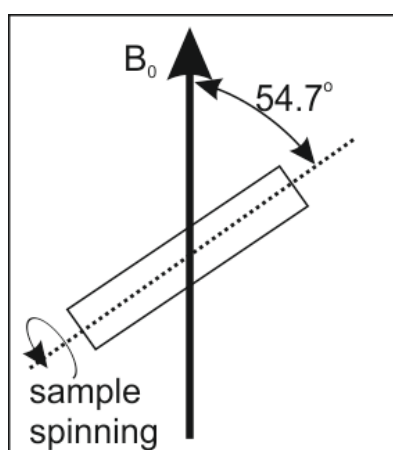

Figure 1.3 In a MAS experiment, the sample is finely powdered, packed tightly into a rotor and spun quickly around an axis at a magic angle of 54.75° with the magnetic field B_0.

in equation (1.7). Orienting the molecule at an angle of 54.7° and rotating at a high frequency helps to average the dipolar interaction (Figure 1.3).[31,32] Provided the rate of spinning is fast compared to homonuclear dipolar coupling linewidth, it will suppress to the formation of spinning sidebands and line broadening due to noncommuting terms in Hamiltonian (1.7).

1.2.1.1 Cross polarization

Low sensitivity and long spin-lattice relaxation times of dilute spin 1/2 nuclei can be overcome through cross polarization. Most dilute nuclei are in proximity of abundant nuclei like ^{1}H with a high gyromagnetic ratio. Polarization can hence be transferred from abundant nuclei to dilute nuclei through cross polarization.[33] A system of two nuclear spins, S and I are simultaneously irradiated with two rf fields B_{1I} and B_{1S} of frequencies ω_I and ω_S close to the Larmor frequencies. The so-called Hartmann-Hahn condition is satisfied when

$$|\omega_{1I}| = |\omega_{1S}|, \tag{1.10}$$

where $\omega_{1I} = -\gamma_{1I}B_{1I}$ and $\omega_{1S} = \gamma_S B_{1S}$.[34] During Hartmann-Hahn matching ^{1}H spins are locked along an effective field, while the ^{13}C spins can be locked on resonance in the xy-plane with a spin-lock pulse on the ^{13}C channel of the spectrometer. Polarization is transferred efficiently from ^{1}H spins to ^{13}C spins since it sets the energy gaps between the rotating frame spin states of ^{1}H and ^{13}C to be equal (Figure 1.4).
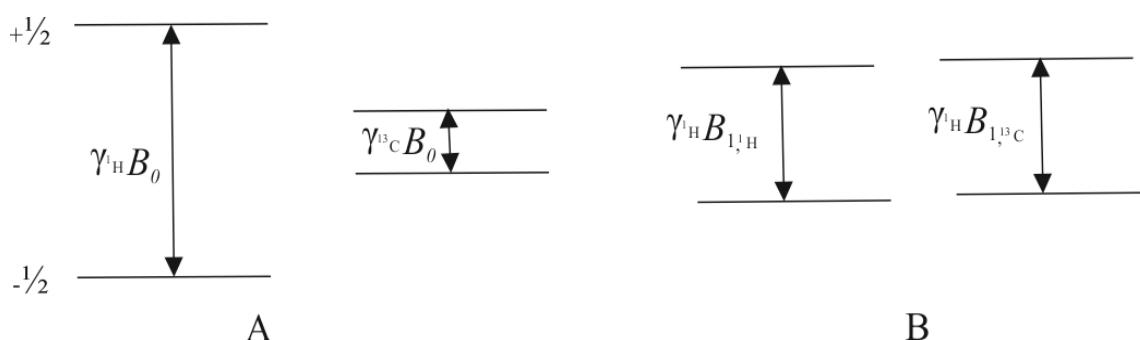

Figure 1.4 Energy levels of ^{1}H and ^{13}C spins in the laboratory frame (A) and the rotating frame (B). Polarization cannot be transferred in the laboratory frame due to energy mismatch. In the rotating frame, the splitting is determined by the *rf* field, and it is possible to tune the energy levels for the transfer of magnetization from ^{1}H to ^{13}C spins.

1.2.1.2 ^{1}H-^{13}C HETCOR and LGCP build up curves

Information about the internuclear distance between two spins can be deduced from the strength of the heteronuclear ^{1}H-^{13}C dipolar interactions. The cross polarization process is a mixture of coherent and incoherent transfer, but it is possible to extract the coherent transfer and measure the distance since the systems under study have sufficiently isolated spin pairs. For systems with ^{13}C at natural abundance, homonuclear ^{1}H decoupling at the LG condition restricts the transfer of polarization between ^{1}H spin pairs. Since ^{13}C is dilute, there are no ^{13}C-^{13}C interactions. Homonuclear dipolar interactions between protons can be averaged to zero by incorporating LG irradiation schemes in a CPMAS experiment (Figure 1.5A).[35,36] The LG technique involves irradiating the ^{1}H continuously with an off-resonance *rf*-field having frequency ω_1 with an off resonance value $\pm\Delta$LG. The LG condition is given by

$$\pm\Delta\text{LG} = \omega_{\pm\Delta LG} - \gamma B_0 = \pm\frac{1}{2}\sqrt{2}\,|\omega_1|, \qquad (1.11)$$

where $\omega_1 = -\gamma B_1$. A series of multiple pulses is used to introduce the LG condition on the proton channel after a 90° pulse to suppress ^{1}H-^{1}H homonuclear dipolar interactions.

For the build-up curves, LGCP data were collected while increasing the CP contact time from 0.1 to 2 ms with increments of 0.1 ms. The LGCP build up curve
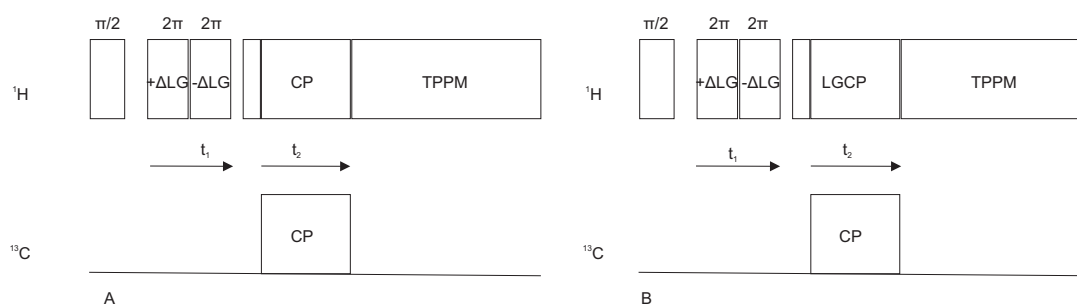
Figure 1.5 A) Pulse program used for ^{1}H-^{13}C LG HETCOR experiments. TPPM decoupling is used to suppress homonuclear coupling between ^{1}H spin pairs.[8] The ^{1}H magnetization is transferred to the ^{13}C spins via the dipolar coupling between ^{1}H and ^{13}C during a contact pulse (CP) applied simultaneously to both spins after a 90° pulse followed by LG conditions applied to the ^{1}H spins. B) Pulse program used for LGCP build up curve experiments. Here the LG condition is applied in the CP region, which suppresses the homonuclear coupling. This eventually helps to extract the LGCP build up curve between selected spin pairs.[11]

is obtained by plotting intensity against mixing time for each ^{13}C species (Figure 1.5B). The distance constraints can be obtained from the analysis of HETCOR and LGCP buildup curves. The LGCP build up curve can be simulated for various internuclear distances and then compared with experimental data to validate a proposed structure.[35]

1.3 Supramolecular crystallography

Packings consist of molecules arranged in a regular and quasi-periodic fashion. Analogous to the unit cell in crystals, packed supramolecular entities can have a repeating unit with intersecting edges labeled '*a*', '*b*' and '*c*' and angles between these edges labeled as '*α*', '*β*' and '*γ*'.[37,38] In addition to the unit cell parameters, space groups could be used to get an insight into the packing of these semicrystalline compounds in three dimension. The symmetry group of a configuration in space, usually in three dimensions is known as space group.[39,40] While there are many reflections in a crystalline structure due to long range order, packings have limited reflections due to limited correlation lengths, typically in the order of 50-100 unit cells, depending on the domain size.[41] Different diffraction patterns arise from the symmetry present in the molecule. Even with limited diffraction data we can still use Friedel's Law, which states that the intensities associated with two points opposite in reciprocal space, are almost equal: *I (h, k, l)*
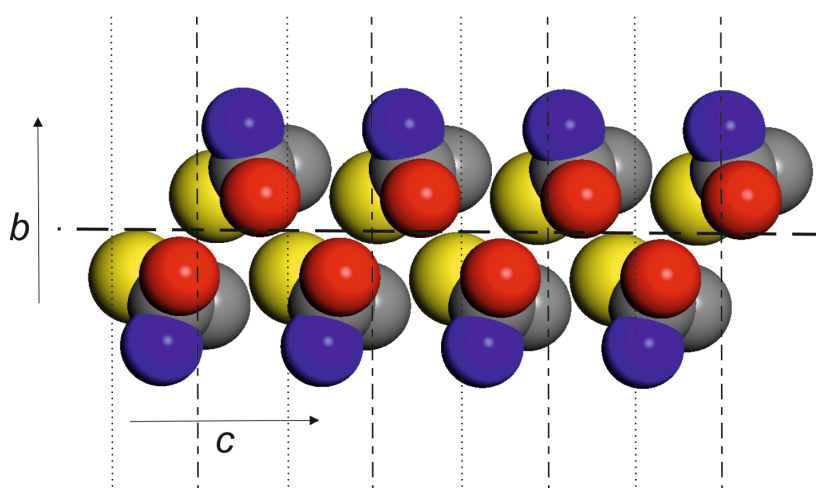

Figure 1.6 A 'c'- glide plane involves reflection on the plane containing the 'c' axis followed by translation along the same plane to accommodate steric hindrance. (adapted from http://pd.chem.ucl.ac.uk/pdnn/symm4/glide.htm)

$\approx I$ *(-h, -k, -l)*.[42,43] Moreover, a pair of reflections with the indices *(h, k, l)* and *(-h, -k, -l)* is known as a Friedel pair.

Packing from the diffraction is determined mainly by two steps, it first involves finding the unit cell parameters.[44-47] The second step is to identify an approximate space group, which involves identifying possible screw axes and glide planes from reflection conditions in the diffraction pattern (Figure 1.6).[48] While screw axes imply rotation and an additional translation, the glide planes imply reflection and an additional translation. A screw axis has a one-dimensional reflection condition, while glide planes have two-dimensional reflection conditions. A twofold axis along the '*a*' axis leads to the reflection condition *h00:h=2n*. A glide plane perpendicular to the '*a*' axis results in the reflection condition *h=2n* onto the zonal plane *0kl*.

Most of the packing in organic molecules falls into three different crystal classes, they are triclinic, monoclinic and orthorhombic with $P2_1$/c, $P\bar{1}$, $P2_12_12_1$, $C2$/c and $P2_1$ as the preferred space groups.[49] Space groups $P1$, $P\bar{1}$, $P1m$, $P12/m1$ and $P121/m1$ do not have any reflection condition. Polar space groups are $P1$, $P2$, $P21$ and $C2$. The CP/MAS NMR spectrum helps to identify the presence of symmetry in the molecule, which gives information about identical sites present in the packing. Polymorph analysis could be used to narrow down the possible crystal structures.[50,51] The number of molecules in the unit cell can be calculated using the equation $z = \frac{\rho * V}{M}$ where ρ is the density of the sample, V is the volume of the unit cell and M is the molecular weight.[20,21,50,52] This work is based on the assumption that the number of molecules in the unit cell should be in correspondence with the number of identical sites from the mathematical operators in the space group, taking into account the symmetry of the molecule. This will allow predominant interplay between bottom up and top down packing constraints. Geometrical optimization helps to converge on a reasonable packing. Furthermore the packing could be validated with simulation of chemical shifts, LGCP build up curves and diffraction patterns.[35,37,53,54] In the later stage, the methodology involving the computational integration of electron diffraction, CP/MAS NMR and modelling could be extended to find the packing in other systems that are heterogeneous in nature (Figure 1.7).
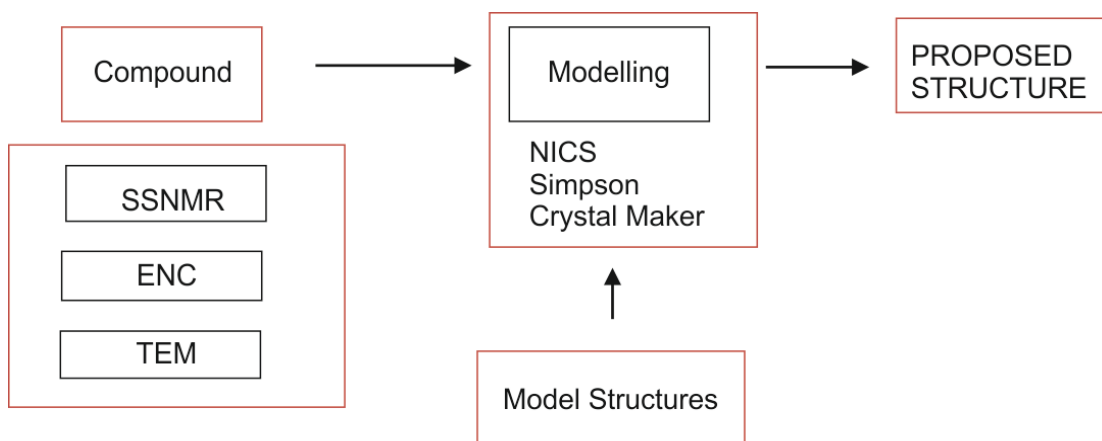
Figure 1.7 Schematic representation of supramolecular crystallography. The concept here is to reduce the uncertainty of the model by reasoning from first principles using the available data from CP/MAS NMR, ENC, and TEM. The logic behind the reconstruction of a model is to search for global packing that can reproduce commonalities in the observed data through simulation.

The scope of this thesis is to perform and develop a methodology for the magnetic resonance and electron diffraction analyses for the evidence-based design of device compatible modules for light harvesting. In this thesis, a concept for solving the packing of pseudocrystalline supramolecular dye assemblies in the solid-state at natural abundance by using MAS NMR in conjunction with electron diffraction is illustrated. This involves the smart use of a glide plane to accommodate steric hindrance to get packing with low energy and high density, which provides a design strategy for solar fuel cell device.

Chapter 2 describes how CP/MAS NMR in combination with cryo-EM can be applied to elucidate the structure of pseudo-crystalline DATZnS(3′-NMe) which forms antiparallel stacking with the $P2/c$ space group. MAS NMR and quantitative chemical shift calculations provide information about the C_2 symmetry and selective distance constraints. Systematic absences from the diffraction pattern give details about the screw axis and glide plane. The electron diffraction pattern and LGCP build up curve between specific pairs were simulated to validate the proposed packing.

In **Chapter 3**, the latest state of the art in electron diffraction, which is the ENC, is used to get the unit cell parameters and space group. This involves rotation of the crystal with continuous exposure to the electron beam over a limited angle.

The nonzero scattering in reciprocal space obtained by ENC is converted into electron density using Phaser molecular replacement with the help of a rigid trial model. Intermolecular correlations help to converge on a centrosymmetric dimer and then bay substituents were grafted to this basic building motif followed by modeling of the structure.[55] Finally the packing is validated with MAS NMR.

A homology modeling approach was used in **Chapter 4**. Here the DATZnS(3'-NMe) in chapter 2 is used as a starting model. MAS NMR and limited data from TEM were feed into the modeling to converge upon an antiparallel packing. This provides insight on how to steer the packing from antiparallel into parallel by using functional groups and steric constraints. This paves the way for evidence based chromophoric design of antenna motifs for artificial photosynthesis.

Finally in **chapter 5**, a summary is given about the results reported in this thesis. In addition, a brief description about the future developments, needed with design of the device and in the field of structural analysis, is given.

References

(1)   Purchase, R. L.; de Groot, H. J. M. *Interface Focus* **2015**, *5, 20150014*.

(2)   Gust, D.; Moore, T. A.; Moore, A. L. *Accounts of Chemical Research* **2009**, *42*, 1890.

(3)   Scholes, G. D.; Fleming, G. R.; Olaya-Castro, A.; van Grondelle, R. *Nat Chem* **2011**, *3*, 763.

(4)   Croce, R.; van Amerongen, H. *Nat Chem Biol* **2014**, *10*, 492.

(5)   Fernando, R.; Etheridge, F.; Muller, E.; Sauve, G. *New Journal of Chemistry* **2015**, *39*, 2506.

(6)   Bensaid, S.; Centi, G.; Garrone, E.; Perathoner, S.; Saracco, G. *ChemSusChem* **2012**, *5*, 500.

(7)   Janna Olmos, J. D.; Kargul, J. *The International Journal of Biochemistry & Cell Biology* **2015**, *66*, 37.

(8)   van Rossum, B. J.; Förster, H.; de Groot, H. J. M. *Journal of Magnetic Resonance* **1997**, *124*, 516.

(9)   Thomas, J. D.; Lee, T.; Suh, N. P. *Annual Review of Biophysics and Biomolecular Structure* **2004**, *33*, 75.

(10)   Demmig-Adams, B.; Adams, W. W. *Nature* **2000**, *403*, 371.

(11)   Bielecki, A.; Kolbert, A. C.; Levitt, M. H. *Chemical Physics Letters* **1989**, *155*, 341.

(12)   Alia, A.; Buda, F.; Groot, H. J. M. d.; Matysik, J. *Annual Review of Biophysics* **2013**, *42*, 675.

(13)   Furumaki, S.; Vacha, F.; Hirata, S.; Vacha, M. *ACS Nano* **2014**, *8*, 2176.

(14)   Jochum, T.; Reddy, C. M.; Eichh; xf; fer, A.; Buth, G.; Szmytkowski, J.; x; drzej; Kalt, H.; Moss, D.; Balaban, T. S. *Proceedings of the National Academy of Sciences of the United States of America* **2008**, *105*, 12736.

(15)   Matenova, M.; Lorelei Horhoiu, V.; Dang, F.-X.; Pospisil, P.; Alster, J.; Burda, J. V.; Silviu Balaban, T.; Psencik, J. *Physical Chemistry Chemical Physics* **2014**, *16*, 16755.

(16)   Saga, Y.; Akai, S.; Miyatake, T.; Tamiaki, H. *Bioconjugate Chemistry* **2006**, *17*, 988.

(17)   Möltgen, H.; Kleinermanns, K.; Jesorka, A.; Schaffner, K.; Holzwarth, A. R. *Photochemistry and Photobiology* **2002**, *75*, 619.

(18)   Kalyanasundaram, K.; Graetzel, M. *Current Opinion in Biotechnology* **2010**, *21*, 298.

(19)   Young, K. J.; Martini, L. A.; Milot, R. L.; Iii, R. C. S.; Batista, V. S.; Schmuttenmaer, C. A.; Crabtree, R. H.; Brudvig, G. W. *Coordination chemistry reviews* **2012**, *256*, 2503.

(20)	Ganapathy, S.; Oostergetel, G. T.; Wawrzyniak, P. K.; Reus, M.; Gomez Maqueo Chew, A.; Buda, F.; Boekema, E. J.; Bryant, D. A.; Holzwarth, A. R.; de Groot, H. J. M. *Proceedings of the National Academy of Sciences* **2009**, *106*, 8525.

(21)	Ganapathy, S.; Sengupta, S.; Wawrzyniak, P. K.; Huber, V.; Buda, F.; Baumeister, U.; Würthner, F.; de Groot, H. J. M. *Proceedings of the National Academy of Sciences* **2009**, *106*, 11472.

(22)	Dubey, R. K.; Inan, D.; Sengupta, S.; Sudholter, E. J. R.; Grozema, F. C.; Jager, W. F. *Chemical Science* **2016**, *7*, 3517.

(23)	Dubey, R. K.; Knorr, G.; Westerveld, N.; Jager, W. F. *Organic & Biomolecular Chemistry* **2016**, *14*, 1564.

(24)	Rombouts, J. A.; Ravensbergen, J.; Frese, R. N.; Kennis, J. T. M.; Ehlers, A. W.; Slootweg, J. C.; Ruijter, E.; Lammertsma, K.; Orru, R. V. A. *Chemistry – A European Journal* **2014**, *20*, 10185.

(25)	Ponnuswamy, N.; Stefankiewicz, A. R.; Sanders, J. K. M.; Pantoş, G. D. In *Constitutional Dynamic Chemistry*; Barboiu, M., Ed.; Springer Berlin Heidelberg: Berlin, Heidelberg, **2012**, 217.

(26)	Tong, L. H.; Pengo, P.; Clegg, W.; Lowe, J. P.; Raithby, P. R.; Sanders, J. K. M.; Pascu, S. I. *Dalton Transactions* **2011**, *40*, 10833.

(27)	Saitô, H.; Ando, I.; Ramamoorthy, A. *Progress in nuclear magnetic resonance spectroscopy* **2010**, *57*, 181.

(28)	Blümich, B. *Advanced Materials* **1996**, *8*, 186.

(29)	Schaefer, J.; Stejskal, E. O. *Journal of the American Chemical Society* **1976**, *98*, 1031.

(30)	Dec, S. F.; Bronnimann, C. E.; Wind, R. A.; Maciel, G. E. *Journal of Magnetic Resonance (1969)* **1989**, *82*, 454.

(31)	Andrew, E. R.; Bradbury, A.; Eades, R. G. *Nature* **1958**, *182*, 1659.

(32)	Lowe, I. J. *Physical Review Letters* **1959**, *2*, 285.

(33)	Hartmann, S. R.; Hahn, E. L. *Physical Review* **1962**, *128*, 2042.

(34)	Lee, M.; Goldburg, W. I. *Physical Review* **1965**, *140*, A1261.

(35)	Ladizhansky, V.; Vega, S. *Journal of the American Chemical Society* **2000**, *122*, 3465.

(36)	Fukuchi, M.; Ramamoorthy, A.; Takegoshi, K. *Journal of magnetic resonance (San Diego, Calif. : 1997)* **2009**, *196*, 105.

(37)	Vosegaard, T.; Tošner, Z.; Nielsen, N. C. In *eMagRes*; John Wiley & Sons, Ltd: 2007.

(38)	Kremer, F. In *Zeitschrift für Physikalische Chemie* **1997**, *200*, 281.

(39)	Opgenorth, J.; Plesken, W.; Schulz, T. *Acta Crystallographica Section A* **1998**, *54*, 517.

(40)	Hestenes, D.; Holt, J. W. *Journal of Mathematical Physics* **2007**, *48*, 023514.

(41)   Ganapathy, S.; Oostergetel, G. T.; Reus, M.; Tsukatani, Y.; Gomez Maqueo Chew, A.; Buda, F.; Bryant, D. A.; Holzwarth, A. R.; de Groot, H. J. M. *Biochemistry* **2012**, *51*, 4488.

(42)   Bijvoet, J. M.; Peerdeman, A. F.; van Bommel, A. J. *Nature* **1951**, *168*, 271.

(43)   Serneels, R.; Snykers, M.; Delavignette, P.; Gevers, R.; Amelinckx, S. *physica status solidi (b)* **1973**, *58*, 277.

(44)   Martineau, C. *Solid State Nuclear Magnetic Resonance* **2014**, *1*,63.

(45)   Ripmeester, J. A.; Wasylishen, R. E. *CrystEngComm* **2013**, *15*, 8598.

(46)   Ashbrook, S. E.; McKay, D. *Chemical Communications* **2016**, *52*, 7186.

(47)   Doerr, A. *Nat Meth* **2006**, *3*, 6.

(48)   Kalman, A.; Argay, G.; Fabian, L.; Bernath, G.; Fulop, F. *Acta Crystallographica Section B* **2001**, *57*, 539.

(49)   Pidcock, E. *Chemical* Communications **2005**, 3457.

(50)   Baias, M.; Dumez, J.-N.; Svensson, P. H.; Schantz, S.; Day, G. M.; Emsley, L. *Journal of the American Chemical Society* **2013**, *135*, 17501.

(51)   Cross, W. I.; Blagden, N.; Davey, R. J.; Pritchard, R. G.; Neumann, M. A.; Roberts, R. J.; Rowe, R. C. *Crystal Growth & Design* **2003**, *3*, 151.

(52)   Baias, M.; Widdifield, C. M.; Dumez, J.-N.; Thompson, H. P. G.; Cooper, T. G.; Salager, E.; Bassil, S.; Stein, R. S.; Lesage, A.; Day, G. M.; Emsley, L. *Physical Chemistry Chemical Physics* **2013**, *15*, 8069.

(53)   Kohn, S. C. *Terra Nova* **1995**, *7*, 554.

(54)   Bak, M.; Rasmussen, J. T.; Nielsen, N. C. *Journal of Magnetic Resonance* **2000**, *147*, 296.

(55)   McCoy, A. J. *Acta Crystallographica Section D: Biological Crystallography* **2007**, *63*, 32.

Chapter 2

Surface-deposited DATZnS(3′-NMe) chromophore light harvesting antennae form parallel molecular stacks in an antiparallel lamellar packing framework

Abstract

The supramolecular packing of the fused napthalenediimide-zinc-salphen based light harvesting chromophore DATZnS(3′-NMe) with a molecular recognition site incorporated into a chromophoric structure and deposited on a surface grid was determined by computational integration of cryo-EM imaging and magic angle spinning (MAS) NMR with ^{1}H-^{13}C heteronuclear dipolar correlation spectroscopy and ^{13}C at natural abundance. Absence of doubling in ^{13}C spectra and calculation of molecular energy point to an intramolecular C_2 symmetry for the chiral DATZnS(3′-NMe) motif. Diffraction patterns obtained by Fourier transformation of TEM images with 0.6 nm resolution indicate a monoclinic packing with the DATZnS(3′-NMe) along the unique axis of 1.685 nm and two shorter axes of 0.547 nm and 2.517 nm under an angle of 102º. This leads to a density of 1.67 g/cm^3 with two molecules in the unit cell. Systematic absences reveal a translational component, either a screw axis or a glide plane to accommodate steric hindrance that predominantly determines the packing. The internal C_2 symmetry and the absence of doubling in the MAS NMR point to a twofold axis in either a chiral packing with two independent positions or an achiral racemic paracrystalline packing with four independent positions to accommodate the two enantiomeric forms of the salphen motif with Λ and the Δ enantiomers present in equal amounts. The only space group that fulfills the requirements is *P*2/*c* with four independent positions that are both necessary and sufficient to account for the internal symmetry of the DATZnS(3′-NMe) as well as the presence of the two

enantiomeric forms. Other space groups either have more independent positions, *e.g.* eight for a racemic packing or four for a chiral packing or they require more than two molecules in the unit cell, or they do not reproduce the systematic absences in the diffraction pattern. In the structure, the molecules are in parallel stack arrangement with the phenazine dipoles head to tail. The two enantiomeric forms lead to sheets running antiparallel to form a 3D structure. The molecular recognition interaction between the salphen and the bromine leads to a pseudo-octahedral arrangement of zinc, which explains the richness in the structure with its two enantiomeric forms. The packing is confirmed by selective NMR distance constraints, between protons from the dimethyl functionalities in the salphen and NDI ring carbons adjacent to the Br, and between the alkyl chains and the phenazine core. Simulations of TEM diffraction reproduce the reflection conditions and allow determining the orientation of the lamellar morphology relative to the surface, which is important in view of the future application in artificial photosynthesis with complex supramolecular motifs bolted onto electrodes. The NDI rings are parallel to the surface, providing an interesting opportunity to make a configuration for *e.g.* injection of charge into a catalyst system.

2.1 Introduction

The world is moving towards a technological transformation, driven by the need to replace fossil fuel by renewables.[1-9] One out of very few options to achieve this is by artificial photosynthesis, which is the fine art of mimicking the processes of natural photosynthesis found in plants and some bacteria.[10-13] Biological systems are complicated with little true complexity. The biological design builds on "responsive matrices", protein complexes for light harvesting, charge separation and catalysis, which proceed with near-unity yield.[14] Any responsive matrix has an energy landscape that is determined by the structure, which on the one hand is stabilized with respect to the denatured or unfolded state, while on the other hand it is broadened by induced misfits and conformational entropy that allows for a quantum coherent functional response.[15,16] In contrast, supramolecular design often aims for tightly fitting assemblies, that leave little room for the frustration and the dynamic shaping that is necessary for steering reactivity and we have to

develop new chemical tools for engineering the packing by molecular recognition motifs, ultimately leading to functional assemblies. Here I explore how a zinc-salphen recognition motif steers the packing when fused to a naphthalene diimide chromophore to form a phenazine and deposited on a surface, a topology of interest to artificial photosynthesis applications. DATZnS(3′-NMe) is a fused NDI-zinc-salphen based chromophore that was designed with the optical and electronic properties of chlorophylls in mind and is much more robust than biological components.[17-25] Like chlorophylls, DATZnS absorbs sunlight by an extended conjugated π-system, has an electric dipole moment that can be utilized for structural and functional control, and has a divalent metal ion that does not interfere with the photochemistry.[17] It can bind with Lewis bases in the surrounding for molecular recognition and scaffolding of the packing in artificial photosynthetic systems.[26-28] Natural dyes can form functional antennae by self-scaffolding, without a protein component. In chlorosome antennae, hundreds of thousands of excitonically coupled bacteriochlorophyll natural dye molecules form the largest light antennae known in nature, capable of rapid transfer of energy over more than 100 nm.[29,30] Chlorosome structures do not depend on proteins for their structural and functional integrity and provide their own scaffolding.[31-33] They may serve as a supramolecular biological paradigm for how to perform structural design of a novel class of extended systems for artificial photosynthesis by molecular recognition and packing.[34] The key to their success is a pseudosymmetric framework where all monomeric building blocks perform the same functional role in well-ordered domains. Alternating chirality of monomers induced by the packing in stacks and sheets leads to induced misfits and conformational entropy.[15]

The aim of this study is to develop a toolbox for structural control in the chemical design of artificial light harvesting systems by packing induced self-assembly of moderately sized building blocks with isomerism. Here it is shown that it is possible to select conformers and isomers by packing and derive systematics for working with racemic paracrystalline materials. While frustration and combination of different functional motifs are necessary for a responsive and reactive chemical design, it will give rise to modulated assembly and lead to paracrystalline supramolecular arrangements. A principal challenge is then how to
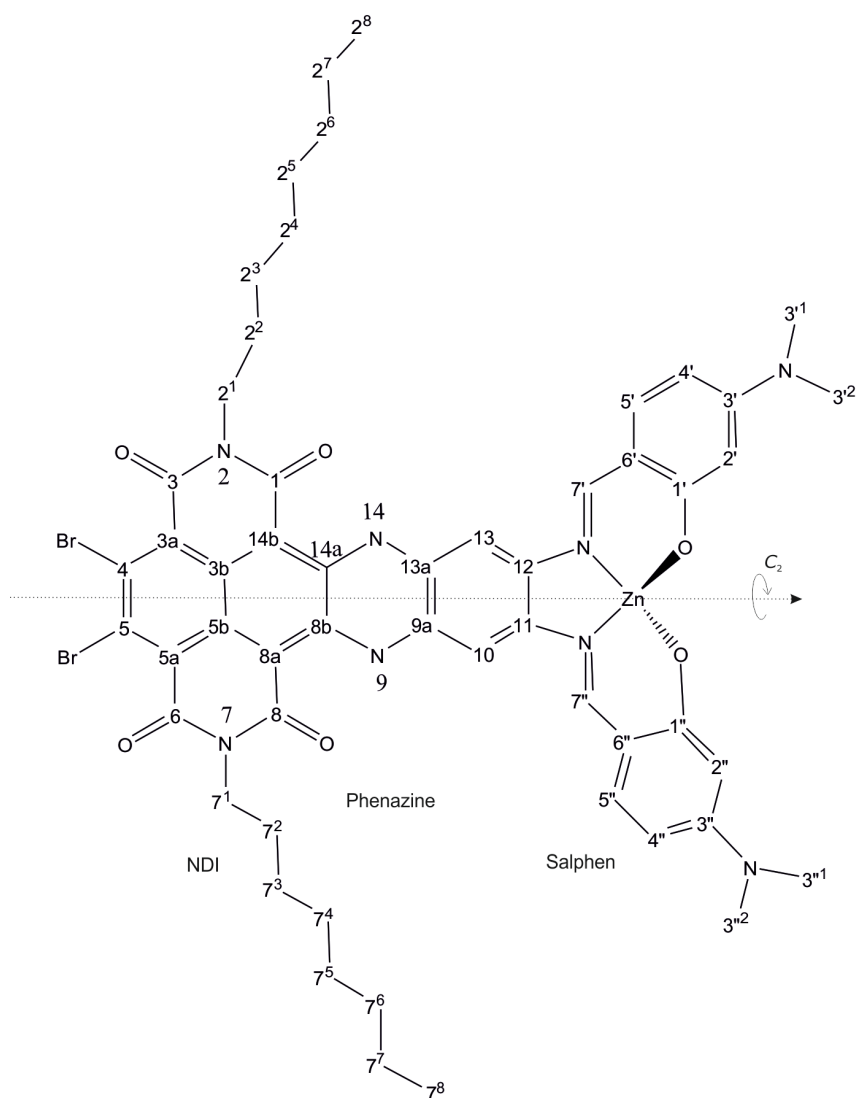
Figure 2.1 Chemical structure of the fused NDI-zinc-salphen based chromophore DATZnS(3′-NMe), a hybrid of NDI, Phenazine and Salphen with a C_2 axis of symmetry along the principal axis. The numbering is according to the IUPAC convention.

resolve the well-determined, limited true complexity from the heterogeneous background. The major challenge is to extract the functionally relevant order that is targeted by the chemical design, in a supramolecular packing that is inaccessible to high resolution X-ray and other diffraction methods for structure determination. Recently Ganapathy *et al.* have addressed this challenge by computational integration of MAS NMR and transmission electron microscopy (TEM) to resolve supramolecular packing order for a natural light collector.[35] In this approach, a library of structures is created based on reflection conditions in TEM imaging,

where the obtainable structure information in reciprocal space was a layer line along the meridian orthogonal to a strong symmetric reflection on the equator in the 2D diffraction pattern.[35] A model for the packing was refined with the help of chemical shifts and a few intermolecular correlation peaks obtained from homonuclear correlation spectroscopy done by proton spin diffusion and ^{1}H-^{13}C heteronuclear correlation data collected at a mixing time of 4 ms.[35] While the previous work concentrated on layer lines to guide the modeling of a helical structure on a cylinder, here I took the next step to resolve the packing for the DATZnS(3′-NMe) dye (Figure2.1), when forming a lamellar morphology on a surface, a technologically demanding configuration of strong relevance to possible future application in electrodes for artificial photosynthesis. I use the symmetry, repeats and reflection conditions obtained from Fourier transforms of TEM images of samples deposited on carbon grids to estimate the unit cell parameters and to identify symmetry operators with a translational component, *i.e.* a screw axis or glide plane. A 3D model for the packing was prepared with Materials studio and validated by simulation of the Fourier transform of the electron diffraction pattern. In addition, distance constraints were extracted from heteronuclear dipolar correlation data by simulating LGCP build up curves to measure ^{1}H-^{13}C distances for selected nuclei. Finally, the preferred orientation of DATZnS(3′-NMe) lamellae on the surface was determined by simulation of the TEM diffraction pattern from a supercell of DATZnS(3′-NMe). The methodology discussed here can be extended to other unlabeled samples for which it is difficult to find packing by more conventional methods.

2.2 Results

2.2.1 Chemical shift assignment and HETCOR analysis

DATZnS(3′-NMe) is a moderately sized molecule with extensive functionalities, arising from fusing functionalized NDI with functionalized salphen and establishing a phenazine bridge. Such chemical richness may be considered intrinsic for future classes of supramolecular architectures with advanced functionality. In addition, as steering the packing with molecular recognition will inevitably give rise to steric hindrance and characteristic aggregation shifts of the

NMR response, this will further contribute to a good resolution compared to the smaller compounds that are currently the standard in NMR crystallography.[35,36] Well in line with the earlier work on self-assembled moderately sized chlorophyll, chlorin and porphyrin type systems, the 1D CP/MAS spectrum of DATZnS(3′-NMe) collected with a spinning frequency of 11 kHz reveals a very good dispersion of ^{13}C chemical shifts, extending over a range of ~170 ppm.[35] This is an essential feature for structure determination of unlabeled materials, as many ^{13}C signals are well resolved in 1D with ^{13}C at natural abundance (Figure S2.3) which are summarized in Table 2.1. The aromatic signals from the NDI cover an extended range, between 150 and 170 ppm, due to the presence of the electronegative Br and keto oxygen substituents that produce extensive downfield shifts for various carbons due to the stabilization of positive charge. Also, the nitrogens in the phenazine motif contribute to the dispersion, in a more moderate way. The 3′-NMe that hyperconjugate to the salphen ring can stabilize negative charge on selected ^{13}C positions with signals shifting upfield to ~100 ppm, in competition with the stabilization of some positive charge from the oxygens bridging to the Zn^{2+} ion. Finally, the aliphatic region of the spectrum remains crowded, with the signals from the alkyl chains at the N2 and N7.

The DATZnS(3′-NMe) and its DAT-diamine precursor (Figure S2.1) are both insoluble, and a conclusive assignment of chemical shifts in the solid state is difficult with ^{13}C at natural abundance. Therefore we perform a homology assignment based on ^{1}H-^{13}C HSQC, ^{1}H-^{1}H COSY and HMBC data collected from the related compound DATZnSTP dissolved in C_6D_6 (Table 2.2). The assignment is validated with ^{1}H-^{13}C HETCOR and NMR chemical shift calculations. A set of 2D HETCOR spectra with a short mixing time of 0.256 ms and a long mixing time of 4 ms was collected (Figure 2.2). The short contact time unambiguously reveals the carbon nuclei with directly bonded protons (Figure 2.2). Due to the good dispersion, a conclusive assignment of the five aromatic C-H signals is straightforward (Table 2.1). The 2^1, 7^1 N-CH$_2$ well as the 3′, 3″ N-CH$_3$ provide a characteristic response around 40 ppm and the terminal CH$_3$ of the alkyl chain resonate most up field at ~13 ppm. None of these signals shows doubling, which provides converging and convincing evidence that the two halves of the molecule are related by symmetry. This provides convincing evidence for a symmetric

DATZnS(3′-NMe) building block, with a twofold axis or a mirror plane running along the center of the phenazine motif. A pseudo octahedral coordination of the zinc salphen motif significantly contributes to the complexity of the system and can provide a handle for steering of the structure by packing effects. The wings of the salphen can be either in the *syn* or *anti*-configuration, and for the *anti*-configuration, two enantiomeric chiral isomers exist for the zinc octahedral surrounding, the Λ and Δ pair. Optimization on the enantiomeric pairs shows that an energy minimum of 10 kcal/mol limits the structure to an *anti*-configuration. The narrow lines with a linewidth of ~1 ppm for selected signals show that the system is at least paracrystalline, as *e.g.* a semicrystalline or disordered system

Table 2.1 Experimental and calculated ^{13}C chemical shifts of the DATZnS(3′-NMe)

Position	$\sigma^{C}_{DATZnS(3'-NMe), expt}$	$\sigma^{C}_{DATZnS(3'-NMe), calc}$
4, 5	154.6, 154.6	152.5, 152.5
3a, 5a	23.8, 123.8	125.6, 125.3
3, 6	166.6, 166.6	162.9, 162.9
3b, 5b	136.9, 136.9	130.0, 130.0
14b, 8a	112.1, 112.1	101.3, 101.3
13a, 9a	123.8, 123.8	129.0, 129.0
13, 10	100.1, 100.1	99.8, 99.8
12, 11	138.1, 138.1	142.1, 142.1
7', 7"	166.6, 166.6	150.2, 150.2
6', 6"	123.8, 123.8	122.7, 122.7
5', 5"	136.9, 136.9	138.2, 138.2
3', 3"	156.7, 156.7	154.1, 154.1
4', 4"	102.1, 102.1	109.1, 109.1
2', 2"	102.1, 102.1	108.5, 108.5
1', 1"	171.7, 171.7	176.7, 176.7
$2^{1}, 7^{1}$	42.4, 42.4	46.9, 46.9
$2^{2}, 7^{2}$	28.6, 28.6	32.3, 32.3
$2^{3}, 7^{3}$	28.1, 28.1	34.5, 34.5
$2^{4}, 7^{4}$	30.7, 30.7	36.7, 36.7
$2^{5}, 7^{5}$	31.8, 31.8	35.1, 35.1
$2^{6}, 7^{6}$	30.7, 30.7	41.8, 41.8
$2^{7}, 7^{7}$	23.2, 23.2	29.3, 29.4
$2^{8}, 7^{8}$	13.7, 13.7	17.8, 17.8
$3'^{1} 3'^{2}, 3''^{1}, 3''^{2}$	39.0, 39.0, 39.0, 39.0	43.3, 43.3, 43.4, 43.4

Table 2.2 Experimental and calculated ^{13}C chemical shifts of the DATZnSTP

Position	$\sigma^C_{\text{DATZnSTP, expt}}$	$\sigma^C_{\text{DATZnSTP, calc}}$
4, 5	140.6, 140.6	152.5, 152.5
3a, 5a	121.7,121.7	125.8,126.3
3,6	160.0,160.0	163.4,163.5
3b,5b	127.3,127.3	130.5,129.9
14b, 8a	95.5, 95.5	101.9, 102.5
1, 8	164.6, 164.6	167.0, 166.8
14a, 8b	127.5, 127.5	139.0, 138.7
13a, 9a	125.7, 125.7	129.8, 129.8
13, 10	102.9, 102.9	104.4, 102.1
12, 11	139.5, 139.5	146.8, 145.7
7', 7"	162.0, 162.0	158.4, 156.4
6', 6"	118.9, 118.9	127.7, 127.1
5', 5"	129.7, 129.7	136.5, 132.0
4', 4"	135.3, 135.3	142.6, 143.0
3', 3"	130.7, 130.7	133.1, 135.8
2', 2"	143.3, 143.3	148.8, 151.5
1', 1"	173.4, 173.4	177.5, 177.4
$4'^1, 4"^1$	34.2, 34.2	44.4, 45.2
$4'^2, 4"^2$	31.8, 31.8	35.3, 33.6
$4'^3, 4"^3$	31.8, 31.8	35.1, 30.4
$4'^4, 4"^4$	31.8, 31.8	30.8, 33.7
$2'^1, 2"^1$	36.3, 36.3	47.7, 46.9
$2'^2, 2"^2$	30.2, 30.2	34.6, 34.8
$2'^3, 2"^3$	30.2, 30.2	30.5, 29.3
$2'^4, 2"^4$	30.2, 30.2	30.1, 29.5
1''', 5'''	149.2, 149.2	149.6, 153.9
5'''	149.2	153.91
2''', 4'''	121.4, 121.4	127.8, 126.0
3'''	161.3	168.2
$3'''^1$	34.4	45.4
$3'''^2, 3'''^3, 3'''^4$	30.0, 30.0, 30.0	34.1, 34.4, 29.4
$2^1, 7^1$	41.5, 41.5	48.4, 49.1
$2^2, 7^2$	28.3, 28.3	33.3, 33.1
$2^3, 7^3$	27.8, 27.8	32.1, 31.9
$2^4, 7^4$	29.8, 29.8	36.6, 41.1
$2^5, 7^5$	29.8, 29.8	29.3, 31.6
$2^6, 7^6$	32.2, 32.2	37.4, 43.1
$2^7, 7^7$	23.1, 23.1	25.0, 32.6
$2^8, 7^8$	14.4, 14.4	14.6, 18.6

would give rise to pronounced susceptibility broadening of signals.[37,38] The remaining aliphatic response is associated with the CH_2 of the aliphatic tail. The quaternary carbon response is detected in the ^1H-^{13}C HETCOR dataset collected with long CP contact time of 4 ms. The 4, 5 ^{13}C adjacent to the Br are assigned to the response at 154.6 ppm, in line with NMR shift calculations for a C_2 symmetric monomer (Table 2.1). The ^{13}C next to the keto oxygens are shifted to 159.8 and 166.6 ppm and are in line with the solution NMR response of the homologue at 160and 164.6 ppm, for the 1, 8 ^{13}C and the 3, 6 ^{13}C, respectively. Similarly the 1', 1" ^{13}C near to the bridging oxygens in the salphen have a characteristic chemical shift of 171.7 ppm, which is in line with the shift of 173.4 ppm for the homologue in solution. Remaining assignments were obtained either by analogy with the solution chemical shifts of the related molecule DATZnSTP (Figure S2.4), or were performed by computation of chemical shifts (Table 2.2). The NMR data are in line with a molecular configuration that has a C_2 axis passing through the centers of NDI and salphen as shown in Figure 2.1.

Intermolecular correlations were obtained from heteronuclear ^1H-^{13}C spectra recorded with a long LGCP contact time of 4 ms (Figure 2.2).[39] Pronounced correlation signals are observed between the $3'^1$, $3'^2$, $3''^1$, $3''^2$ protons resonating with 0.6 ppm ^1H chemical shift on salphen and 4, 5 ^{13}C nuclei on the NDI motif and are indicated with an asterisk. These correlation signals can be attributed to long-range transfer since they are not observed in the dataset collected with a short mixing time. The nearest intramolecular ^1H are the 2^1, 7^1 CH_2 at a distance of 4.8 Å that resonates with a different ^1H chemical shift of 0.4 ppm. The long range transfer between 3'-NMe and 4, 5 ^{13}C provides strong NMR evidence that molecular recognition between the NDI part of the molecule and the salphen motif of an adjacent molecule is steering the packing. In addition, long-range correlation peaks are observed between protons on the alkyl chain and 11, 12, 3b, 5b, 13a, 9a, 14b, 8a, 10, 13 ^{13}C nuclei on the phenazine backbone. These long-range correlation signals could be inter or intramolecular and provide information about the positioning of the alkyl chain in the packing.

Figure 2.2 Contour plot sections of ^{1}H-^{13}C heteronuclear MAS NMR dipolar correlation spectra of DATZnS(3′-NMe) recorded in a magnetic field of 17.6 T employing a spinning rate of 11 kHz and data were collected at a sample temperature of 298 K. CP contact times of 4 ms (red) and 1 ms (black) were used to distinguish inter and intramolecular correlation peaks. The left panel shows the aromatic and carbonyl region, while the aliphatic response is shown in the right panel. Correlation peaks are indicated by numbers corresponding to the assignment listed in Table 2.1. The position of the alkyl chain is confirmed from long range correlation peaks observed between 11, 12, 3b, 5b, 13a, 9a, 14b, 8a, 10, 13 carbon atoms and protons on the aliphatic tail. The intermolecular correlations between the 3′1, 3′2, 3′′1, 3′′2 and the 4, 5 ^{13}C are indicated with an asterisk. Many correlations in the dataset recorded with a long mixing time are intermolecular.

2.2.2 LGCP build up curve

To validate the interpretation of the HETCOR data shown in Figure 2.2, LGCP build up curves (Figure 2.3) were collected with the sequence of van Rossum *et al.* (Figure S2.8B).[40] Homonuclear decoupling was achieved by applying pulses at the ± LG condition during the CP contact time. The LGCP build up curves for the 4, 5 and 13a, 9a ^{13}C can be resolved in the dataset of Figure S2.3-2.4 and are plotted against mixing time from 0 to 2 ms in Figure 2.3 with a red and green trace, respectively. Heteronuclear distances between selective nuclei can be estimated from such LGCP build up curves by simulation for various ^{1}H-^{13}C distances using the SIMPSON virtual spectrometer software.[41] Both traces are in line with a simulation for a single ^{1}H-^{13}C pair of spins separated by ~3 Å, corresponding to a dipolar coupling frequency of -1.1 kHz. The relatively short intermolecular distance may indicate the parallel transfer of polarization from a proton cloud to a nearby ^{13}C nucleus. The observation that two different build up signals from nearby abundant ^{1}H nuclear species into a ^{13}C at natural abundance can be
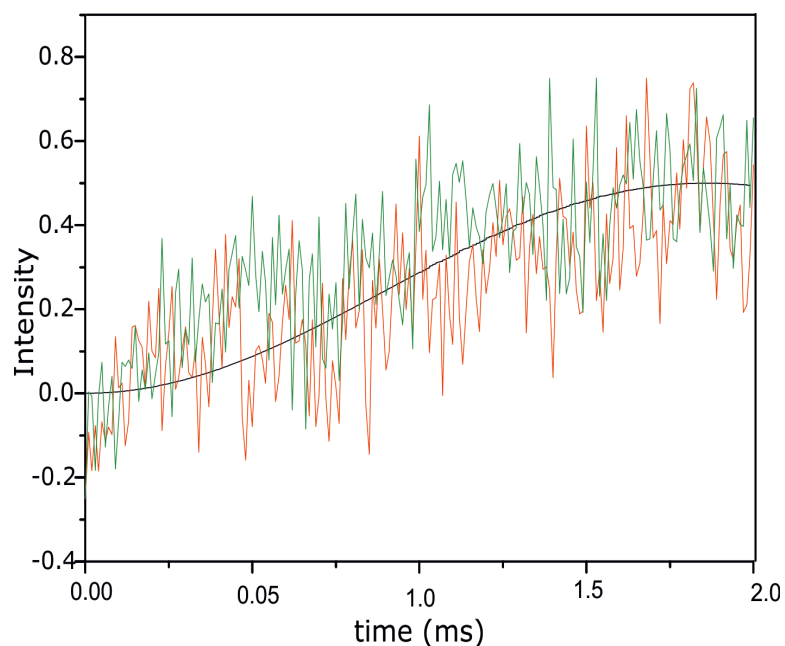
Figure 2.3 2-D LGCP build-up curves of 4/5 carbon nuclei (red) and 13a/9a carbon nuclei (green) were compared with a simulated buildup for a heteronuclear [1]H-^{13}C spin pair separated by 3 Å (black).

superimposed onto one another and yield similar coherent buildup transfer is intriguing. It may indicate a general property of intermolecular heteronuclear buildup in rigid systems, which can serve as a practical rule for structure determination of moderately sized molecular systems with ^{13}C at natural abundance. The 3b, 5b ^{13}C in the central part of the NDI motif correlate with the 2^1 and 7^1 CH_2 protons. The intramolecular distance is 4.4 Å, which is rather long. The correlation, therefore, can be intermolecular, indicative of the formation of J-aggregates with a slipped arrangement of the NDI moieties since this would position the alkyl tail above the plane of a neighbouring molecule and would imply that the correlations and buildup from protons at the alkyl chain to 13a, 9a ^{13}C are intermolecular. Similarly, the buildup of CP intensity from the alkyl CH_2 to the quaternary ^{13}C on the phenazine core can be considered intermolecular from the abundant ^{1}H nuclei on the alkyl chain. There are no intramolecular correlation signals for the 10, 13 or other aromatic protons with their quaternary neighbours. In addition, the 9 N-H was found to resonate downfield $\sim$ 10 ppm in the homologue and there are no correlation signals in this region in the HETCOR dataset with a long mixing time as well (data not shown).

2.2.3 Cryo EM measurements

A high-resolution TEM image of the DATZnS(3′-NMe) deposited on a carbon electrode reveals a layered periodic arrangement (Figure 2.4A). Fourier transformation of the selected region indicated by a dashed square shows periodic spacings of 1.685 nm and 0.547 nm in mutually orthogonal directions (Figure 2.4B). This represents the preferred orientation, as it was difficult to find other alignments with clear reflections. The TEM data thus provide enough evidence to converge on a monoclinic packing with the molecule along the unique axis of 1.685 nm, parallel to the surface. This is in line with the head to tail molecular recognition deduced from the NMR distance constraints. The reflections cannot all be of first order, as this would lead to a density that is at least a factor two too high, depending on the number of molecules in the unit cell. Along the direction of 1.685 nm, there are two strong centrosymmetric reflections, which can be of first order since the size of the molecule along the long axis is around 1.685 nm. In addition, higher order weak reflections without any systematic absence are also observed in the same direction. Perpendicular to the direction of 1.685 nm there are series of reflection spots with a systematic absence pointing to reflection condition *h0l*: *l = 2n*. This systematic absence implies a translational component, a screw axis or glide plane, in the symmetry operations for the packing space group. The 1.24 nm reflection observed (Figure S2.5) at high magnification should be either a first order reflection with one molecule per unit cell or a second order reflection with two enantiomers per unit cell to arrive at a density around 1.67 g/cm^3 and account for the symmetry in the NMR response. Interestingly there is also a 0.74 nm reflection spot (Figure S2.5), which could be a higher order reflection of the third axis. Although at this point considering the strength of the reflection spots, other polymorphs cannot be excluded.

2.3 Discussion

2.3.1 Antiparallel lamellar packing of DATZnS(3'-NMe)

For moderately sized molecules with functionalities protruding, packing will inevitably lead to steric conflicts unless screw axes or glide planes, symmetry operations containing a translational component, are invoked that allow for an

interpenetration of parts of the structure containing symmetry-related molecules. This is the reason why by far most of the nonchiral organic packings are in the $P2_1/c$ space group, which as both a 2_1 screw axis and a c-glide plane. This implies two independent, symmetry related positons in a chiral packing with a twofold axis, or two enantiomers can be present in an equal amount to establish a racemic packing with four inequivalent sites, two from the twofold axis in the DATZnS(3'-NMe) and two from the enantiomeric pair (Figure 2.1). The monoclinic space groups with a twofold axis are $P2$, $C2$, $P2/m$, C2/m, P$2/c$, and $C2/c$. Of these, $P2$ and $P2/m$ do not have reflection conditions and can be discarded. The chiral space group $C2$ has four independent positons while only two are needed for a chiral packing. Likewise, the achiral space groups $C2/m$, and $C2/c$ have eight independent positions, while only four are needed for a racemic packing. This effectively limits the space group to $P2/c$, with unidirectional donor-on-donor and acceptor-on-acceptor columnar arrays in an extended and layered antiparallel monoclinic unit cell with a twofold axis and a glide plane (Figure 2.5).[42] The $P2/c$ space group has reflection conditions in line with the experimental diffraction pattern. The molecular arrangement was modeled in a $P2/c$ unit cell with dimensions a = 0.547 nm, b = 1.685 nm, c = 2.517 nm and β = 102°, taken from the TEM images (Figure 2.4). First, a monomer was optimized with the Dreiding force field in FORCITE and refined at the DFT level with DMol^3 to determine the atomic charges. The total charge was set to zero, and the molecule was then positioned with the C_2 molecular axis aligned onto the twofold symmetry axis in the unit cell, second setting with B-Unique, Cell1 in Materials Studio. The four symmetry operations then generate two pairs of enantiomers, and only one set of enantiomers was kept. With a density of 1.67 g/cm^3, the position along the twofold axis was varied to minimize steric hindrance. The structure was optimized with FORCITE, leading to an energy of 170.5 kcal/mol. To validate the structure, we performed an optimization without constraining the cell, which led to virtually the same result, and we performed a polymorph analysis with Materials Studio to verify the possibility of other packings with higher density and lower energy across the five most frequent space groups, which we were not able to find. The $P2/c$ has by far the highest density and lowest lattice energy among the packings with other possible space groups.
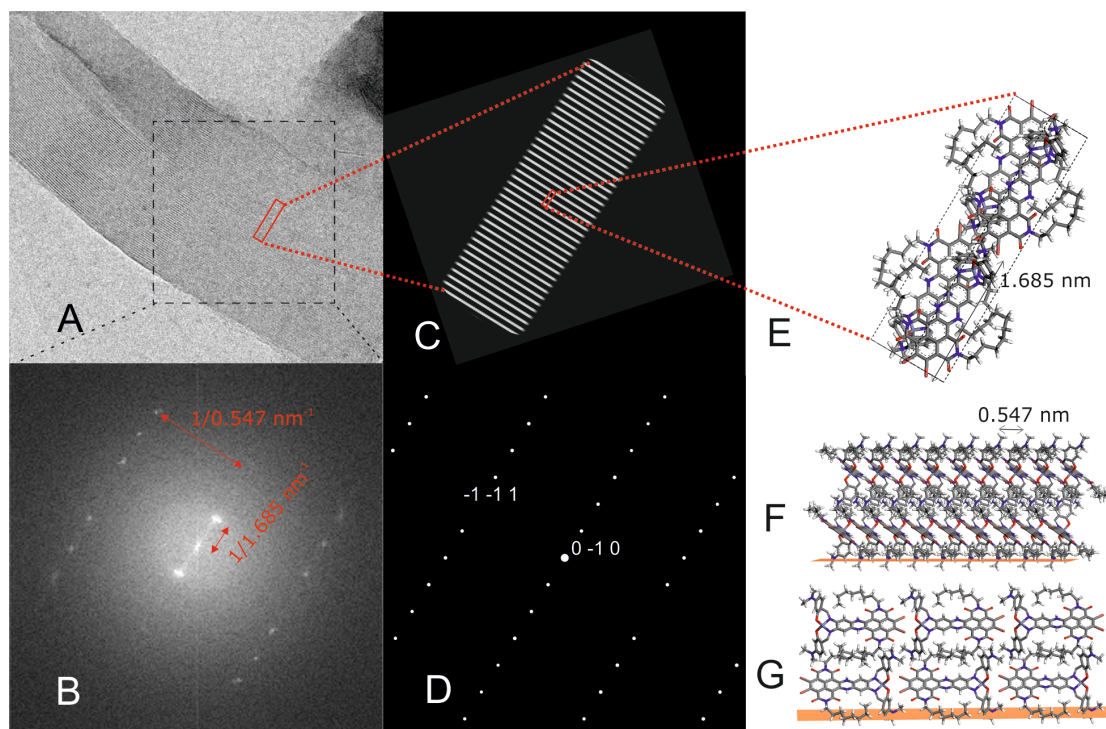
Figure 2.4 Integration of TEM and MAS NMR data to resolve the DATZnS(3′-NMe) structure. (A) TEM image of the DATZnS(3′-NMe) deposited on a carbon grid, revealing the lamellar character of the compound and (B) the Fourier transform of the selected region showing the TEM diffraction pattern with systematic absences. In (D) the simulated diffraction pattern obtained with the NMR derived geometry optimized DATZnS(3′-NMe) stacks in the $P2/c$ space group (E) is shown. The projection of the electron density map with a 40*20*2 supercell is shown in panel (C). The orientation of the compound on the carbon grid is schematically indicated in (F) and (G).

The DATZnS(3′-NMe) forms a tightly packed J-aggregate with a distance of 0.36 nm between NDI planes. Such short distances are commonly encountered for various classes of aggregated aromatic dyes.[43-45] Strong π-π stacking interactions and aligned electric dipoles may explain why the molecule has a high density and a low energy and is virtually insoluble. The aliphatic tails are oriented in the same direction as the salphen wings and are in voids between the phenazine moieties. A tight packing with the alkyl chains folded along the phenazine bridge of a neighbouring molecule explains the observation of strong heteronuclear correlation signals between the abundant aliphatic ^{1}H and rare phenazine ^{13}C spins, with distances between 0.2 and 0.4 nm providing very effective pathways for polarization transfer (Figure 2.3). The molecular recognition that leads to the head to tail orientation and distorted octahedral surrounding of the Zn^{2+} ion puts

the 3′-NMe of a salphen at a distance of 0.32 nm from the 4, 5 ^{13}C in the NDI, which is also in quantitative agreement with the LGCP buildup kinetics data and the SIMPSON analysis shown in Figure 2.3.

For the simulation of the diffraction pattern the model was read into CrystalMaker, oriented, and projected onto the TEM diffraction pattern in SingleCrystal (Figure 2.4D). The model was oriented by performing visual matching of the simulated diffraction with the observed Fourier transform. A view direction along the 0.69, 0, 0.69 lattice vector gave the best match on an average orientation for the DATZnS(3′-NMe) on the EM grid, with the indexing of the diffraction image as indicated in Figure 2.4D. The analysis validates the systematic absence of reflections from the c-glide plane in the $P2/c$ space group, and shows that -1 0 1 and 1 0 -1 are quenched (Figure 2.4B). The strong 0 1 0 and 0 -1 0 are from the lamellar spacing and alternating regions of zinc salphen and NDI. The alternating electron density observed in the TEM image was reproduced from a 40*20*2 super cell constructed out of a unit cell along the surface. An electron density map was generated and then projected onto a plane with the EMAN electron microscopy processing suite, which is in correspondence with TEM image (Figure 2.4C). In the preferred orientation the DATZnS(3′-NMe) molecules are oriented parallel to the electrode surface as in Figure 2.4F. The phenazine dipoles are aligned along the surface while the NDI stacks are running at an angle of 45° with the plane of the NDI rings parallel to the surface (Figures 2.4E, F).

2.3.2 Insight into the packing

In Figure 2.5 it is shown how the molecular recognition leads to a hierarchy in the suprastructure. At the basis there is twofold C_2 symmetry of the DATZnS(3′-NMe) (Figure 2.5A). In the competition between accommodating functionalities by screw axes and glide planes, apparently, the screw axis is suppressed in favour of a twofold axis to accommodate the C_2 symmetry. This is possible because of a rich structural variability introduced with the nonplanar metal salphen that has Λ and Δ enantiomer. The structural variability allows for an overall packing in an achiral $P2/c$ space group with a racemic mixture of the two enantiomeric species, thereby circumventing the need for a screw axis in favour of a c-glide plane with inversion symmetry in the structure. Thus, while $P2_1/c$ is by far the most common space
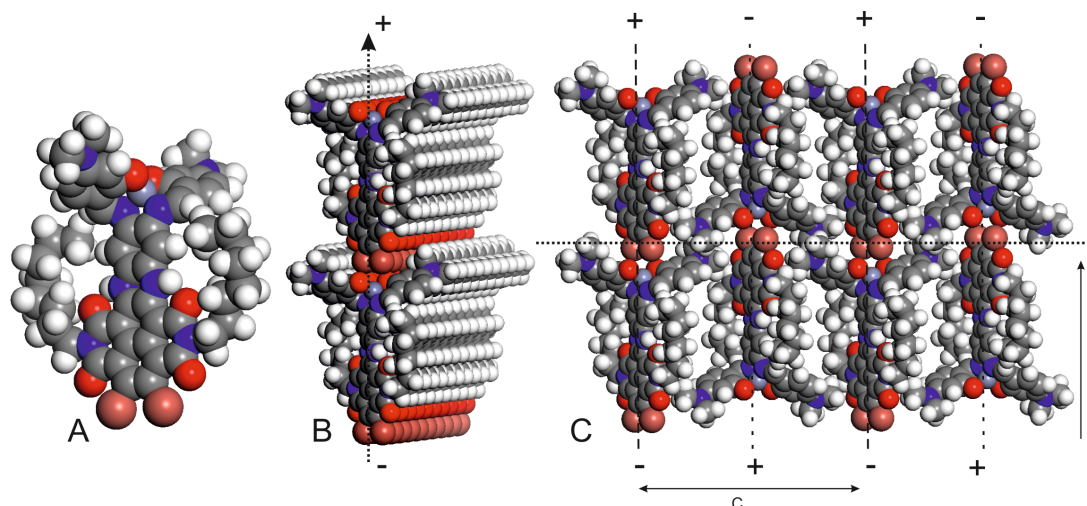
Figure 2.5 Molecular recognition for steering the packing of DATZnS(3′-NMe) starts from chiral building blocks with C_2 symmetry (A). These self-assemble into enantiomerically pure polar layers with a $P2$ surface symmetry to accommodate the twofold axis. The layers comprise arrays of aligned dipoles with a positive salphen side and negative Br side (B). Alternating layers with opposite chirality self-assemble with a c-glide to release steric hindrance and establish a dense packing with quenching of electric dipoles (C).

group for optically active organic species, here in this work, it is managed to steer away by molecular recognition and chemical programming of a twofold axis at the molecular level, which does not "fit" in a $P2_1/c$ framework. This is similar to the concept of an induced fit or misfit in biological samples.[15]

2.3.3 Orientation of the molecule on the surface

With the C_2 molecular symmetry preserved, the DATZnS(3′-NMe) self assembles into polar planes without inversion symmetry elements (Figure 2.5B). Here the selectivity induced by the chirality that emerges at the salphen motif is essential. Chiral expression at surfaces and planes has attracted considerable attention in recent years. Only five possible chiral space groups can exist at a surface and the DATZnS(3′-NMe) is forced into a $P2$ plane by the molecular C_2 symmetry, the molecular recognition and for energetic reasons.[46] The electric dipoles align and form extended arrays with a positive and a negative side, which may be of interest to support charge separation following light absorption in the NDI columns running perpendicular to the electric field direction in the $P2$ plane of chiral molecules (Figure 2.5B). It is easy to create chirality in a 2D system since a surface

45

cannot possess a center of inversion and can only maintain reflection mirror symmetry planes normal to the surface, which leads to the $P2/c$ arrangement shown in Figure 2.5C with the two enantiomeric species forming planes of alternating chirality. In the proposed 3D model the net dipole moment cancels due to the antiparallel stacking of layers. Hence, the DATZnS(3′-NMe) forms extended chiral domains arising from the planar arrangements of the individual $C2$ motifs, a concept known as organizational chirality.[46] Because of the close analogy between surfaces and planes, it is anticipated that this molecular steering concept can be further developed for the chemical design of functional electrodes. With the DATZnS(3′-NMe) forming polar layers, there is the possibility to deliver electrons at the salphen side to an electrode or tailor the template to incorporate a catalyst in a solar fuel cell device architecture. In parallel introduction of electron donating or withdrawing groups to the core of the naphthalene shifts the optical absorption, making it suitable for tuning the optoelectronic properties.[47,48]

2.4 Conclusions

The molecular structure and packing of paracrystalline DATZnS(3′-NMe) oriented on a surface grid was studied in detail in the solid state. DATZnS(3′-NMe) lamella pack in a $P2/c$ space group with alkyl chains folding along the phenazine and the zinc in a pseudo octahedral environment with adjacent bromine atoms. Symmetry and distance constraints obtained from CP/MAS NMR in association with reflections in the diffraction pattern were used to converge on a racemic packing with four independent positions starting from chiral building blocks with C_2 symmetry. The system combines a high density of 1.67 g/cm^3 with a low energy in comparison with other polymorphs. The molecular recognition and molecular symmetry are used to steer the packing and associated functional characteristics by forcing the system into a racemic packing and use a c-glide plane with inversion symmetry to release steric hindrance. The combination of MAS NMR, cryo-EM and molecular modeling with periodic boundary conditions in the form of a space group provides a promising approach that can be of use in the future to investigate structure and properties of other unlabeled moderately sized supramolecular systems.

2.5 Materials and methods

2.5.1 Sample preparation

For the purpose of this study Zinc(II) 6,6'-((1E,1'E)-((4,5-dibromo-2,7-dioctyl-1,3,6,8-tetraoxo-1,2,3,6,7,8,9,14-octahydro-[3,8] phenanthrolino [1,10-abc] phenazine-11,12-diyl) bis (azanylylidene)) bis (methanylylidene))bis(3-(dimethylamino)phenolate) (DATZnS(3'-NMe)) molecule is used (Figure 2.1).[17] The DATZnS scaffold is a hybrid material with a core expanded naphthalene diimide (cNDI) supramolecularly coupled with a zinc bis-salicyimide phenylene (salphen) moiety and can be functionalized with 3′-NMe or 2′,4′-tBu functional groups (Figure S2.2).[17] For the synthesis, anhydrous N,N-dimethylformamide (DMF) was obtained from Sigma-Aldrich and used as received. Melting points were measured using $\Delta T = 1$ °C min^{-1} on a Stuart Scientific SMP3 melting point apparatus and are uncorrected. Infrared (IR) spectra were recorded neat using a Shimadzu FTIR-8400s spectrophotometer and wavelengths are reported in cm^{-1}. Unless stated otherwise, all reagents were used as received from commercial vendors.

Synthesis of DAT-diamine: In a small round bottom flask, 15 mL of 98% H_2SO_4 was degassed for 15 min using an N_2 stream. DATTs[49] was added as a solid (131 mg, 0.12 mmol) and the resulting turquoise solution was stirred under N_2 atmosphere for 4 days. The reaction mixture was transferred under vigorous stirring into a 1 L flask containing 500 mL of H_2O and 200 mL of dichloromethane, after which $NaHCO_3$ was added as a saturated aqueous solution until gas evolution ceased. The organic phase was separated and concentrated under vacuum. A dark blue solid (DAT-diamine) was obtained in quantitative yield (85 mg). This solid readily aggregates in solution, prohibiting recording of ^1H and ^{13}C solution NMR spectra. FTIR: 3456, 3416, 3362, 3339, 2953, 2914, 2849, 1678, 1570, 1489, 1452, 1425, 1286, 1234, 1134, 1094, 1013, 874, 812, 660 cm^{-1}. The first four frequencies are indicative of the presence of aniline like N-H stretching vibrations.

Synthesis of DATZnS(3'-NMe): DAT-diamine intermediate (142 mg, 0.18 mmol) was prepared from DATTs, was dissolved in 15 mL dry, degassed DMF under an Ar atmosphere and heated to 110 °C in the dark. In a separate flask, 4-

dimethylaminosalicylaldehyde (60 mg, 0.37 mmol) and zinc acetate dihydrate (320 mg, 1.75 mmol) were dissolved in dry, degassed DMF (5 mL) and kept under Ar. This mixture was stirred for 5 minutes and added to the hot DMF solution via a syringe. After 4 hours, the reaction mixture was cooled down to room temperature and diluted with 25 mL saturated aqueous $NaHCO_3$ solution to induce precipitation. The dark blue precipitate was collected on a filter and washed with water, ethanol and chloroform to afford (after vacuum drying) 221 mg of a dark blue solid (95 % yield from DAT-diamine). IR (ATR FTIR): 3497, 3371, 2923, 2856, 1684, 1610, 1570, 1560, 1448, 1431, 1375, 1358, 1279, 1246, 1182, 1151, 843, 669, 660, 661, 584 cm^{-1}. Mp: > 300° C

2.5.2 NMR measurements

NMR spectra with high sensitivity and high resolution were obtained by exploiting heteronuclear cross polarization (CP) along with magic angle spinning (CPMAS), in which polarization is transferred from abundant ^{1}H spins to the dilute ^{13}C nuclei, followed by the observation of the signals from the carbon. MAS NMR experiments were performed on a Bruker AV-750 spectrometer equipped with a 4 mm triple resonance MAS probe head, using a ^{13}C radio frequency of 188.6 MHz and data were collected at a sample temperature of 298 K. The ^{79}Br resonance from KBr was used to set the magic angle. A spinning frequency of 11 kHz ± 5Hz was used for the 2D ^{1}H-^{13}C heteronuclear correlation experiments. The ^{1}H spins were decoupled during acquisition using the two-pulse phase modulation TPPM scheme. Two-dimensional ^{1}H-^{13}C heteronuclear correlation data sets were obtained with the Phase Modulated Lee Goldburg (PMLG) experiment with a short CP time of 0.256 ms and a long CP time of 4 ms (Figure S2.2A). The ^{1}H chemical shift was calibrated with a HETCOR dataset collected from tyrosine.HCl salt. A Frequency-Switched Lee-Goldburg (FSLG) scale factor of 0.571 reproduces the ^{1}H chemical shifts for Tyrosine in solution. To collect the data set for the LGCP build up curves, the sequence in Figure S2.8b was used. LG conditions were applied during CP and the contact time was increased from 0.1 to 2 ms.[39] NMR data were processed using the TopSpin 3.2 software (Bruker, Billerica, MA). OriginPro 9.1 (OriginLab Corporation, Northampton, MA) was used to process the LGCP build up curves for the selected ^{13}C nuclei and to do the Fourier transformation. LGCP build up curve

simulations were performed using the open-source simulation software SIMPSON for ^{1}H–^{13}C spin systems with REPULSION powder averaging over a set of 66 Euler angles with 8 γ angles at 11 kHz spinning and a static field corresponding to 750 MHz for ^{1}H (S2.6).

2.5.3 Cryo-EM measurements

Samples for CryoEM were prepared by gently "crushing" the material with a small spatula onto a glass slide. It was suspended in ethanol and after settling a droplet from the upper half of the suspension containing the smaller fragments was put onto a carbon-coated grid, blotted, and dried in air. The samples were cooled down to -180° in the microscope and imaged with 300 kV electrons. Electron microscopy was performed with a Tecnai G2 Polara electron microscope (FEI, Hillsboro, OR) equipped with a Gatan energy filter at 115,000× magnifications (Gatan, Pleasanton, CA). Images were recorded in the zero-loss imaging mode, by using a slit-width of 20 eV, with a slow-scan CCD camera at 1 μm under focus, to have optimal phase contrast transfer at 300 kV for details with a periodicity of ≈2 nm. 3D electron density was simulated from atomic coordinates at 0.6 nm resolution by using the EMAN pdb2mrc program. The electron density map was projected onto a plane using the EMAN proc3d program to get a simulated EM image. Simulation of the TEM diffraction was performed with SingleCrystal (Crystalmaker Software Ltd, Oxford) after orienting the crystal structure in the CrystalMaker (Crystalmaker Software Ltd, Oxford) software.[50,51]

2.5.4 Structure modeling and chemical shift calculation

Computational modeling was performed with the Biovia Materials Studio Suite (Biovia, San Diego, CA). Racemic packings were obtained for different space groups. A set of unit cells with a twofold axis was selected to accommodate the C_2 symmetry. The monomer was positioned along the twofold axis in a unit cell with the parameters obtained from TEM. The monomer was shifted and rotated to minimize steric hindrance and spurious doublings were removed by hand to obtain a reasonable density. The structure was then optimized using the FORCITE module with the Dreiding force field and ESP charges calculated with DMol^3 for the molecule in its C_2 configuration. Calculations were performed with DMol^3 as

implemented in DMol^3 package. The generalized gradient approximation (GGA) with the Perdew–Burke–Ernzerhof (PBE) functional is employed. In this work, the double numerical atomic orbital augmented by a polarization p-function (DNP) is chosen as the basis file 3.5. Global orbital cutoff value is 3.9 Å.

NMR chemical shift calculations for monomers were performed by optimizing the structure using the Gaussian 03 software package (Gaussian, Inc., Wallingford, CT) with the Becke, Lee, Yang, and Parr (BLYP) exchange-correlation functional with 6-311G basis set and using the NMR module in Gaussian 03.[52]

References

(1)	Cook, T. R.; Dogutan, D. K.; Reece, S. Y.; Surendranath, Y.; Teets, T. S.; Nocera, D. G. *Chemical Reviews* **2010**, *110*, 6474.

(2)	Chu, S.; Majumdar, A. *Nature* **2012**, *488*, 294.

(3)	Lewis, N. S.; Nocera, D. G. *Proceedings of the National Academy of Sciences* **2006**, *103*, 15729.

(4)	Abbott, D. *Proceedings of the IEEE* **2010**, *98*, 42.

(5)	Kutal, C. *Journal of Chemical Education* **1983**, *60*, 882.

(6)	Kim, D.; Sakimoto, K. K.; Hong, D.; Yang, P. *Angewandte Chemie International Edition* **2015**, *54*, 3259.

(7)	Listorti, A.; Durrant, J.; Barber, J. *Nat Mater* **2009**, *8*, 929.

(8)	Wondraczek, L.; Tyystjärvi, E.; Méndez-Ramos, J.; Müller, F. A.; Zhang, Q. *Advanced Science* **2015**, *2*, n/a.

(9)	Faunce, T. A.; Lubitz, W.; Rutherford, A. W.; MacFarlane, D.; Moore, G. F.; Yang, P.; Nocera, D. G.; Moore, T. A.; Gregory, D. H.; Fukuzumi, S.; Yoon, K. B.; Armstrong, F. A.; Wasielewski, M. R.; Styring, S. *Energy & Environmental Science* **2013**, *6*, 695.

(10)	Gust, D.; Moore, T. A. *Science* **1989**, *244*, 35.

(11)	Young, K. J.; Martini, L. A.; Milot, R. L.; Snoeberger Iii, R. C.; Batista, V. S.; Schmuttenmaer, C. A.; Crabtree, R. H.; Brudvig, G. W. *Coordination Chemistry Reviews* **2012**, *256*, 2503.

(12)	Bottari, G.; Trukhina, O.; Ince, M.; Torres, T. *Coordination Chemistry Reviews* **2012**, *256*, 2453.

(13)	Eisenberg, R.; Nocera, D. G. *Inorganic Chemistry* **2005**, *44*, 6799.

(14)	Purchase, R. L.; de Groot, H. J. M. *Interface Focus* **2015**, *5*.

(15)	Alia, A.; Buda, F.; Groot, H. J. M. d.; Matysik, J. *Annual Review of Biophysics* **2013**, *42*, 675.

(16)	Purchase, R. L.; de Groot, H. J. M. *Interface Focus* **2015**, *5*, 20150014.

(17)	Rombouts, J. A.; Ravensbergen, J.; Frese, R. N.; Kennis, J. T. M.; Ehlers, A. W.; Slootweg, J. C.; Ruijter, E.; Lammertsma, K.; Orru, R. V. A. *Chemistry – A European Journal* **2014**, *20*, 10285.

(18)	Lin, C.-C.; Velusamy, M.; Chou, H.-H.; Lin, J. T.; Chou, P.-T. *Tetrahedron* **2010**, *66*, 8629.

(19)	Grunder, S.; Muñoz Torres, D.; Marquardt, C.; Błaszczyk, A.; Krupke, R.; Mayor, M. *European Journal of Organic Chemistry* **2011**, *2011*, 478.

(20)	Hendsbee, A. D.; McAfee, S. M.; Sun, J.-P.; McCormick, T. M.; Hill, I. G.; Welch, G. C. *Journal of Materials Chemistry C* **2015**, *3*, 8904.

(21)	Shao, H.; Parquette, J. R. *Chemical Communications* **2010**, *46*, 4285.

(22)	Whiteoak, C. J.; Salassa, G.; Kleij, A. W. *Chemical Society Reviews* **2012**, *41*, 622.

(23)	Clarke, R. M.; Storr, T. *Dalton Transactions* **2014**, *43*, 9380.

(24)	Wu, S.; Zhong, F.; Zhao, J.; Guo, S.; Yang, W.; Fyles, T. *The Journal of Physical Chemistry A* **2015**, *119*, 4787.

(25)	Bhosale, S. V.; Jani, C. H.; Langford, S. J. *Chemical Society Reviews* **2008**, *37*, 331.

(26)	Paulo, P. M. R.; Costa, S. M. B. *Journal of Photochemistry and Photobiology A: Chemistry* **2012**, *234*, 66.

(27)   Aratani, N.; Kim, D.; Osuka, A. *Accounts of Chemical Research* **2009**, *42*, 1922.

(28)   Beletskaya, I.; Tyurin, V. S.; Tsivadze, A. Y.; Guilard, R.; Stern, C. *Chemical Reviews* **2009**, *109*, 1659.

(29)   Han, D.; Du, J.; Kobayashi, T.; Miyatake, T.; Tamiaki, H.; Li, Y.; Leng, Y. *The Journal of Physical Chemistry B* **2015**, *119*, 12265.

(30)   Kim, H.; Li, H.; Maresca, J. A.; Bryant, D. A.; Savikhin, S. *Biophysical Journal* **2007**, *93*, 192.

(31)   Fujita, T.; Huh, J.; Saikin, S. K.; Brookes, J. C.; Aspuru-Guzik, A. *Photosynthesis Research* **2014**, *120*, 273.

(32)   Pšenčík, J.; Collins, A. M.; Liljeroos, L.; Torkkeli, M.; Laurinmäki, P.; Ansink, H. M.; Ikonen, T. P.; Serimaa, R. E.; Blankenship, R. E.; Tuma, R.; Butcher, S. J. *Journal of Bacteriology* **2009**, *191*, 6701.

(33)   Pšenčík, J.; Arellano, J. B.; Ikonen, T. P.; Borrego, C. M.; Laurinmäki, P. A.; Butcher, S. J.; Serimaa, R. E.; Tuma, R. *Biophysical Journal* **2006**, *91*, 1433.

(34)   Chakrabarty, R.; Mukherjee, P. S.; Stang, P. J. *Chemical reviews* **2011**, *111*, 6810.

(35)   Ganapathy, S.; Oostergetel, G. T.; Wawrzyniak, P. K.; Reus, M.; Gomez Maqueo Chew, A.; Buda, F.; Boekema, E. J.; Bryant, D. A.; Holzwarth, A. R.; de Groot, H. J. M. *Proceedings of the National Academy of Sciences* **2009**, *106*, 8525.

(36)   Baias, M.; Dumez, J.-N.; Svensson, P. H.; Schantz, S.; Day, G. M.; Emsley, L. *Journal of the American Chemical Society* **2013**, *135*, 17501.

(37)   Blümich, B.; Hagemeyer, A.; Schaefer, D.; Schmidt-Rohr, K.; Spiess, H. W. *Advanced Materials* **1990**, *2*, 72.

(38)   Kaźmierski, S.; Pawlak, T.; Jeziorna, A.; Potrzebowski, M. J. *Polymers for Advanced Technologies* **2016**, n/a.

(39)   van Rossum, B. J.; de Groot, C. P.; Ladizhansky, V.; Vega, S.; de Groot, H. J. M. *Journal of the American Chemical Society* **2000**, *122*, 3465.

(40)   Ladizhansky, V.; Vega, S. *Journal of the American Chemical Society* **2000**, *122*, 3465.

(41)   Bak, M.; Rasmussen, J. T.; Nielsen, N. C. *Journal of Magnetic Resonance* **2000**, *147*, 296.

(42)   Jin, S.; Ding, X.; Feng, X.; Supur, M.; Furukawa, K.; Takahashi, S.; Addicoat, M.; El-Khouly, M. E.; Nakamura, T.; Irle, S.; Fukuzumi, S.; Nagai, A.; Jiang, D. *Angewandte Chemie International Edition* **2013**, *52*, 2017.

(43)   Würthner, F.; Kaiser, T. E.; Saha-Möller, C. R. *Angewandte Chemie International Edition* **2011**, *50*, 3376.

(44)   Prokhorov, V. V.; Perelygina, O. M.; Pozin, S. I.; Mal'tsev, E. I.; Vannikov, A. V. *The Journal of Physical Chemistry B* **2015**, *119*, 15046.

(45)   Wang, Y. J.; Li, Z.; Tong, J.; Shen, X. Y.; Qin, A.; Sun, J. Z.; Tang, B. Z. *Journal of Materials Chemistry C* **2015**, *3*, 3559.

(46)   Barlow, S. M.; Raval, R. *Surface Science Reports* **2003**, *50*, 201.

(47)   Sakai, N.; Mareda, J.; Vauthey, E.; Matile, S. *Chemical Communications* **2010**, *46*, 4225.

(48)   Etheridge, F. S.; Fernando, R.; Golen, J. A.; Rheingold, A. L.; Sauve, G. *RSC Advances* **2015**, *5*, 46534.

(49)   Banerji, N.; Bhosale, S. V.; Petkova, I.; Langford, S. J.; Vauthey, E. *Physical Chemistry Chemical Physics* **2011**, *13*, 1019.

(50)   Yin, Y. W. *Journal of the American Chemical Society* **2004**, *126*, 14996.

(51)   Kohn, S. C. *Terra Nova* **1995**, *7*, 554.

(52)   Frisch, M. J.; Trucks, G. W.; Schlegel, H. B.; Scuseria, G. E.; Robb, M. A.; Cheeseman, J. R.; Scalmani, G.; Barone, V.; Mennucci, B.; Petersson, G. A.; Nakatsuji, H.; Caricato, M.; Li, X.; Hratchian, H. P.; Izmaylov, A. F.; Bloino, J.; Zheng, G.; Sonnenberg, J. L.; Hada, M.; Ehara, M.; Toyota, K.; Fukuda, R.; Hasegawa, J.; Ishida, M.; Nakajima, T.; Honda, Y.; Kitao, O.; Nakai, H.; Vreven, T.; Montgomery Jr., J. A.; Peralta, J. E.; Ogliaro, F.; Bearpark, M. J.; Heyd, J.; Brothers, E. N.; Kudin, K. N.; Staroverov, V. N.; Kobayashi, R.; Normand, J.; Raghavachari, K.; Rendell, A. P.; Burant, J. C.; Iyengar, S. S.; Tomasi, J.; Cossi, M.; Rega, N.; Millam, N. J.; Klene, M.; Knox, J. E.; Cross, J. B.; Bakken, V.; Adamo, C.; Jaramillo, J.; Gomperts, R.; Stratmann, R. E.; Yazyev, O.; Austin, A. J.; Cammi, R.; Pomelli, C.; Ochterski, J. W.; Martin, R. L.; Morokuma, K.; Zakrzewski, V. G.; Voth, G. A.; Salvador, P.; Dannenberg, J. J.; Dapprich, S.; Daniels, A. D.; Farkas, Ö.; Foresman, J. B.; Ortiz, J. V.; Cioslowski, J.; Fox, D. J.; Gaussian, Inc.: Wallingford, CT, USA, 2009.
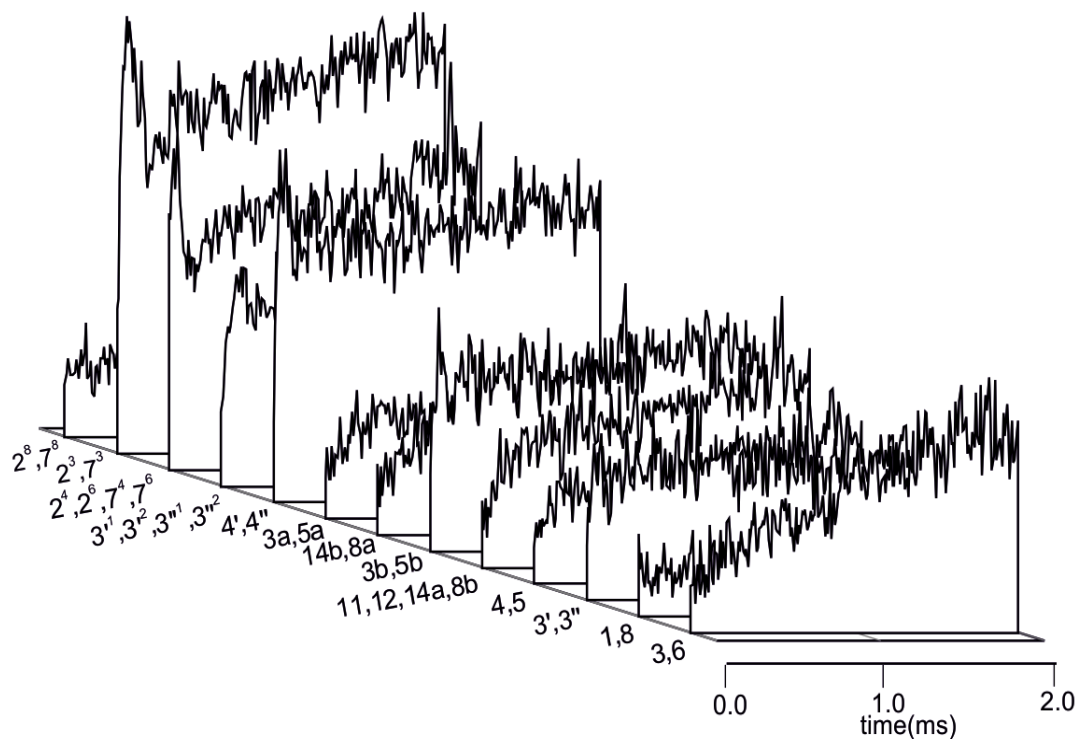
Figure S2.1 1D ^{13}C CP-MAS spectrum of DATZnS(3′-NMe). The data were collected in 3092 scans with a MAS rotation frequency of 11 kHz. Spinning side bands were identified by collecting the spectrum at different spinning frequency.

Figure S2.2 Structure of DATZnSTP homologue used for the solution state NMR assignment. Chemical shifts of corresponding carbon atoms are explained in Table 2.2.

Figure S2.3 LGCP build curve plotted for selected [13] C nuclei.
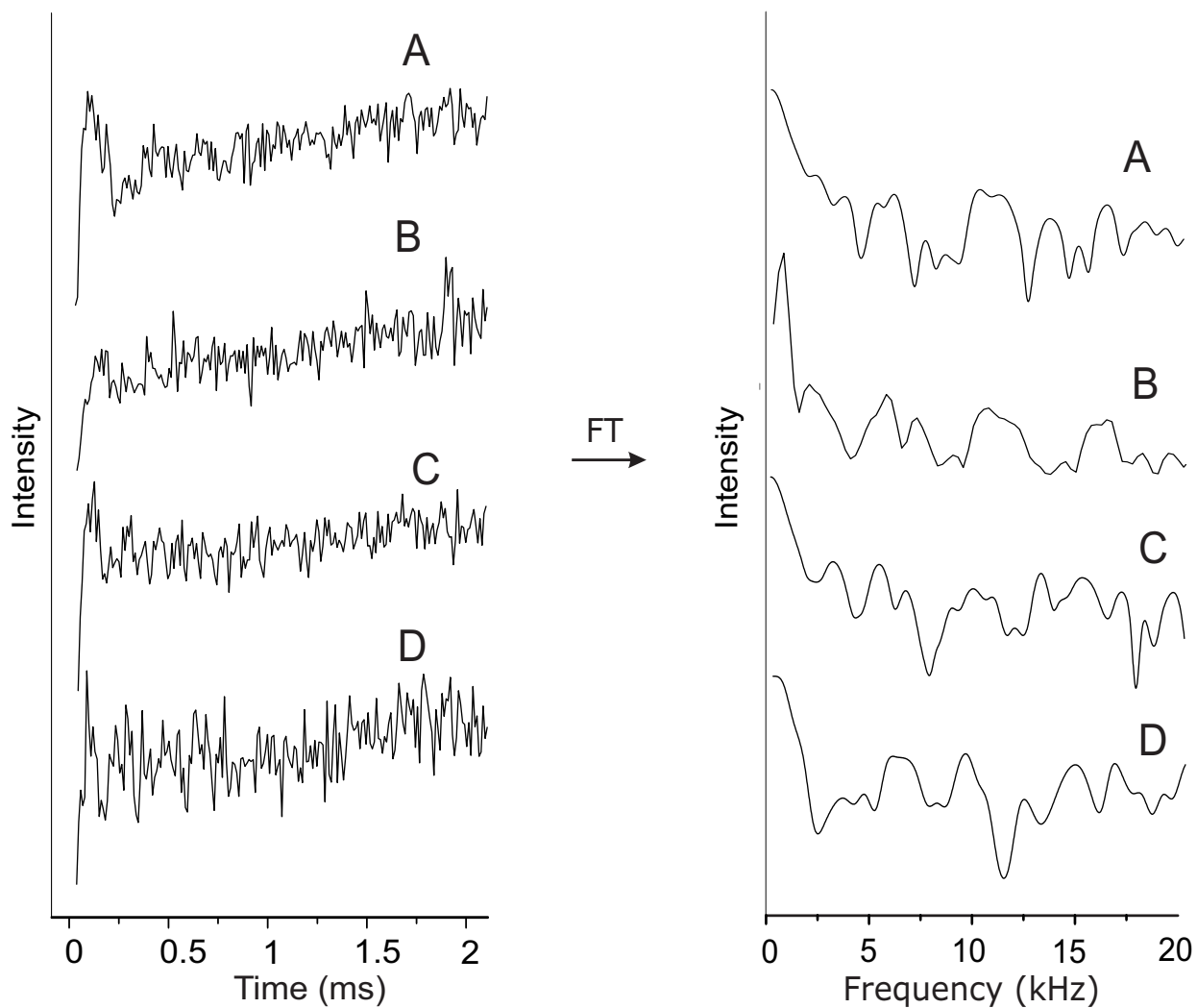
Figure S2.4 LGCP build up curve and its Fourier transform of (A) 2^3, 7^3 (B) $3'^1$, $3'^2$,$3''^1$, $3''^2$ (C) $4'$, $4''$ and (D) $5'$, $5''$ ^{13}C nuclei. Initial sharp rise in the LGCP build up curve is due to the directly attached proton on the carbon atom. This validated the assignment of these chemical shifts to proton attached carbon atoms.
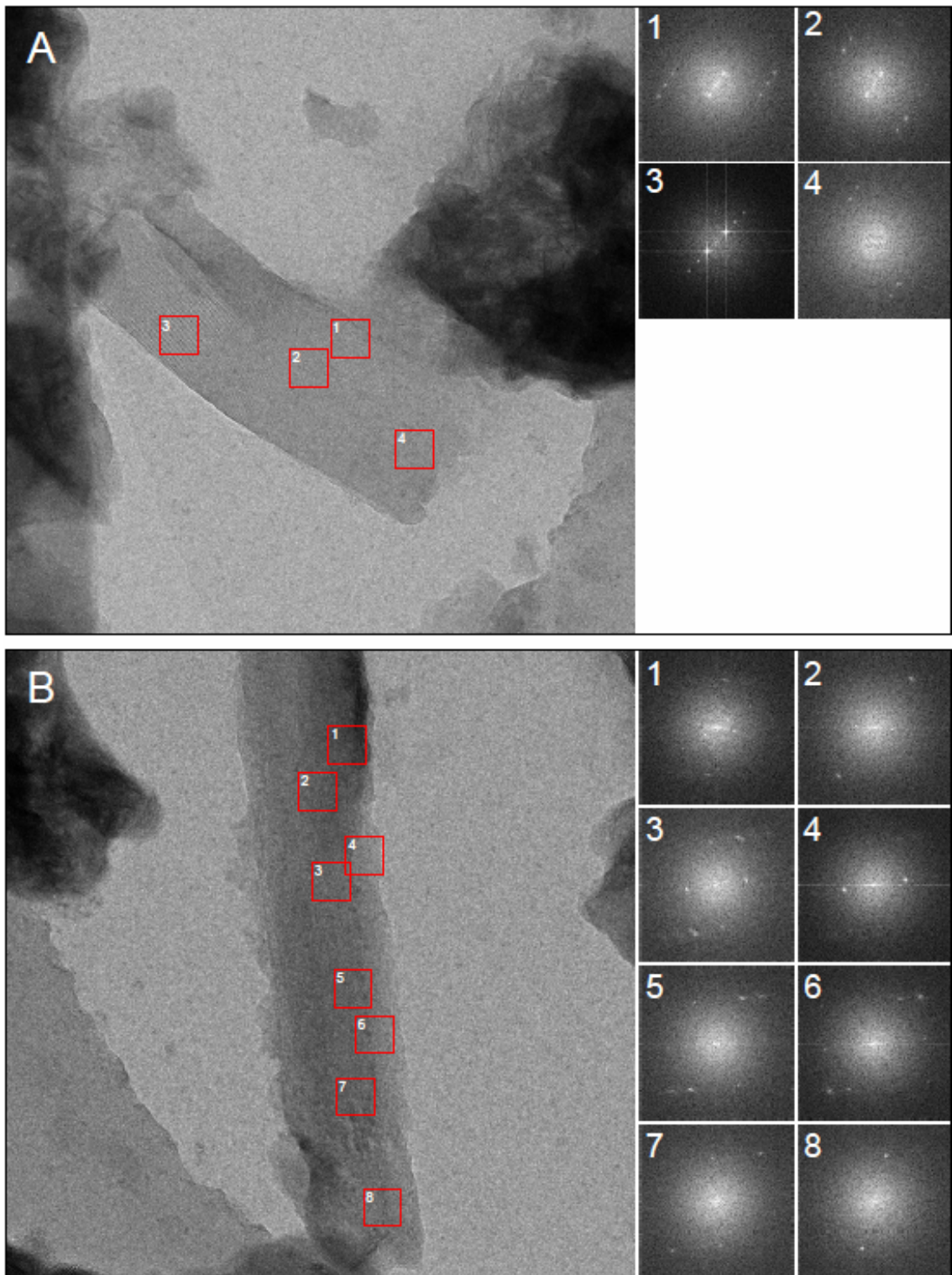
Figure S2.5 TEM image in two different orientation (A) and (B) and its Fourier transforms of selected regions showing multiple reflection spots, which are of higher order diffraction.

S2.6 Input file used for SIMPSON simulation

```
spinsys {
  channels 1H 13C
        nuclei 1H  13C
        dipole 1 2 -1118.9  0 0 0
}
par {
  method       direct
        start_operator  Inz-I2z
        detect_operator I2p
        crystal_file    rep66
        spin_rate       11000
        np          512
        gamma_angles    8
        sw          1000000
  variable   tsw 1.0e6/sw
}
proc pulseq {  } {
  global par
  pulseid 5 50000 y 0 0
  acq_block {
    pulse $par(tsw) 50000 x 40000 x
        }
}
proc pulseq_lg {} {
        global par
        set effH 50000
  set taup [expr 54.74/90.0*5]
  pulseid $taup 50000 y 0 0
  set offset [expr $effH/sqrt(3.0)]
        set rfH [expr $effH/sqrt(1.5)]
  offset $offset 0
  acq_block {
    pulse $par(tsw) $rfH x 40000 x
        }
}
proc main {} {
  global par
        set f [fsimpson]
        fsave $f $par(name).fid -binary
  set par(pulse_sequence) pulseq_lg
  set f [fsimpson]
        fsave $f $par(name)_lg.fid -xreim
}
```
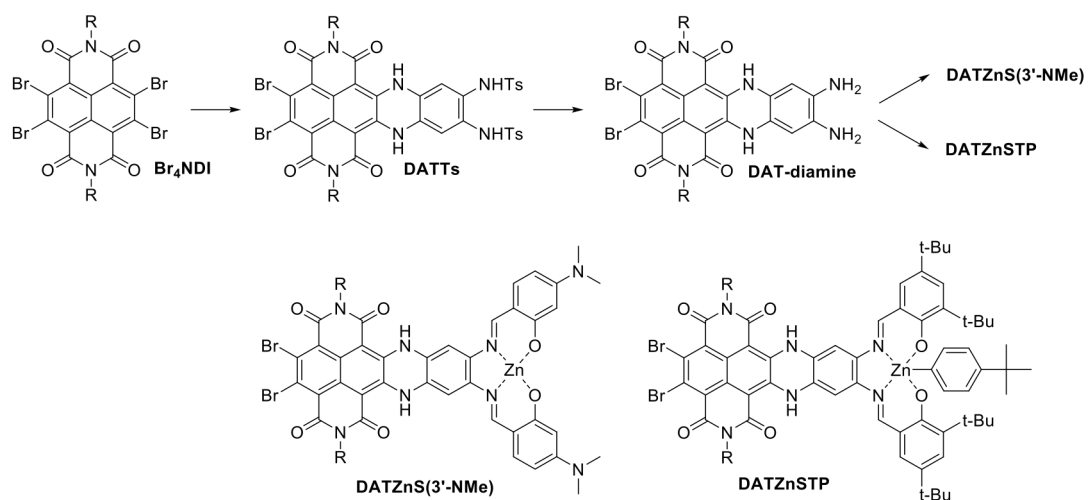
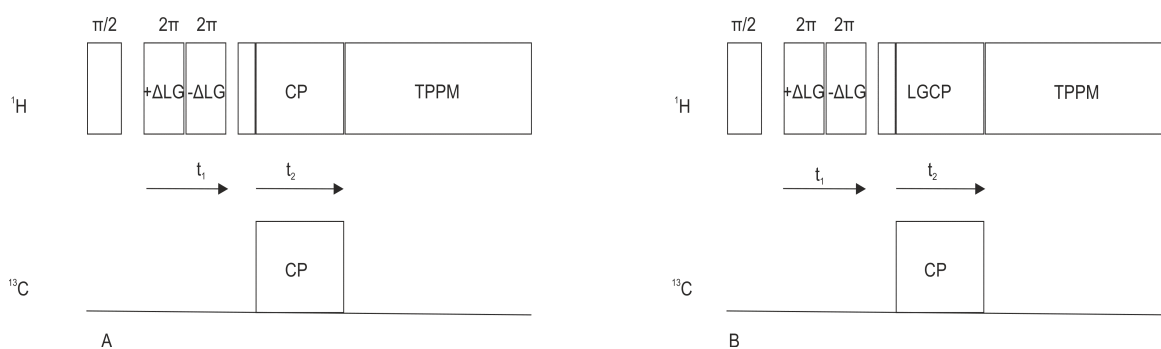Figure S2.7 Overview of synthetic strategy towards DATZnS-dyads. R = ^{n}octyl.

Figure S2.8 Pulse sequence used for (A) ^{1}H-^{13}C HETCOR experiment (B) for LGCP build up curve experiment.

De novo structure determination of an artificial bichromophoric light-harvesting antenna system by integrating MAS NMR and Electron Nano Crystallography

Abstract

Naphthalene monoimide (D1) functionalized 1,7-perylene-3,4,9,10-tetracarboxylic monoimide dibutylester (A2) is a light harvesting antenna molecule that forms antiparallel centrosymmetric dimers with disordered bay substituents projecting out in an overall 3D para crystalline framework. In the antenna molecule (D1A2), there is a substantial overlap of the D1 emission with the A2 absorption spectrum, resulting in an efficient transfer of energy through Förster Resonance Energy Transfer (FRET) from the donor D1 to the acceptor A2. The molecular geometry and the packing of the bichromophoric light-harvesting antenna, D1A2 have been determined by an interdisciplinary approach, which involves the computational integration of magic angle spinning (MAS) NMR and electron nano crystallography (ENC) followed by modelling. MAS NMR chemical shifts were used to generate a truncated 1,7-perylene-3,4,9,10-tetracarboxylic monoimide dibutylester motif as the building block for the molecular replacement. This motif is optimized with Density functional theory (DFT) in a C_2 molecular symmetry and used in a biased molecular replacement approach to generate a partial 3D electron density map. Grafting of the bay substituents to the centrosymmetric dimers is guided by the inversion symmetry in the unit cell and the distance constraints obtained from [1]H-^{13}C HETCOR at longer mixing time. The structure was then optimized with force field modeling with charges obtained from DMol[3]. This is the first example of structure determination by integrating MAS NMR with ENC for a molecule with a molecular weight of 1460 g/mol using supramolecular crystallography.

3.1 Introduction

One out of very few routes to a sustainable and uninterrupted supply of energy on a meaningful scale is to mimic the processes of natural photosynthesis, which has been remarkably conserved across taxonomies during three billion years of evolution.[1,2] Its successful operation is based on a very limited set of functionally independent subsystems dedicated to light harvesting,[3,4] charge separation and catalysis.[5] The molecular building blocks in photosynthetic complexes are interlinked by weak couplings that are well-balanced for optimal performance. Key structure-function relationships allow for a robust design with sufficient complexity for efficient solar energy conversion close to the thermodynamic limit while avoiding redundancy.

In photosynthetic antennae, dye molecules are embedded in responsive matrix architectures for efficient exciton transport. The chemical programming of artificial molecular scaffolds that replicate the commonalities of the photosynthetic responsive matrices in a controlled way is a challenge. An essential element of such a response matrix is chirality, since this allows the matrix to undergo conformational twisting upon excitation for a coherent conversion with near unity yield.[6-11] The functional entities involved in photosynthesis are known, and chemical engineering[12] involves finding similar counterparts in robust organic molecules. From the available building blocks with high molar absorptivity in the visible region, perylene and naphthalene monoimide chromophores stand out because of their photochemical robustness, tunability of opto electronic properties and versatility of applications.[13-15] In addition to archetypal perylene bisimides, a new class of peri-substituted perylene tetracarboxylic acid derivatives has been developed with potentiality for application in artificial photosynthesis.[13,16] Here studies about the packing of 4-(isopentylthio)naphthalene monoimide D1, as energy-donor and 1,7-perylene-3,4,9,10-tetracarboxylic monoimide dibutylester (A2)[17] as an acceptor on the way to an artificial responsive matrix is done. Similar to antennae in the photosynthetic machinery, D1 can harvest light and transfer the energy to the perylene through Förster Resonance Energy Transfer (FRET),[18,19] since both chromophores have complementary absorption with good overlap
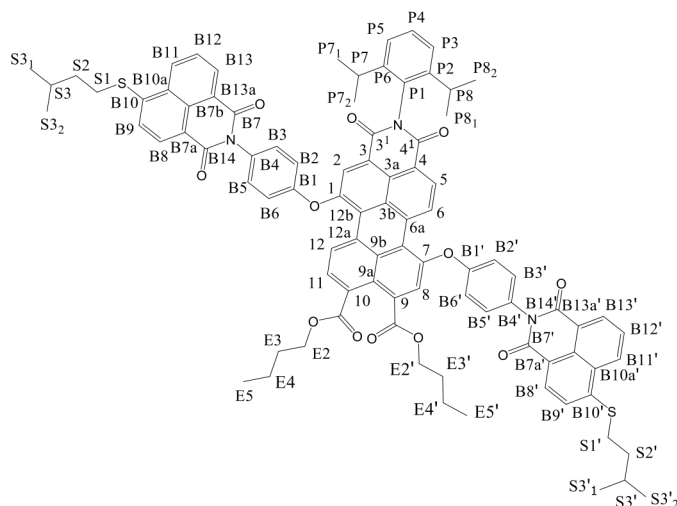
Figure 3.1: Chemical structure of D1A2, which is an asymmetric perylene with a phenoxy derivative of napthalenemonoimide as bay substituents. Here the perylene core is numbered based on the conventional numbering scheme while the bay substituents are numbered starting with B1 and B1′. Similarly alkyl tail attached to sulphur with S1 and S1′, imide substituents as P1 and alkyl group on ester as E1 and E1′.

between the emission of D1 and the absorption of A2. Generally, perylene derivatives tend to undergo facile charge separation when coupled to moderately electron rich chromophores like naphthalene monoimide. However, electron transfer has not been observed in D1A2, which may be ascribed to rigid and non-conjugated phenoxy spacers between the constituent chromophores.[16]

For the rational design and optimization of artificial responsive matrices, it is essential to understand the mechanisms of self-assembly. This is because self-assembly determines the conformational entropy and how the misfits in the packing steer the morphology and dynamic structure of the responsive matrix towards the desired direction. This requires resolving the packing order against a background of pronounced heterogeneity that makes the structure elucidation of these systems inaccessible to X-ray and other diffraction methods. The supramolecular packing of heterogeneous self-assembly is resolved in chapter 2 by computational integration of MAS NMR and low-resolution electron microscopy.[20,21] Based on the characteristic pattern of the nonzero diffraction intensities extracted from Fourier transformed transmission electron microscopy (TEM) images, long range information about the supramolecular framework was

Table 3.1 ^{13}C solid state (σ_s^C) and solution state (σ_{liq}^C) chemical shifts of D1A2.

Position	σ_s^{C*}, ppm	σ_{liq}^C, ppm	$\Delta\sigma = \sigma_s^C - \sigma_{liq}^C$
8	127.39	126.66	0.73
9	131.36	132.05	-0.69
9a	120.97	118.87	2.1
9b	121.74	121.62	0.12
6b	128.53	128.66	-0.13
7	152.71	152.49	0.22
10	132.97	133.99	-1.02
11	132.41	131.27	1.14
12	128.27	128.15	0.12
12a	129.29	129.41	-0.12
12b	126.31	126.46	-0.15
3b	121.17	118.84	2.33
6a	126.89	126.77	0.12
E′	162.43	163.49	-1.06
E1	162.43	164.17	-1.74
3a	122.1	123.29	-1.19
4	130.93	131.32	-0.39
5	129.35	129.73	-0.38
6	128.27	128.58	-0.31
1	152.71	152.31	0.4
2	122.54	125.34	-2.8
4	132.97	133.21	-0.24
3^1	167.02	167.38	-0.36
4^1	167.02	168.21	-1.19
E2	65.59	65.55	0.04
E3	29.42	30.48	-1.06
E4	18.76	19.21	-0.45
E5	14.85	13.8	1.05
E2′	65.59	65.88	-0.29
E3′	29.4	30.64	-1.24
E′	18.76	19.29	-0.53
E5′	14.85	13.8	1.05
P1	146.88	146.3	0.58

P2, P6	126.31	125.6	0.71
P3, P5	132.88	131.27	1.61
P4	120.55	122.55	-2.00
P8, P7	28.92	29.13	-0.21
P8$_1$, P8$_2$	23.79	22.42	1.37
P7$_1$, P7$_2$	23.79	24.09	0.3
B1, B1$'$	152.71	155.6	-2.89
B2, B6, B2$'$, B$'$	129.35	130.64	-1.29
B3, B5, B3$'$, B$'$	119.95	118.65	1.3
B4, B4$'$	146.88	146.37	0.51
B7, B7$'$	162.43	162.82	-0.39
B7a, B7a$'$	130.09	131.06	-0.97
B7b, B7$'$	122.83	123.13	-0.3
B13a, B13a$'$	129.29	129.64	-0.35
B14, B14$'$	162.43	164.2	-1.77
B8, B8$'$	129.35	129.51	-0.16
B9, B9$'$	122.54	124.01	-1.47
B10, B10$'$	143.69	145.74	-2.05
B10a, B10a$'$	121.56	122.79	-1.23
B11, B11$'$	129.87	130.53	-0.66
B12, B12$'$	127.39	126.66	0.73
B13, B13$'$	132.41	132	0.41
S1, S1$'$	36.6	37.11	-0.51
S2, S2$'$	30.97	30.32	0.65
S3, S3$'$	22.95	27.69	-4.74
S3$_1$, S3$_2$, S3$'_1$, S3$'_2$	24.94	22.17	2.77

*Analogous assignment based on solution state NMR

obtained. The chemical shifts and limited set of intermolecular distance constraints allowed to fill the framework with molecular building blocks, to resolve a model that captures the essential properties of the heterogeneous structure.

This chapter explains a next step in this methodology by integrating MAS NMR with ENC to determine directly the nonzero scattering in reciprocal space, representing ~60% of the maximum scattering intensity that can be expected for a

well ordered rigid D1A2 system. This shows that part of the system diffracts, while a significant part is disordered or dynamic. A biased molecular replacement approach is used to generate a partial electron density map, with the input from reflection spots obtained from ENC. This allows determining the cell parameters and leads to a *P*-1 space group as most likely solution. A rigid A2 motif was modeled in a C_2 molecular symmetry, guided by the information from NMR chemical shifts. This was used for molecular replacement and allowed to position a centrosymmetric A2 in a packing cell. The electron density is consistent with dimeric A2. Limited sets of NMR distance restraints were used to refine the packing and position the naphthalene monoimide bay substituents. The structure was further optimized with molecular modeling to resolve any packing conflicts. In this way a pseudocrystalline structure scaffolded by a network of centrosymmetric perylene dimers with induced P and M core chirality in racemic packing is converged. The network is supported by the bridges formed out of the phenoxy and naphthalene monoimide bay substituents that extend towards the next row of perylene dimers, effectively providing non-covalent crosslinks involving the isopentylthio functionalities. Such a scaffold would provide a matrix for tuning the static and dynamic properties of the naphthalene monoimide.

3.2 Results

In the D1A2 light harvesting donor-acceptor molecule, the blue light absorbing naphthalene monoimide energy donor, D1, is covalently attached to a green light absorbing energy acceptor perylene derivative, A2, at the 1,7-bay-positions (Figure 3.1). While the perylene core does not possess any stereogenic center, core chirality can be induced by steric interactions.[22] Here sterically demanding aromatic phenoxy spacers that are non-conjugating due to nonplanar conformations at both the energy donor and the acceptor motifs is used. Bridging the donor and acceptor chromophores without direct electronic communication suppresses electron transfer that would compromise the antenna function.[23,24] It has been shown previously that perylene derivatives containing substituents in the bay position like D1A2 indeed exist as atropo enantiomers represented as P and M and can form centrosymmetric dimers.[22,25-28]

3.2.1 Chemical shift assignments

To determine the packing of the D1A2 in the condensed state, analysis of the CP/MAS data shown in Figure S3.1 is done. The data were collected with a mixing time of 1 ms and a good signal to noise from cross polarization suggests uniform enhancement over both the donor and the acceptor. A good dispersion over 170 ppm is observed for the ^{13}C response. There is no evidence for doubling due to different fractions. The strongest signals are detected upfield between 10 and 70 ppm. The most downfield responses in this region are from the alkyl ^{13}C connected to the ester and thioether bridges in the A2 and D1, respectively. Between 115 and 135 ppm the aromatic signals of the A1 and D1 are found, while downfield the characteristic regions for the phenoxy ($\sim$152 ppm), the aromatic thio response $\sim$145 ppm and the keto ^{13}C $\sim$165 ppm all comprise relatively strong signals. Both the donor and the acceptor motif have comparable NMR responses from functionalities and extended π conjugation, while the thio and phenoxy groups are better resolved. To arrive at an assignment from the MAS NMR is therefore not straight forward. However, the D1A2 light harvesting molecule is built from well-secondary and quaternary carbon atoms. The solid state MAS NMR chemical shifts have been tentatively assigned by comparing to the solution NMR response (Table 3.1 and 2). With this approach, a difference $|\Delta\sigma| \leq 2$ ppm in ^{13}C NMR chemical shifts between solution σ_{liq}^{C} and solid σ_{s}^{C} state is obtained (Table 3.1).

Some moderate differences in linewidth between the responses from the donor and the acceptor point to partial disorder for the donor substituents. In particular, the width of the B4, B4′ signals from the phenoxy spacer in the middle of the bay substituent are $\sim$2 ppm, while the responses of the keto C3^1 and the C4^1 towards the head of the perylene core are narrow ($\sim$1 ppm), and also the E2, E2′ signal from the acceptor is $\sim$1 ppm wide. This suggests that the bay substituents may be heterogeneous relative to the core. For the alkyl chains attached to the naphthalene monoimide substituents the assignment of the resonances to the different atoms is less clear. For the B10, B10′ a linewidth of $\sim$1 ppm is observed, while the S1, S1′ signals are relatively broad, $\sim$2 ppm. With solid state HETCOR spectra collected with a short mixing time of 256 μs, specific ^{13}C-^1H pairs can be

Table 3.2 ^{1}H solid state (σ_s^H) and solution state (σ_{liq}^H) chemical shifts of D1A2.

Position	σ_s^H, ppm	σ_{liq}^H, ppm	$\Delta\sigma = \sigma_s^H - \sigma_{liq}^H$
8	7.84	8.54	-0.7
11	7.6	8.66	-1.06
12	7.05	9.4	-2.35
5	7.33	8.1	-0.77
6	7.05	9.35	-2.3
2	7.59	7.94	-0.35
E2	3.44	4.31	-0.87
E3	1.31	1.79	-0.48
E4	1.01	1.45	-0.44
E5	0.94	0.97	-0.03
E2′	3.44	4.36	-0.92
E3′	1.31	1.79	-0.48
E4′	1.01	1.51	-0.5
E5′	0.94	1.00	-0.06
P3	7.69	8.49	-0.8
P4	8.01	7.55	0.46
P5	7.69	8.49	-0.8
P8	2.41	1.82	0.59
P7	2.41	1.82	0.59
P8$_1$, P8$_2$	0.8	0.98	-0.18
P7$_1$, P7$_2$	0.8	0.98	-0.18
B2, B6, B2′, B6′	7.33	7.32	0.01
B3, B5, B3′, B5′	7.93	7.24	0.69
B8, B8′	7.33	7.44	-0.11
B9, B9′	7.59	7.31	0.28
B11, B11′	7.67	8.6	-0.93
B12, B12′	7.85	7.75	0.1
B13, B13′	7.6	8.63	-1.03
S1, S1′	1.17	1.69	-0.52
S2, S2′	1.09	3.16	-2.07
S3, S3′	1.05	1.82	-0.77
S3$_1$, S3$_2$, S3′$_1$, S3′$_2$	0.88	0.98	-0.1
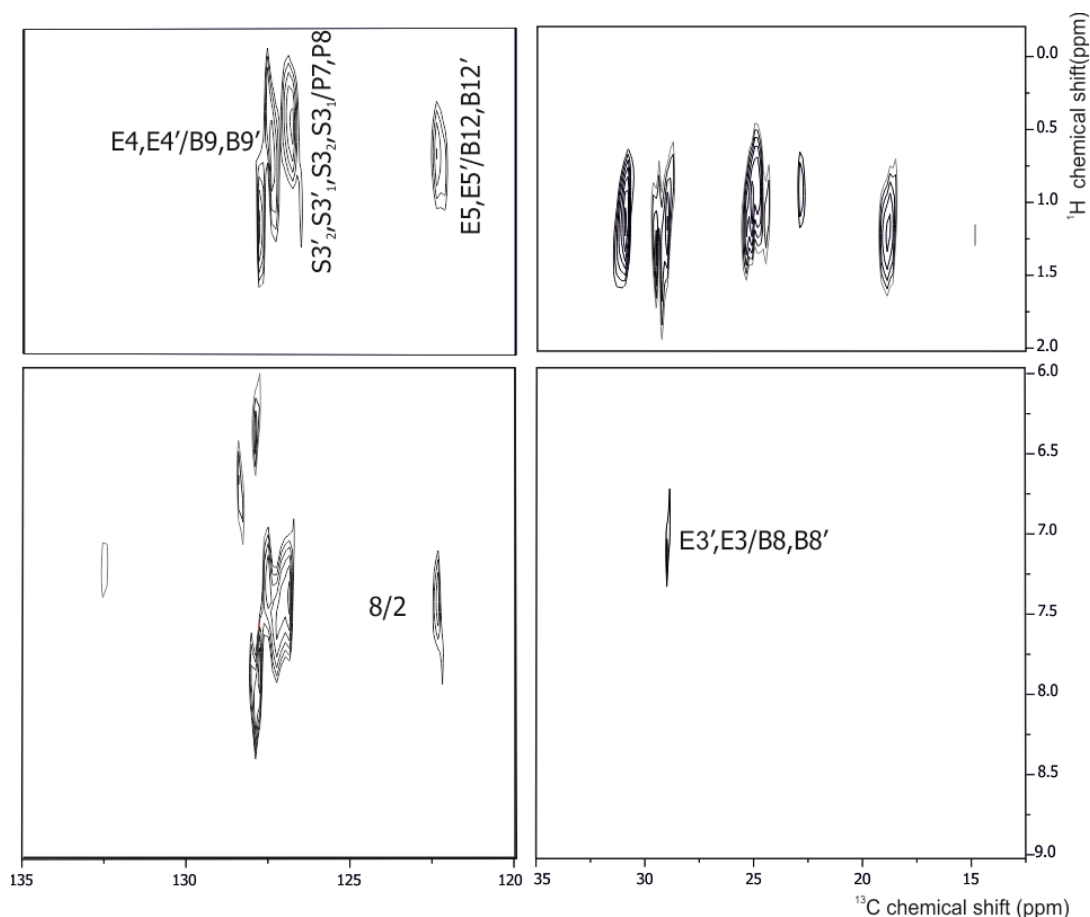
Figure 3.2 ^{13}C-^{1}H 2D HETCOR spectra of D1A2 at natural abundance collected at room temperature with 1 ms mixing time. The MAS frequency and the number of scans are 13 kHz and 1 k respectively. Intermolecular correlations, for resolving the packing, are indicated. The HETCOR spectrum is divided into four panels. The left bottom part indicates the interaction of the aromatic region with aromatic protons, while the left top indicates the interaction of aliphatic protons with aromatic carbons and the right bottom indicates the interaction between aromatic protons and aliphatic carbons that are unique to find the position of tails.

 resolved (Figure S3.8). Diverse functionalities present in the molecule help to have a reasonable dispersion of chemical shift for assigning. Interestingly, even though the two naphthalene monoimides are attached to different bay positions they exhibit very similar chemical shifts, indicating identical environments for the two donors pointing towards pseudosymmetry in the packing. Similarly, the dispersion of responses from the methyl groups of the imide substituent 2,6-diisopropyl phenyl and the isopentyl tail is only moderate, despite core chirality and asymmetric bay substituents. Due to the electronegative sulphur, the shifts of the

adjacent CH_2 groups are around 36 ppm. Similarly, the CH_2 groups E2 and E2′, attached to carboxyl functionalities, have a distinguishable chemical shift around 65 ppm. Terminal alkyl groups E5 and E5′ have a characteristic upfield chemical shift of 14 ppm and this signal is well resolved. The E4 and E4′ resonate with a chemical shift of 18.76 ppm. A close analogy between solution and solid-state NMR chemical shifts validates our inference that the bricks or building blocks are not very sensitive to the differences between the dissolved and condensed states. Pronounced deviation of ~2.35 ppm in the ^1H NMR chemical shift in solution state and solid state indicate conformational stress from the phenoxy spacers (Table 3.2) Specific internuclear distance constraints between carbon nuclei and proton nuclei were obtained from a HETCOR dataset collected with a long mixing time of 1 ms, which can be used to map the packing. In Figure 3.2 four panels are shown that comprise the observed correlation signals and intermolecular correlations are labeled following the numbering scheme in Figure 3.1. Since B12′C and B12C are located at the far end of the bay substituent and the E5H and E5′H are at the terminal methyl of the aliphatic chains attached to the perylene core, intramolecular relayed transfer along the carbon backbone is unlikely. Also, long range transfer across the same molecule would require a pronounced conformational change with respect to the relaxed, extended state, which would compromise the general similarity between solution and solid state shifts. Thus, we attribute this cross peak to intermolecular transfer. It is known from chapter 2 that clusters of protons are capable of efficient relayed polarization transfer over 3-5 Å. Similarly long-range correlation peaks can be observed between E4H, E4′H and B9C, B9′C respectively. This could only be intermolecular since naphthalene monoimide is far away from alkyl chain attached to perylene core to have an intramolecular transfer. Interestingly, a long-range correlation signal can be observed between aromatic protons and aliphatic carbons, represented as E3′H, E3H and B8′C, B8C in Figure 3.2, which is also an intermolecular correlation. A correlation peak is observed between 2H and 8C in the aromatic ring. This long-range transfer should be intermolecular since 8 Å distance between 8H and 2C is too large for an intramolecular transfer event. This intermolecular correlation points towards centrosymmetric dimers of perylene with opposite core chirality. A

Table 3.3 Data processing statistics. The electron diffraction data of D1A2 was successfully indexed using the XDS software package.

Space group	*P*-1
Cell dimensions	
a, b, c (Å)	14.53, 15.55, 19.53
α, β, γ (°)	96.366, 107.158, 108.898
Resolution (Å)	5.38-1.92 (2.03-1.92)
R_{sym} (%)	13.3 (21.2)
I/σ	3.13 (1.72)
R_{meas} (%)	18.8 (30.0)
$CC_{1/2}$	97.9 (96.2)
Completeness (%)	25.2 (26.1)
Redundancy	1.93 (1.88)

*Highest resolution shell is shown in parenthesis

long range correlation between the 2,6-diisopropyl phenyl P7C and P8C carbons with the proton response associated with the terminal $S3_1$, $S3_2$, $S3_1{}'$ and $S3_2{}'$ methyl groups on the isopentyl thiol tail should be intermolecular.

Electron nano crystallography (ENC) was used to determine the unit cell dimensions of a single flat D1A2 nanocrystal of 400x1000x200 nm^3 (Figure 3.3). The nanocrystal was rotated continuously at room temperature in a highly parallel electron beam from -20.0° to +27.7° with an angular increment of 0.028° per frame (data not shown). [34] Data were collected at low dose conditions of no more than 0.018 $e^-Å^{-2}s^{-1}$, and the total accumulated exposure dose did not exceed 3.3 $e^-/Å^2$. The camera length, the distance between the sample and detector, was calibrated at 524 mm. Prior to data analysis, frames were integrated to an angular increment of 0.112°. The electron diffraction data was successfully indexed by XDS to obtain the unit cell parameters *a* = 1.453 nm, *b* = 1.55 nm, *c* = 1.95 nm, α = 96.36°, β = 107.15°, γ = 108.89° and V =3.89 nm^3.[29]
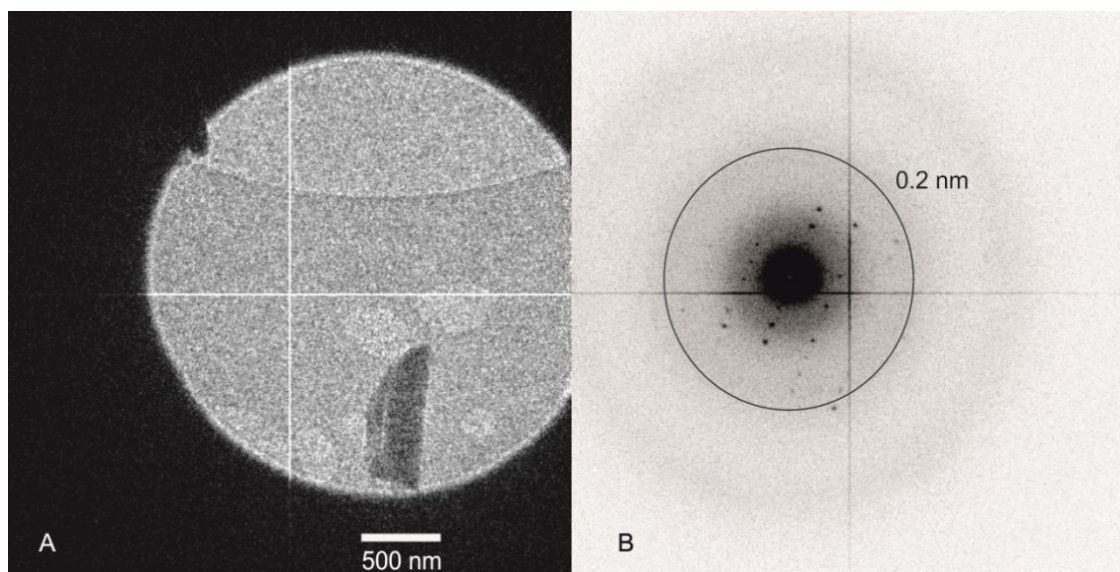
Figure 3.3 ENC recorded from the D1A2 showing an image (A) of the thin rod like shaped nanocrystals with dimensions of 400x1000x200 nm^3 at 5.3 k times magnification and a diffraction pattern (B) with a spots to a resolution up to 2 Å, which is integrated over 1.0 degree of rotation from -10.8 to -9.8°.

While it can be determined from the reflections with high confidence that the packing is triclinic, a distinction between the two possible space groups $P1$ and P-1 is not straightforward. A most likely centrosymmetric P-1 space group was determined from the XDS *hkl* output with POINTLESS, with a probability of 0.577, and a probability of 0.423 for the alternative $P1$, yielding a space group confidence of 0.3 for the best solution P-1 (Table 3.3).[30,31] Since the standard settings of POINTLESS are for proteins, they were changed with the CHIRALITY NONCHIRAL keyword to allow for centrosymmetric space groups. As there is a single space group with the highest score, P-1 was selected for further processing. This is in line with the NMR results, which reveal an intermolecular correlation between 2H and 8C that provides strong evidence for a centrosymmetric packing of antiparallel dimers. Data were processed with AIMLESS to resolve 502 reflections out of 956 observations down to a final resolution of 1.9 Å (Table 3.3).[32] The intensities were truncated and converted to amplitudes with CTRUNCATE.[33] The scattering data are highly anisotropic, indicating that the crystal is poorly ordered along one direction. Data completeness was limited to 25% (Table 3.3).

To generate an electron density map, the intensities were analyzed with the PHASER molecular replacement (MR) package in PHENIX. Single component MR

was performed with a truncated C_2 symmetric rigid perylene core model with methyl ester tails and without the bay substituents. Selection of the trial structure was guided by the NMR results, where very similar chemical shifts between the two halves of the perylene core point to a pseudosymmetric packing of $C2$-type motifs (Table 3.1 and 3.2). The core structure was optimized with the DMol[3] DFT tool in Materials Studio prior to molecular replacement. A wavelength of 0.02508 Å was applied in PHENIX by changing the settings from X-Ray to electron diffraction. Since the purpose of our analysis is to generate structure factors with the help of a model, the packing test was omitted at this stage, and only performed later when the NMR distance constraints were taken into account. This is an essential feature of this approach, where the aim is to resolve the principle elements of the packing, rather than solving a structure at high resolution, which is meaningless in a heterogeneous environment. Here reciprocal space is used to average the details and let the commonality between packing cells emerge. This can imply tolerating colliding molecules at an early stage, and resolving the collisions at a later stage by force field modeling of the heterogeneous structure. Extensive investigation of perylene bisimides has provided converging and convincing evidence that packing induced core chirality can lead to centrosymmetric dimers in a racemic material or J-aggregate formation for the pure enantiomer.[22]

3.3 Discussion

3.3.1 Structure determination of bichromophoric antenna system
Computational integration of MAS NMR and TEM was recently developed to elucidate the supramolecular packing of moderately sized molecules in a pseudosymmetric scaffolding with gross heterogeneity that gives rise to regions in reciprocal space where the structure factor is not systematically zero.[20,21] Use was made of how reflections are grouped into layer lines to determine the arrangement of molecules in the suprastructure, which was complemented by the measurement of NMR chemical shifts and internuclear transfer of polarization to determine the conformation and positioning of the molecules in the packing framework. In chapter 2 images were collected to visualize repeats in the supramolecular packing and Fourier transforms were explored to determine where scattering can occur in
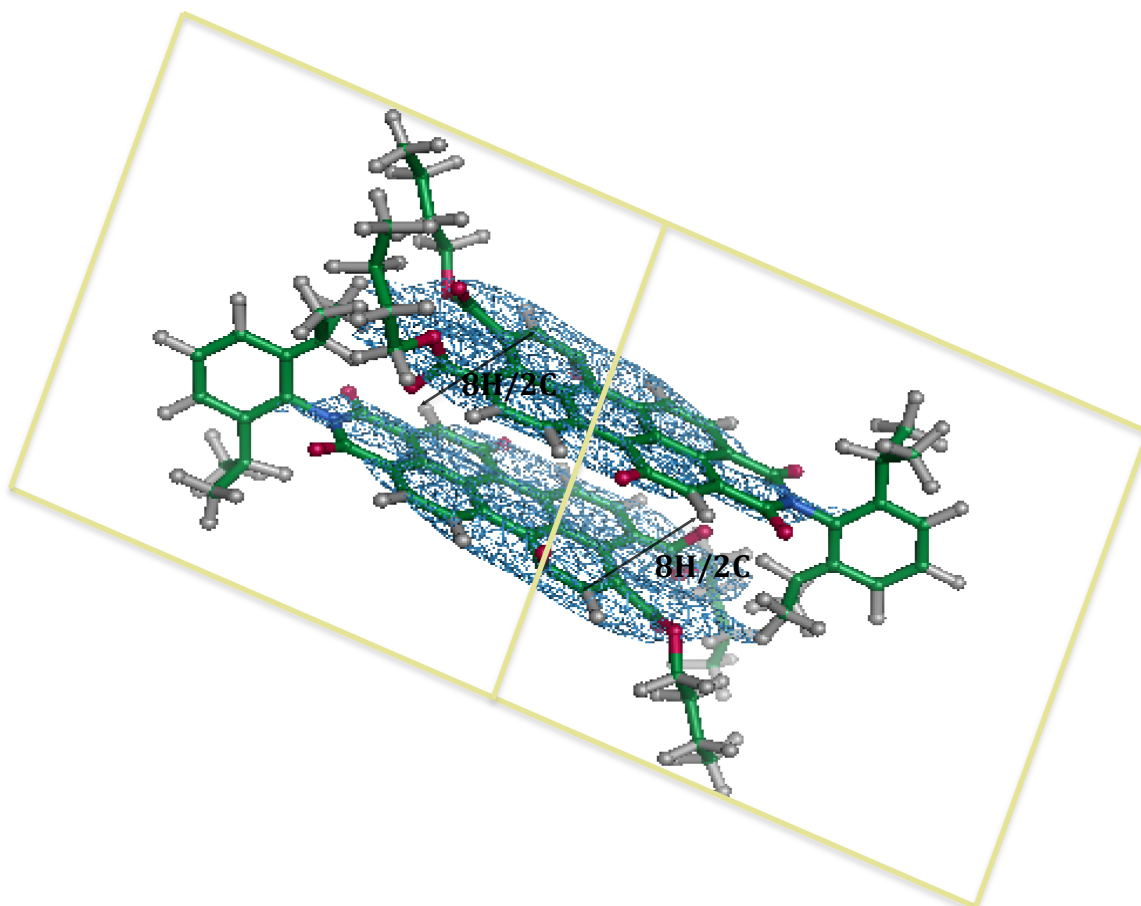
Figure 3.4 Integration of ENC with MAS NMR. Global packing can be derived from the electron density, which reveals dimeric centrosymmetric perylene motifs in the unit cell. This is well in line with the NMR distance constraint between 8H and 2C. The orientation of the dimers in the unit cell is shown in the right panel. Perylene dimers with pseudo C_2 symmetry form the basic building block on which bay substituents were grafted.

reciprocal space. Systematic absences allowed determining the space group that describes the packing. Here the methodology is extended to the next level by performing an ENC experiment to observe directly the scattering intensity in reciprocal space. This allows determining the unit cell parameters and the Laue class of the packing. The coherent scattering intensity is considerably less than expected from the molecular weight (Table 3.3), and I used different building blocks of the supramolecular structure as trial models to determine that mainly the perylene part is diffracting and that phenoxy and naphthylmonoimide fragments may be disordered or mobile and do not give rise to nonzero structure factors in the ENC. The density of perylene type solids is ~1.25 g/cm^3.[34] From consideration of the atomic volumes and space group, it is deduced that there should be two molecules in the unit cell *i.e.* Z=2. A racemic material built from

centrosymmetric dimers in a *P*-1 setting, the most likely space group from ENC, is confirmed by the distance constraints observed between 8H and 2C in the NMR. It is known that clusters of protons are capable of efficient relayed polarization transfer over 3-5 Å to quaternary carbon nuclei. The model bias in the molecular replacement allows to add relevant phase angles to the scattering intensities and generate a low resolution electron density map in the unit cell for positioning of molecules with NMR shift and distance constraints (Figure 3.4). In PHASER analyses with naphthalene monoimide and isopentylthio fragments, the match with the electron density map was rather poor, compared to the perylene core trial structure. For the naphthalene monoimide, which is a flat rigid object with a molecular weight of 197 Da, PHASER reproduces an electron density of the centrosymmetric perylene dimer. On the one hand this gives confidence that molecular bias helps to converge upon the desired result, while on the other hand it confirms that the diffracting species is primarily the perylene. Hence, naphthalene monoimide predominantly represents the disordered or mobile fraction not involved in coherent scattering, which also explains the broad naphthalene monoimide response in the ^{13}C- 1D MAS spectra.

3.3.2 Insight into packing

With the principal scattering component positioned in the unit cell (Figure 3.4), the bay substituents can be attached for geometrical optimization using the FORCITE module in Materials Studio to fill the space and compare with the partial electron density map. The final model obtained in this way is shown in Figure 3.5 with naphthalene monoimide positioned in between perylene dimers. Propellor shaped centrosymmetric dimers with P and M chirality are positioned diagonally across the unit cell, with the 2, 6 diisopropyl phenyl group perpendicular to perylene plane to diminish steric hindrance (Figure 3.4).[35] A 3D network is formed by the stretched phenoxy and naphthalene monoimide bay substituents, that extend towards the next second row of perylene dimers, effectively providing non-covalent crosslinks with the isopentylthio functionalities and positioning the naphthalene monoimide donor blocks in between the perylene dimers of the first next row (Figure 3.5). In this way both rigidity and softness can be realized within the same scaffolding, which paves the way for the design and engineering of
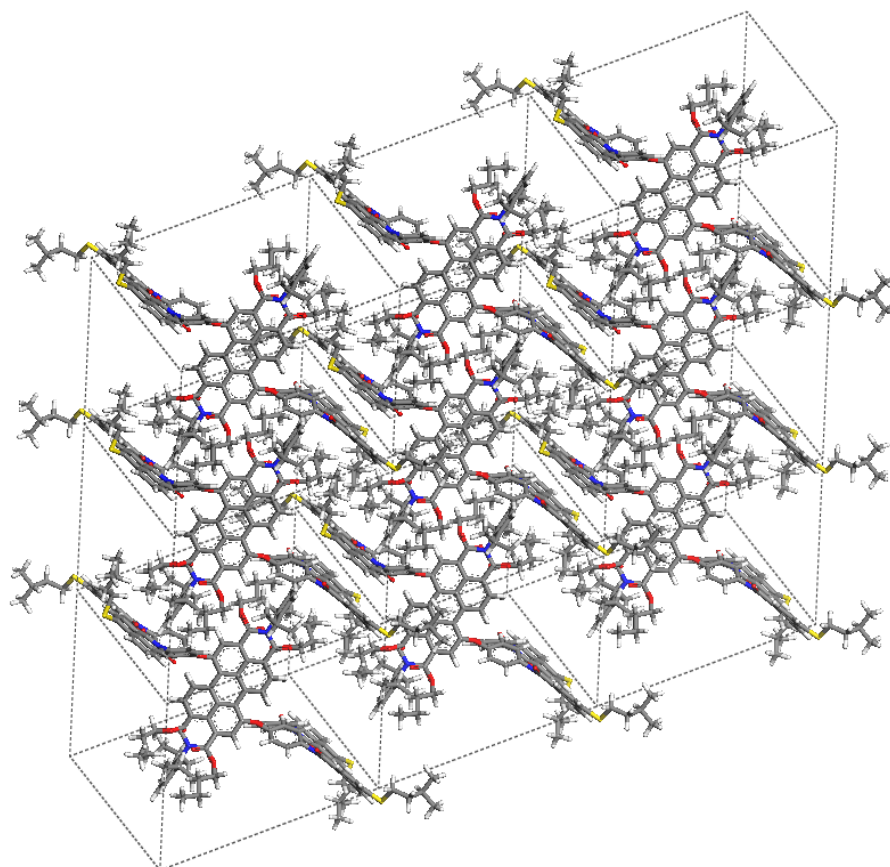
Figure 3.5 Proposed packing of D1A2 with the *P*-1 space group. The orientation of the perylene core in the unit cell is in accordance with the partial electron density map obtained from PHENIX. With electron diffraction the unit cell and Laue group of the packing are determined, while NMR shifts provide information about the structure of the diffracting unit and provide information about its molecular symmetry that can be used to generate structure. This is a major step forward relative to the previous approach, instead of having separate images and models, here there is fully integrated analysis where the nonzero scattering intensity in reciprocal space is translated into a 3D electron density contour in real space that is projected onto a tangible 3D molecular structure with the periodic commonality of the packing represented by a unit cell and space group. The perylene cores forms centerosymmetric dimers with the napthalenemonoimide moieties extending outwards. Even though the molecule is chiral, the barriers for the flipping of both wings are relatively very low. Here the enantiomers are running in opposite directions and related by an inversion symmetry operation.

artificial photosynthesis materials. The molecules self-assemble in a racemic packing of P and M enantiomers with core-induced handedness. The induced misfit necessary for the responsive matrix operation could be achieved through the

positioning of the naphthalene monoimide donor motives in the cavities in the network. In the proposed model NMR constraints shown in Figure 3.2 are accommodated and lead to a viable model packing with an overall energy of 230 kcal/mol. In the electron density map and the structure, the distance between perylene planes in the dimer is ~4.1 Å after modeling. A shorter distance of 3.8 Å has been reported before for perylene dimers from X-ray data.[36]

Blue light-absorbing naphthalene monoimide energy donors, harvest the photons and transfer the energy to the green light-absorbing perylene derivatives, which are energy acceptors. This energy transfer can probably procced through FRET since there is a good overlap between the donor's emission and the acceptor's absorption.[16] The perylene dimers form rods along the *a* axis with an edge-to-edge distance of 0.28 nm between dimers, which is favorable for FRET (Figure 3.5). Both along the *b* axis and along the *c* axis the edge-to-edge distances are longer, ~0.8 nm and ~1 nm, respectively. Such morphology offers an interesting prospect for chemical programing of the molecular scaffold for responsive matrix device concepts.

3.4 Conclusions

Computational integration of ENC and MAS NMR with a molecular replacement approach is used to determine the molecular geometry and packing of a bichromophoric light-harvesting donor-acceptor antenna system D1A2 that forms a racemic packing of centrosymmetric P and M dimers due to core induced chirality in the solid state. This results enable a direct molecular level approach to axiomatic design and improvement of light-harvesting antenna systems D1A2 with naphthalene monoimide (D1) and perylene monoimide diester (A2) as molecular entities. The rod type morphology of D1A2 in the solid state leads to a contiguous column of acceptors, with naphthalene monoimide antennas projecting out to harvest photons and feed into the system through FRET via their positioning in between dimers. This methodology opens the way for the studies of pseudocrystalline supra molecular systems with ^{13}C at natural abundance and could be used for underpinning the design of complex self-assembling systems for artificial photosynthesis.

3.5 Materials and Methods

3.5.1 Sample preparation

The studied antenna system D1A2 was synthesized by the reaction between perylene derivative *N*-(2,6-diisopropylphenyl)-1,7-dibromo-perylene-3,4,9,10-tetracarboxy monoimide dibutylester and a naphthalene derivative *N*-(4′-hydroxyphenyl)-4-(isopentylthio)naphthalene-1,8-dicarboxy Monoimide.[16] [17]

3.5.2 NMR measurements

The MAS NMR spectra were recorded with a Bruker AV-750 MHz spectrometer (Bruker, Billerica, MA) equipped with a 4 mm triple MAS probe operating with a spinning frequency of 13 kHz ± 5 Hz. The Two Pulse Phase Modulation scheme was used to decouple the proton spins during acquisition.[37] Two-dimensional ^{1}H-^{13}C heteronuclear correlation data were collected by using the frequency-switched Lee-Goldburg (FSLG) experiment,[38] with two different CP times of 256 µs and 1024 µs for the detection of short range and long range dipolar correlations respectively (Figure S3.9). For the PMLG a ^{1}H 90° pulse of 3.1 µs was employed. The ^{1}H chemical shift was calibrated from a solid spectrum of solid tyrosine-HCl salt with an FSLG scale factor of 0.571 that reproduces the ^{1}H chemical shift in the solution state NMR. The solution state data were recorded with an 850 MHz spectrometer at a concentration of 60 mM and chloroform as the solvent. The ^{1}H and ^{13}C NMR spectra were measured at a temperature of 298 K with TMS as internal standard. All data were processed using the Bruker TopSpin3.2 data processing software (Bruker, Billerica, MA).

3.5.3 Cryo-EM measurements

Prior to data collection the sample was gently crushed into a fine powder between two microscopy glass slides. The crushed sample was applied to a holey carbon films on 300 mesh Copper grid (Agar Scientific Ltd, Essex) creating a random size and orientation distribution of nanocrystals.[34] Electron diffraction data were collected from a single D1A2 nano crystal. The experimental setup for the electron diffraction measurements was a Philips-FEI CM30 LaB6 transmission electron microscope (University of Barcelona, CciTUB services) operated at 200 kV (λ =

0.02508 Å) fitted with a Timepix detector chip-assembly.[39] Electron diffraction data were collected under parallel beam conditions from a single nanometer sized crystal that was rotated in a single tilt holder at room temperature without the need for cryo-cooling the sample.

3.5.4 Structure modeling and chemical shift calculation

Computational modelling was done with the Biovia Materials Studio Suite (Biovia, San Diego, CA). A unit cell was created with the lattice parameters from ENC using the FORCITE Module. The geometrically optimized molecule is then placed along the *P*-1 symmetry axis. Inverse symmetry in the *P*-1 space group generates the enantiomers. The structure is then optimized with the FORCITE Module using the Universal force field under periodic boundary conditions. *P*-1 symmetry preserves the intrinsic chirality of the molecule during geometry optimization. Smart algorithm with a convergence tolerance of energy about $2.0\ e^{-5}$ kcal/mol and force of 0.001 kcal/mol with Universal force field and charge obtained from $DMol^3$ is employed for FORCITE optimization.

References

(1)   Purchase, R. L.; de Groot, H. J. M. *Interface Focus* **2015**, *5*.

(2)   McConnell, I.; Li, G.; Brudvig, G. W. *Chem Biol* **2010**, *17*, 434.

(3)   Croce, R.; van Amerongen, H. *Nat Chem Biol* **2014**, *10*, 492.

(4)   Demmig-Adams, B.; Adams, W. W. *Nature* **2000**, *403*, 371.

(5)   Alia, A.; Buda, F.; Groot, H. J. M. d.; Matysik, J. *Annual Review of Biophysics* **2013**, *42*, 675.

(6)   Breton, J.; Geacintov, N. E. In *Ciba Foundation Symposium 61 - Chlorophyll Organization and Energy Transfer in Photosynthesis*; John Wiley & Sons, Ltd.: 2008, p 217.

(7)   Koester, V. J.; Fong, F. K. *The Journal of Physical Chemistry* **1976**, *80*, 2310.

(8)   Fenna, R. E.; Matthews, B. W. *Nature* **1975**, *258*, 573.

(9)   Scholes, G. D.; Rumbles, G. *Nat Mater* **2006**, *5*, 683.

(10)   Khlbrandt, W.; Wang, D. N. *Nature* **1991**, *350*, 130.

(11)   Jordan, P.; Fromme, P.; Witt, H. T.; Klukas, O.; Saenger, W.; Krausz, N. *Nature* **2001**, *411*, 909.

(12)   Thomas, J. D.; Lee, T.; Suh, N. P. *Annual Review of Biophysics and Biomolecular Structure* **2004**, *33*, 75.

(13)   Wasielewski, M. R. *Accounts of Chemical Research* **2009**, *42*, 1910.

(14)   Huang, C.; Barlow, S.; Marder, S. R. *The Journal of Organic Chemistry* **2011**, *76*, 2386.

(15)   Bhosale, S. V.; Jani, C. H.; Langford, S. J. *Chemical Society Reviews* **2008**, *37*, 331.

(16)   Dubey, R. K.; Inan, D.; Sengupta, S.; Sudholter, E. J. R.; Grozema, F. C.; Jager, W. F. *Chemical Science* **2016**, *7*, 3517.

(17)   Sengupta, S.; Dubey, R. K.; Hoek, R. W. M.; van Eeden, S. P. P.; Gunbaş, D. D.; Grozema, F. C.; Sudhölter, E. J. R.; Jager, W. F. *The Journal of Organic Chemistry* **2014**, *79*, 6655.

(18)   Kashida, H.; Takatsu, T.; Sekiguchi, K.; Asanuma, H. *Chemistry – A European Journal* **2010**, *16*, 2479.

(19)   Şener, M.; Strümpfer, J.; Hsin, J.; Chandler, D.; Scheuring, S.; Hunter, C. N.; Schulten, K. *Chemphyschem : a European journal of chemical physics and physical chemistry* **2011**, *12*, 518.

(20)   Ganapathy, S.; Oostergetel, G. T.; Wawrzyniak, P. K.; Reus, M.; Gomez Maqueo Chew, A.; Buda, F.; Boekema, E. J.; Bryant, D. A.; Holzwarth, A. R.; de Groot, H. J. M. *Proceedings of the National Academy of Sciences* **2009**, *106*, 8525.

(21)   Ganapathy, S.; Sengupta, S.; Wawrzyniak, P. K.; Huber, V.; Buda, F.; Baumeister, U.; Würthner, F.; de Groot, H. J. M. *Proceedings of the National Academy of Sciences* **2009**, *106*, 11472.

(22)   Safont-Sempere, M. M.; Stepanenko, V.; Lehmann, M.; Wurthner, F. *Journal of Materials Chemistry* **2011**, *21*, 7201.

(23)   González-Rodríguez, D.; Torres, T.; Herranz, M. Á.; Echegoyen, L.; Carbonell, E.; Guldi, D. M. *Chemistry – A European Journal* **2008**, *14*, 7670.

(24)   Li, C.; Yan, H.; Zhao, L.-X.; Zhang, G.-F.; Hu, Z.; Huang, Z.-L.; Zhu, M.-Q. *Nat Commun* **2014**, *5*.

(25)   Osswald, P.; Würthner, F. *Chemistry – A European Journal* **2007**, *13*, 7395.

(26)   Safont-Sempere, M. M.; Osswald, P.; Radacki, K.; Würthner, F. *Chemistry – A European Journal* **2010**, *16*, 7380.

(27)   Osswald, P.; Reichert, M.; Bringmann, G.; Würthner, F. *The Journal of Organic Chemistry* **2007**, *72*, 3403.

(28)   Osswald, P.; Würthner, F. *Journal of the American Chemical Society* **2007**, *129*, 14319.

(29)   Kabsch, W. *Acta Crystallographica Section D* **2010**, *66*, 125.

(30)   Evans, P. *Acta Crystallographica Section D* **2006**, *62*, 72.

(31)   Evans, P. *Acta Crystallographica Section D* **2011**, *67*, 282.

(32)   Evans, P. R.; Murshudov, G. N. *Acta Crystallographica Section D* **2013**, *69*, 1204.

(33)   Winn, M. D.; Ballard, C. C.; Cowtan, K. D.; Dodson, E. J.; Emsley, P.; Evans, P. R.; Keegan, R. M.; Krissinel, E. B.; Leslie, A. G. W.; McCoy, A.; McNicholas, S. J.; Murshudov, G. N.; Pannu, N. S.; Potterton, E. A.; Powell, H. R.; Read, R. J.; Vagin, A.; Wilson, K. S. *Acta Crystallographica Section D* **2011**, *67*, 235.

(34)   S. Budavari, M. J. O. N., A. Smith, and P. E. Heckelman, *"The Merck Index, Merck & Co,"* Inc., Rahway, NJ **1989**, *vol. 1606*.

(35)   Shi, Y.; Qian, H.; Li, Y.; Yue, W.; Wang, Z. *Organic Letters* **2008**, *10*, 2337.

(36)   Briseno, A. L.; Mannsfeld, S. C. B.; Reese, C.; Hancock, J. M.; Xiong, Y.; Jenekhe, S. A.; Bao, Z.; Xia, Y. *Nano Letters* **2007**, *7*, 2847.

(37)   Bennett, A. E.; Rienstra, C. M.; Auger, M.; Lakshmi, K. V.; Griffin, R. G. *The Journal of Chemical Physics* **1995**, *103*, 6951.

(38)   Van Rossum, B. J.; Förster, H.; De Groot, H. J. M. *Journal of Magnetic Resonance* **1997**, *124*, 516.

(39)   van Genderen, E.; Clabbers, M. T. B.; Das, P. P.; Stewart, A.; Nederlof, I.; Barentsen, K. C.; Portillo, Q.; Pannu, N. S.; Nicolopoulos, S.; Gruene, T.; Abrahams, J. P. *Acta Crystallographica. Section A, Foundations and Advances* **2016**, *72*, 236.
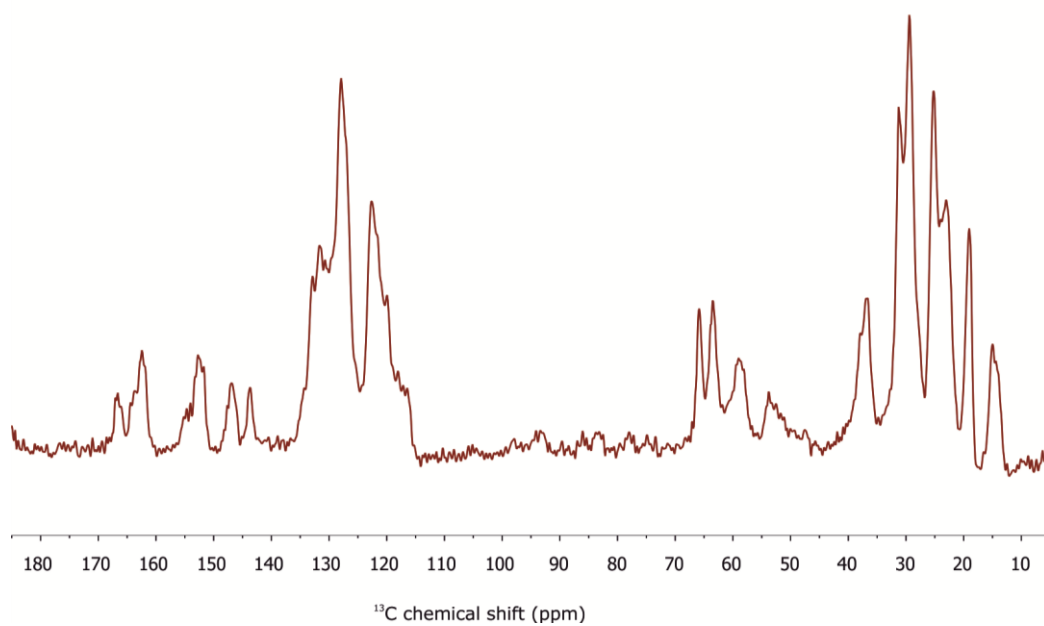
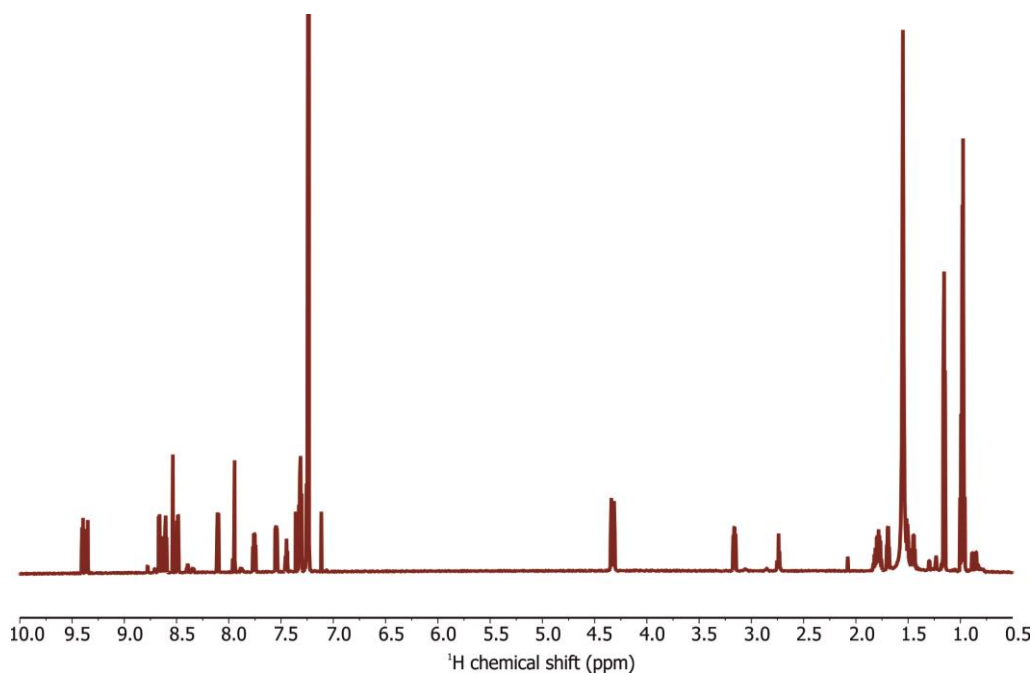Figure S3.1 1D ^{13}C CPMAS spectrum of D1A2 collected at a spinning frequency of 13 kHz.

Figure S3.2 ^{1}H NMR spectrum of D1A2.

Figure S3.3 ^{1}H-^{1}H COSY spectrum of D1A2 showing aliphatic region.

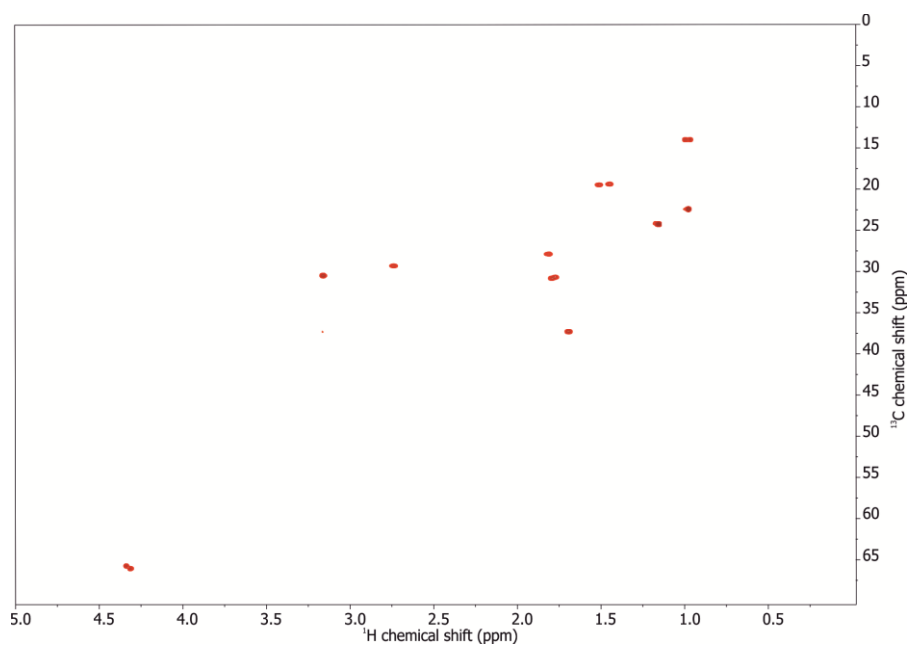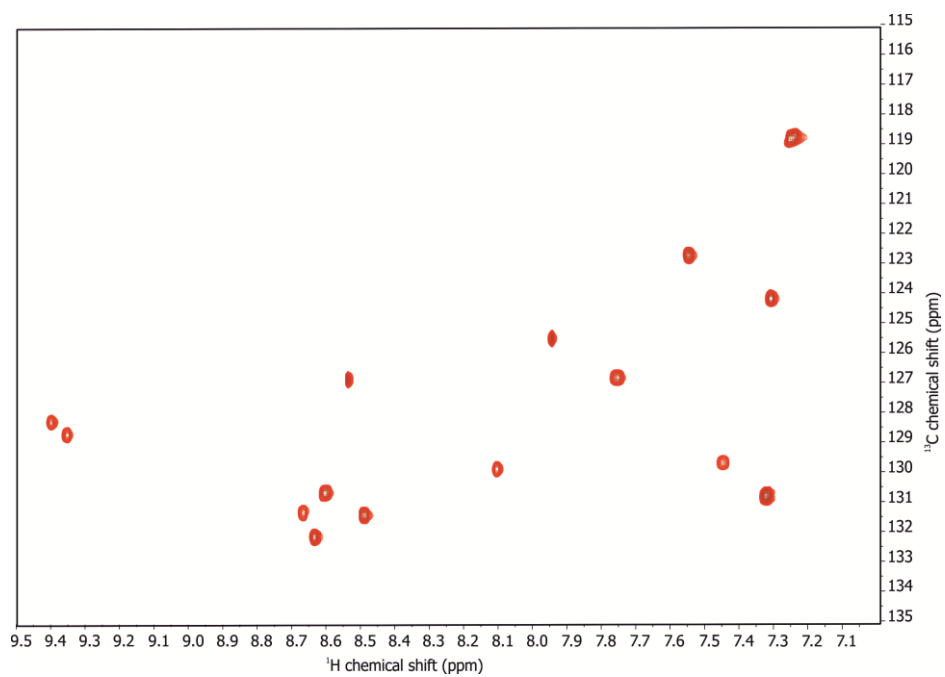Figure S3.4 ^{1}H-^{1}H COSY spectrum of D1A2 showing aromatic region.

Figure S3.5A ^{13}C-^{1}H HSQC spectrum of D1A2 showing aliphatic region.

Figure S3.5B ^{13}C-^{1}H HSQC spectrum of D1A2 showing aromatic region.

Chapter 4

Structural analysis of DATZnS(4H) using homology modelling

Abstract

The packing of DATZnS(4H) is deduced from CP/MAS NMR, TEM, and unit cell parameter optimization with force field modelling. C_2 molecular symmetry of the DATZnS(4H) is obtained from MAS NMR and DFT modeling. Spatial correlations obtained from HETCOR spectra collected with a long mixing time of 2 ms point towards an antiparallel stacking. The packing constraints and limited data from Fourier transformation of a TEM image are used to construct a structural model with the $P2/c$ space group obtained from the DATZnS(3′-NMe) parent compound for which the structure has been solved (chapter 2). The data indicates that the packing of fused naphthalene diimide-salphen bichromophoric antenna forming a phenazine motif with a dipole moment in a $P2/c$ supramolecular scaffold can be steered by a functional group between antiparallel dipoles and parallel dipoles in a layer. The packing of fused NDI-salphen chromophores forming a phenazine motif with a dipole moment in a $P2/c$ supramolecular scaffold can be steered by chemical substituents between antiparallel dipoles and parallel dipoles in a sheet.

4.1 Introduction

With the looming energy crisis and pollution coming out of conventional fuels, scientists are trying to find an alternative by mimicking the primary processes of photosynthesis.[1-6] In nature, plants harvest light for solar to fuel conversion using photosynthetic antennae complexes.[7-9] Even though nature has given the blue prints to convert energy from sunlight through photosynthesis, a principal challenge lies in finding suitable molecules that mimic the chemical characteristics of chlorophylls for application in artificial systems.[10-12] Self-assembly is the underlying principle behind the antenna complexes that harvest the solar flux efficiently.[13] Unique features of antenna complexes in photosynthesis is their well-

defined three dimensional architecture, which plays a significant role in absorbing the sunlight and funnel the resulting excited-state energy to a designated site.[14-16] The challenge is to find a suitable scaffold, which has the ability to harvest light into which the water splitting catalyst can be attached.[6,17]

DATZnS(4H) is a bichromophoric antenna, which is prepared by fusing naphthalene diimide with zinc salphen, thereby generating a phenazine bridge (Figure 4.1). [18-22] This molecule belongs to a class of molecules, which exhibit the properties of zinc salphen to form a metal organic framework while the NDI and the phenazine can be involved in π-π stacking.[18-20] In addition, the extended π conjugation from the salphen to NDI in the molecule enhances the π-π stacking.[21] The opto-electronic tunability[22] due to the possibility to substitute various heteroatoms and functional groups makes this molecule a versatile building block for chemical engineering purposes.[23,24] The aliphatic tails present in the molecule are an added advantage. They enhance the solubility and allow for modification at a later stage, *e.g.* by using them as a linker to attach antenna systems to functionalized electrode surfaces. The vacant orbitals present in the Zn^{2+} of the salphen can accommodate an additional ligand. For instance, a catalyst can be attached through a coordination bond to the scaffold.[14,25-27]The phenazine molecule possesses an aromatic surface which is flat and electron rich.[28] This creates the possibility of attractive van der Waals and charge transfer interactions similar to supramolecules built from porphyrins.[29-32] The properties and applications of these organometallic frameworks can be altered by changing the Zn^{2+} by other metals or by introducing a functionalized ligand. The efficiency of light harvesting and possibly also charge separation depends on the packing of the molecule in a three dimensional framework. The packing effects that derive from the scaffolding play a crucial role in determining the functional properties of these antenna complexes, such as mixing in charge transfer states into the excited state.[33,34] In particular, since the fused salphen-phenazine-NDI motif has an electric dipole moment, this provides a handle for functionalization and chemical engineering by steric control for steering the packing. The stability of this molecule is another attractive feature. Self-organization is driven by supramolecular noncovalent interactions such as π-π stacking, hydrogen bonding, and a hydrophobic packing environment. To design a supramolecule with a designated
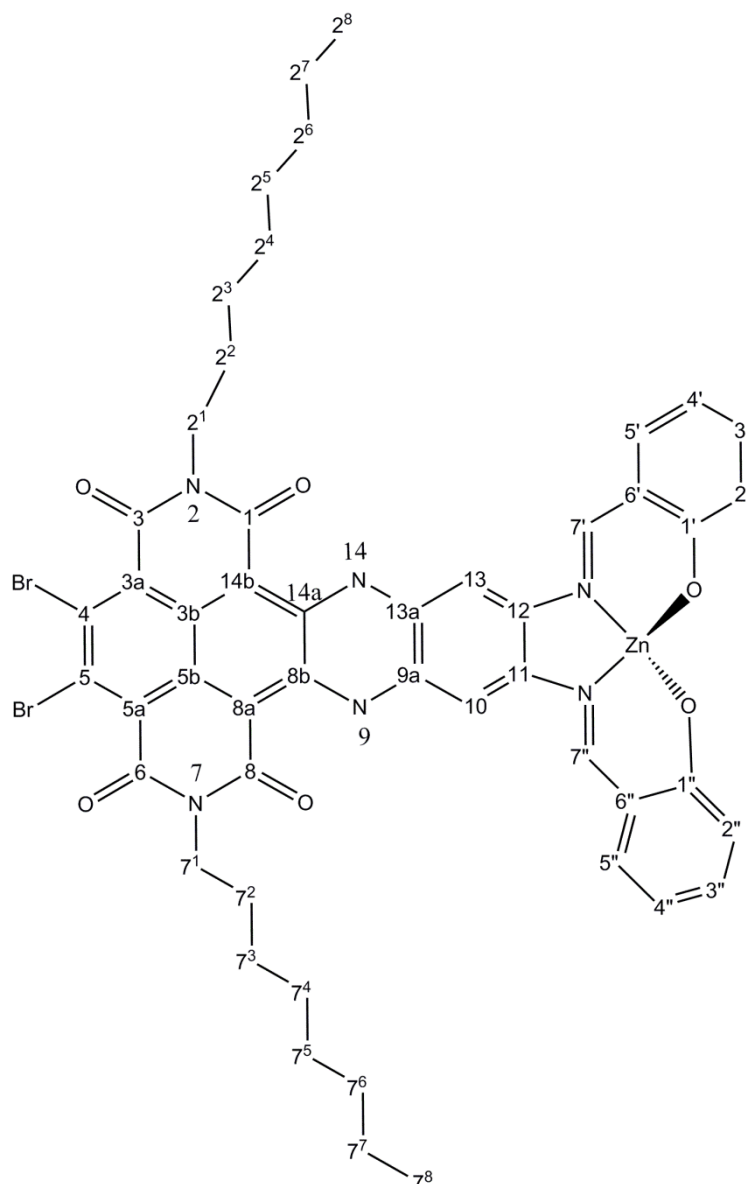
Figure 4.1 Chemical structure of the DATZnS(4H) molecule with numbering according to the IUPAC convention. DATZnS(4H) is a member of a class of fused NDI-zinc-salphen based chromophore (salphen = bis-salicylimide phenylene) which are catching interest in the field of chemical design of light harvesting antenna molecules. These molecules are both robust and versatile with respect to optical tuning and other chromophoric chemical properties. The dipole moment of the molecule is aligned along the principal axis of the molecule.

property like efficient light harvesting, we have to deepen our knowledge about how molecular characteristics influence the self-assembly.[35] The DATZnS(4H) dyad has the possibility to be tailored for incorporation into flexible large area devices. Compact π-π stacking arising from the phenazine helps to form a rigid scaffold to attach the catalyst.[36] The wavelength at which photons are absorbed in

the dyad can be adjusted with the functional groups so that it can cover the broad range of the solar spectrum. The introduction of different metals in the salphen[18] part can be used to tune the photophysical and electronic properties.[37,38] Finally, these systems can produce the high chromophore density that is considered essential for efficient light harvesting, as explained in chapter 2.

To mimic the engineering principles of nature we have to understand how the molecules can be packed.[39] Moreover, packing studies are essential for getting insight in to the solid state physical properties of aggregates. Overall dimensions and shapes of the final assemblies are determined by various packing factors, both steric and electronic. A supramolecular strategy based on DATZnS(4H) with diverse functional groups offers the opportunity to steer the packing in desired directions. In parallel, profound mechanistic insight into packing effects will pave the way for investigating and optimizing the functional properties using theoretical and experimental studies ahead of experimental realization.

Computational integration of CP/MAS NMR and Cryo-EM for resolving the packing is opening a new horizon to visualize supramolecular structures with well defined scaffolding and intrinsic heterogeneity at the molecular level.[39] By carefully analyzing regions of nonzero diffraction in reciprocal space, either obtained directly from electron diffraction or indirectly from Fourier transforms of TEM images, packing order can be detected and combined with chemical shift and distance constraints obtained by MAS NMR to average static heterogeneity and resolve a very detailed model for the supramolecular organization in the absence of true translation symmetry. In chapter 2, it is explained how the systematic absences in reciprocal space can be acquired by Cryo-EM. Along with chemical shift information and distance constraints obtained by CP/MAS NMR and ^{1}H-^{13}C heteronuclear correlation spectroscopy data collected from samples with ^{13}C at natural abundance, a space group could be identified. In chapter 3, electron nano crystallography is used to determine the unit cell parameters and space group, while the packing is filled in combination with CP/MAS NMR. In this chapter, it is shown that very limited Cryo-EM, in combination with chemical shift and HETCOR data can guide the state of the art molecular mechanics modeling of the packing organization in a periodic framework with limited correlation length. Spatial correlation peaks are obtained from HETCOR data collected at longer mixing time.

Here a unique unit cell with twofold axis can be deduced from EM since the NMR and DFT modeling point to C_2 molecular symmetry of the DATZnS(4H) and a racemic packing of the delta and lambda forms. The unit cell parameters are optimized using the FORCITE module in the Materials Studio software. In addition, the principle reflection in reciprocal space deduced from the EM was reproduced using Crystal Maker to validate the packing. Finally it is tempting to conclude that steric control by bulky substituents allows for a switch between parallel and antiparallel stacking of the DATZnS motif.

4.2 Results

4.2.1 Chemical shift assignments

DATZnS(4H) is a fused NDI-zinc-salphen based chromophore (salphen = bis-salicylimide phenylene). Moderately sized molecules like DATZnS(4H) with low symmetry and few protons, which are on the extended network of conjugated aromatic rings, make it feasible to identify selective intermolecular polarization transfer events, to spatially probe the structure.[40] ^{13}C 1D CP/MAS NMR data were collected to start with the structural analysis (Figure S4.1). The spectrum is well dispersed over 170 ppm, which makes a reasonable assignment based on chemical shifts possible. This dispersion of chemical shifts is achieved through rich functionalities, as there are four carbonyl groups, two phenoxy, and two imide groups present in the fused NDI-zinc-salphen based chromophore. The narrow lines in the 1D CP/MAS NMR spectrum point to a homogeneous, nearly crystalline microstructure.

CP/MAS NMR ^{13}C chemical shifts $\sigma_i{}^C$ were assigned by comparison with computational chemical shifts using Gaussian 03 and solution state NMR of the DATZnSTP molecule introduced in chapter 2 (Table 4.1). Assignments of the primary, secondary and tertiary carbon atoms can be confirmed with the aid of HETCOR data acquired with a short mixing time of 0.256 ms, to limit spin diffusion through intermolecular pathways (Figure 4.2). The spectrum is divided into two panels for the aliphatic region and the aromatic region. The aliphatic region is spread from 10 ppm to 50 ppm, while the aromatic region is from 100 ppm to 170 ppm. The aromatic CH protons are reasonably resolved in the HETCOR spectra,
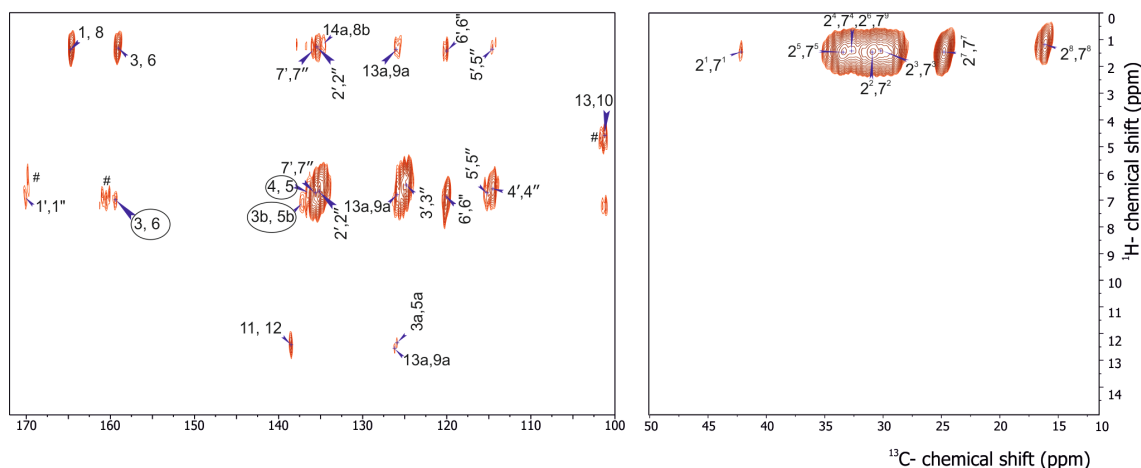
Figure 4.2 Contour plot sections of ^{1}H-^{13}C heteronuclear dipolar correlation spectra at 2 ms, which is showing long range correlations signals recorded in a field of 17.6 T by using a spinning frequency of 13 kHz. The spectrum is divided over two panels, aliphatic on the right and aromatic on the left. Folding of the tails along the phenazine can be deduced from a set of correlation peaks between the ^{1}H from the aliphatic tail and the ^{13}C on the phenazine backbone. Formation of a pseudo octahedral recognition motif involving the Zn^{2+} and the two bromine of adjacent molecules transpires from an intermolecular correlation indicated by circles arising from the interaction between salphen and NDI. # indicates the side bands.

and the data are well in line with the results from the computational chemical shift (Table 4.1). The terminal methyl group in the alkyl chain has a characteristic shift of 13.7 ppm, while the alkyl group attached to the electronegative nitrogen resonates with a chemical shift of 40.7 ppm. The 2^7, 7^7 responses are well resolved with identical shifts of 22.6 ppm, revealing symmetry in the molecule and in the packing. The 13, 10 in the phenazine ring are also symmetry related and have a characteristic shift of 100.1 ppm.

4.2.2 Analysis of HETCOR at longer mixing time

In the HETCOR spectra at longer mixing time, there are many long-range correlation signals arising from the heteronuclear dipolar transfer between proton and carbon nuclei, which could be inter or intramolecular (Figure 4.2).[39] For the DATZnS(4H) molecule the protons attached to the tertiary carbon nuclei are well resolved in the 2D HETCOR at short mixing times (Figure S4.2). This is important for the selective detection of long range correlations at a cross polarization time of 2 ms, to resolve the spatial arrangement of the DATZnS(4H) molecules in the

89

Table 4.1 Experimental CP/MAS NMR chemical shifts compared with computational results from Gaussian 03 calculations for the DATZnS(4H).

Position	$\sigma^C_{DATZnS(4H), expt}$	$\sigma^C_{cDATZnS(4H), calc}$
1, 8	163.6	162.5
3, 6	158.3	157.8
4, 5	135.4	152.3
14b, 8a	99.0	101.7
14a, 8b	133.5	136.7
3a, 5a	124.8	125.1
3b, 5b	136.1	130.7
13a, 9a	125.0	128.1
13, 10	100.3[1]	99.1
11, 12	137.5	140.4
1', 1''	169.1	176.2
2', 2''	133.9[1]	129.2
3', 3''	123.6[1]	128.4
4', 4''	113.6[1]	104.8
5', 5''	113.9[1]	120.6
6', 6''	118.9	107.8
7', 7''	134.3[1]	139.5
2^1, 7^1	46.40	42.4
2^2, 7^2	31.75	28.6
2^3, 7^3	31.86	28.1
2^4, 7^4	33.63	30.7
2^5, 7^5	30.85	31.8
2^6, 7^6	37.79	30.7

2^7, 7^7	26.31	23.2
2^8, 7^8	14.44	13.7

[1]Assignment based on the computational chemical shift and HETCOR at short mixing time of 0.256 ms.

packing.

Long-range correlations between protons attached to the carbon atoms on the tail with the 1, 8, 3, 6 carbonyl group and aliphatic tail are observed in the HETCOR dataset collected with 2 ms mixing time. These can be intramolecular. For instance, the carbonyl group could get polarization from the 2^1, 7^1 CH_2 alkyl groups over an intramolecular distance of less than 4 Å, depending on the conformation. The transfer of polarization from protons on the alkyl chain to 14a, 8b, 13a, 9a, 6′, 6″ 5′, 5″ 2′, 2″, 7′ and 7″ carbon nuclei gives information about the folding and positioning of the tails in the packing. While transfer to 14a, 8b, 13a, 9a ^{13}C could be intramolecular or intermolecular, intramolecular transfer to 6′, 6″, 5′, 5″, 2′, 7′ is difficult, and the correlations point to intermolecular transfer and antiparallel stacking. Heteronuclear correlation signals involving the quaternary ^{13}C in the highly unsaturated NDI part and the salphen are very useful for structure determination, since there are no protons on the NDI motif for intramolecular transfer. Extensive polarization transfer from aromatic protons on the salphen part to 4, 5, 3, 6, 3b, and 5b quaternary carbon atoms corroborate an antiparallel stacking arrangement. For a cross polarization time of 2 ms, a spatial correlation is observed between the 14-NH proton and 3a, 5a, 4 and 5 ^{13}C. A rapid buildup of signal indicates it concerns primarily intramolecular transfer.

4.2.3 Cryo-EM

Stripes observed in the cryo-EM image lead to two strong reflections in the Fourier transform that give information about the periodic arrangement (Figure 4.3). These spots correspond to a distance of 1/1.87 nm. They occur in various images, indicating periodic repetition of the molecule in a preferred orientation.(data not shown) Since no other distinct spacing could be observed in the TEM images, there is considerable heterogeneity in the sample and packing.
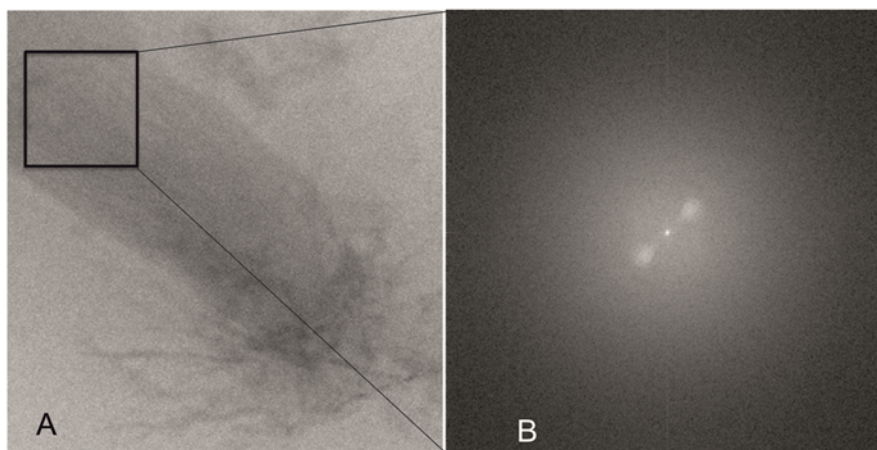
Figure 4.3 (A) TEM image of the DATZnS(4H) loaded on a carbon grid revealing a lamellar arrangement. (B) Fourier transform of the selected region indicated with a black square shows a 1.87 nm periodic repetition

4.3 Discussion

4.3.1 Structure determination of DATZnS(4H)

Since there is only one set of NMR signals for the two halves of the molecule, this reveals molecular symmetry, either nonchiral σ_v or chiral C_2, with the latter being the lowest in energy according to DFT calculations. This imposes a twofold molecular axis, while the molecules should form lamellar packing according to the TEM. To model the structure, a homology approach is employed. The molecule was placed with its C_2 symmetry axis on the twofold axis of a unit cell of the P2/c space group. The cell parameters from the DATZnS(3′-NMe) homologue were used, and the DATZnS(4H) was positioned in the cell on the twofold axis. One molecule corresponds to twice the asymmetric unit and to eliminate the spurious images, the unit cell was converted to $P1$. The redundant fragments were selected and deleted and the cell was converted back to $P2/c$ with the find symmetry command in Materials Studio. Two settings were considered, the original setting with parallel stacking and a setting, where the a and c axis were interchanged to get antiparallel stacking (Figure S4.3). Optimizations of unit cell parameters and molecule were performed with FORCITE in Materials Studio for both settings and it was found that the antiparallel stacking is stabilized by 37 kcal/mol with parameters a = 1.47 nm, b = 1.83 nm, c = 9.6 nm, α = 90°, β = 109° and γ = 90° (Figure 4.4).

The antiparallel model in Figure 4.4 contrasts with the parallel stacking deduced for the DATZnS(3′-NMe) homologue in chapter two, where only correlations were observed between the NDI motif and the dimethylamine functionalities, which are thought to play a decisive role in steering the packing configuration of the latter compound. The extensive polarization transfer to 4, 5, 3, 6, 3b, and 5b from aromatic protons on the salphen part to the NDI part indicated in Figure 4.2 with a circle confirms the antiparallel stacking, which has short distances of ~3.5-4 Å between the salphen protons and NDI carbons. This matches very well with the heteronuclear distance determined from the quantitative numerical analysis of LGCP buildup curves in the related DATZnS(3′-NMe) compound in Figure 2.3 in chapter 2. The alternative, recognition between the NDI and the salphen part with extended overlap in the parallel stack model is difficult to reconcile with the characteristic heteronuclear transfer in Figure 4.2, since in the parallel model for the DATZnS(4H) not only the enthalpy is higher in the modeling because of steric hindrance but also the distances are larger, in the range of 5 Å. Finally, the HETCOR data for the DATZnS(3′-NMe) homologue in chapter 2 do not exhibit the characteristic correlations indicated with the circle in Figure 4.2 Thus, the heteronuclear transfer from the salphen to the NDI is a critical observation for structure validation.

4.3.2 Insight into packing

The structure shows π-π overlap between the phenazine moieties, which may help to drive the packing along the b axis. The distance between two molecules in the direction perpendicular to the plane of the molecule is 0.36 nm,[41] indicating strong π - π stacking. The tails are projecting outwards into the space between the two stacks. The ring structure locks the keto group into co-planarity with the phenazine ring resulting in substantial π-electron conjugation involving the keto and the phenazine ring. The presence of the carbonyl group and the nitrogen with the lone pair induces an extended π electron delocalization. Due to this extended conjugation phenazine derivatives adopt a planar geometry.[42,43] The electropositive Zn^{2+} in the Λ and Δ chiral salphen functionalities produce a cavity to which the electronegative bromine of the next molecule along the c axis is attracted to form the pseudo-octahedral recognition motif, similar to the

DATZnS(3′-NMe) homologue (Chapter 2). This electrostatic attraction and head to tail alignment of electric diploes can help to stabilize the packing along the axial direction of the molecule. The pseudo octahedral coordination of the zinc follows
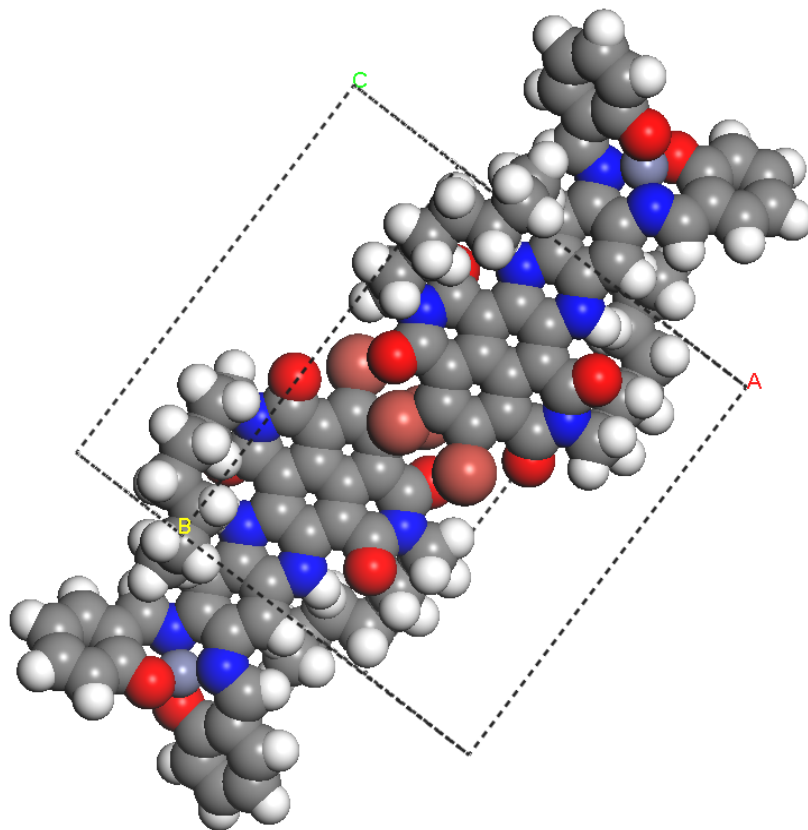

Figure 4.4 Proposed structure of antiparallel DATZnS(4H) in a 3D packing with the space group $P2/c$. In comparison with the parent structure of the DATZnS(3′-NMe) homologue in chapter 2, the dipole moments are compensated between the stacks and antiparallel rows of head to tail DATZnS(4H). Since the only difference between the two compounds is the NCH_3 functional groups, chemical control over the dielectric characteristics at the supramolecular level is achieved.

the packing induced chirality with enantiomeric pairs of lambda and delta form alternating along the antiparallel stack.

In the TEM pattern of Figure 4.3, the stripes are from alternating regions of high electron density containing Zn^{2+} with regions of phenazine. Along the antiparallel stack the dipole moments are aligned in the opposite directions, which constitute the scaffold of the packing. With the dipoles compensated at the level of the antiparallel arrangement within the stack, there is no emerging electrostatic component for stabilization of planes as in the DATZnS(3′-NMe) homologue. This

may explain why the DATZnS(4H) structure appears much less ordered in the TEM, with only the two reflections of the long repeat along the c axis in the Fourier transform. Tight packing of dyads within the self-assembled stacks provides a high chromophore density to harvest the solar light efficiently. The pseudo-octahedral recognition motif is a characteristic of the supramolecular packing, and is consistent with the antiparallel arrangement that transpires from the spatial correlation peaks between salphen and NDI. The structure accommodates the folding of the tails along the phenazine, in line with the HETCOR data at longer mixing time. Steric hindrance from the salphen part restricts parallel stacking.

4.4 Conclusions

Based on the energy, density, intermolecular correlations from CP/MAS, reflection spots in the Fourier transform of the TEM image and homology modelling, we converge upon an antiparallel stacking for the DATZnS(4H) forming lamellar sheets in a $P2/c$ packing arrangement. Pseudo-octahedral coordination of the Zn^{2+} and C_2 molecular symmetry produces the twofold axis, while the two enantiomeric forms Λ and Δ produced by a c-glide symmetry operation lead to a racemic packing with the alkyl chains folded along the phenazine. This structure is a homologue of the DATZnS(3′-NMe) structure determined in chapter 2, and suggests that the NCH_3 functional group can be used to steer the aggregation from a parallel sheet in DATZnS(3′-NMe) to an antiparallel sheet in DATZnS(4H). This concept paves the way for the chemical design of supramolecular scaffolds for light harvesting and charge separation, on the way to organic solar fuel cell device concepts that can be programmed to quench the internal field in an antiparallel arrangement, *e.g.* for light harvesting, or exploit the internal field from aligned dipole moments, *e.g.* for the injection of charge in catalysts for water splitting. With access to detailed structure information of heterogeneous supramolecular assembly in the DATZnS(4H), rational design of functional based material for light harvesting and charge separators may become reality.

4.5 Materials and methods

4.5.1 Sample preparation

8,9-Dibromo-5,12-dihydro-5,12-diazatetracene di-*n*-octylimide diamine intermediate (103 mg, 0.13 mmol), prepared from 2,3-(*p*-Toluenesulfonamido)-8,9-dibromo-5,12-dihydro-5,12-diazatetracene di-*n*-octylimide was dissolved in 9 mL dry, degassed DMF under an Ar atmosphere and heated to 80 °C in the dark.[44] In a separate flask, salicylaldehyde (40 mg, 0.33 mmol) and zinc acetate dihydrate (265 mg, 1.32 mmol) were dissolved in dry, degassed DMF (5 mL) and kept under Ar. This mixture was stirred for 5 minutes and added to the hot DMF solution via a syringe. After 6 hours, the reaction mixture was cooled down to room temperature, diluted with 5 mL H_2O and stored overnight at -20 °C to induce precipitation. The dark blue precipitate was collected on a filter and washed with water, ethanol and dichloromethane to afford (after vacuum drying) 89 mg of a dark blue solid (59 % yield from 8,9-Dibromo-5,12-dihydro-5,12-diazatetracene di-*n*-octylimide-diamine). IR (ATR FTIR): 2953, 2922, 2851, 1686, 1572, 1528, 1499, 1448, 1431, 1315, 1281, 1225, 1200, 1173, 1150, 1128, 1105, 1076, 1030, 964, 914, 847, 584 cm^{-1}. Mp > 300 ° C

4.5.2 NMR measurements

The solid-state CP/MAS spectra were recorded with a 750 MHz spectrometer, equipped with 4 mm triple resonance CP/MAS probes in dual ^{1}H-^{13}C mode with a spinning frequency of 13 kHz ± 5 Hz. The pulse sequence for the 2-D heteronuclear polarization transfer experiment is shown in Figure S4.3. The 2D sequence starts with a magic angle preparation pulse on the ^{1}H channel, followed by FSLG LGCP to transfer the magnetization from the protons to carbons during a variable time t_1. The ^{1}H dimension of the heteronuclear dipolar interaction correlation experiment can be obtained by Fourier transformation with respect to t_1. The TPPM scheme was used to decouple proton spins during acquisition while the ^{13}C free induction decays (FIDs) were recorded in the t_2 domain (Figure S4.4). For short range polarization transfer from ^{1}H directly bonded to ^{13}C, a CP contact time of 0.256 ms was used, and for longer range polarization transfer and the detection of intermolecular correlations, a CP time of 2 ms was employed. The ^{1}H chemical shift

was calibrated from a spectrum of solid tyrosine-HCl salt.[40] A scale factor of 0.57 for the FSLG was verified with solid tyrosine HCl salt. The data were processed using the Bruker TopSpin 3.2 software (Bruker, Billerica, MA).

4.5.3 Cryo-EM measurements

For electron microscopy, samples dissolved in ethanol were applied to a carbon grid at 83 K with a Vitrobot vitrification system (FEI, Hillsboro, OR). Electron microscopy was done with a Tecnai G2 Polara electron microscope (FEI, Hillsboro, OR) equipped with a Gatan energy filter at 115,000 magnification (Gatan, Pleasanton, CA). Images were recorded in the zero-loss imaging mode, by using a slit width of 20 eV, with a slow-scan CCD camera at 1 micrometer under focus, to have optimal phase contrast transfer at 300 kV.

4.5.4 Structure modeling and chemical shift calculation

Computational chemical shifts were obtained with the Gaussian 03 software package (Gaussian, Inc., Wallingford, CT) using the Becke, Lee, Yang, and Parr (BLYP) exchange-correlation functional with 6-311G basis set. The molecule was geometrically optimized prior to NMR chemical shift calculation.

Biovia Materials Studio Suite (Biovia, San Diego, CA) was used for computational modeling. A monomer structure of the DATZnS(4H) core without the aliphatic tails was obtained by optimization with Gaussian 03 (Gaussian, Inc., Wallingford, CT) and placed in the $P2/c$ unit cell determined for the homologue in chapter 2 as described in the results section. Optimization of the cell parameters was performed with the FORCITE module. For geometry optimization with Forcite, the "smart" algorithm setting in materials studio was used and a convergence tolerance of 0.001 kcal/mol for energy and 0.5 kcal/mol/Å for the force parameter were applied. For the full molecule including the tails, DMol[3] calculations were conducted to get the ESP charges. The generalized gradient approximation (GGA) with the Perdew Burke Ernzerhof (PBE) functional with double numerical atomic orbital augmented by a polarization p-function (DNP) basis set was used for DMol[3] calculations.

References

(1)   Purchase, R. L.; de Groot, H. J. M. *Interface Focus* **2015**, *5*.

(2)   Listorti, A.; Durrant, J.; Barber, J. *Nat Mater* **2009**, *8*, 929.

(3)   House, R. L.; Iha, N. Y. M.; Coppo, R. L.; Alibabaei, L.; Sherman, B. D.; Kang, P.; Brennaman, M. K.; Hoertz, P. G.; Meyer, T. J. *Journal of Photochemistry and Photobiology C: Photochemistry Reviews* **2015**, *25*, 32.

(4)   Wigginton, N. S. *Science* **2016**, *352*, 1185.

(5)   Wong, K.-T.; Bassani, D. M. *NPG Asia Mater* **2014**, *6*, e116.

(6)   Yoneda, Y.; Noji, T.; Katayama, T.; Mizutani, N.; Komori, D.; Nango, M.; Miyasaka, H.; Itoh, S.; Nagasawa, Y.; Dewa, T. *Journal of the American Chemical Society* **2015**, *137*, 13121.

(7)   Blankenship, R. E.; Olson, J. M.; Miller, M. In *Anoxygenic Photosynthetic Bacteria*; Blankenship, R. E., Madigan, M. T., Bauer, C. E., Eds.; Springer Netherlands: Dordrecht, 1995, p 399.

(8)   Hermant, R. M.; Liddell, P. A.; Lin, S.; Alden, R. G.; Kang, H. K.; Moore, A. L.; Moore, T. A.; Gust, D. *Journal of the American Chemical Society* **1993**, *115*, 2080.

(9)   van Gammeren, A. J.; Hulsbergen, F. B.; Erkelens, C.; de Groot, H. J. M. *JBIC Journal of Biological Inorganic Chemistry* **2004**, *9*, 109.

(10)   Gust, D.; Moore, T. A.; Moore, A. L. *Accounts of Chemical Research* **2001**, *34*, 40.

(11)   Stanier, R. Y.; Smith, J. H. C. *Biochimica et Biophysica Acta* **1960**, *41*, 478.

(12)   Pandit, A.; de Groot, H. J. M. *Photosynthesis Research* **2012**, *111*, 219.

(13)   McConnell, I.; Li, G.; Brudvig, G. W. *Chemistry & biology* **2010**, *17*, 434.

(14)   Schmid, S. A.; Abbel, R.; Schenning, A. P. H. J.; Meijer, E. W.; Herz, L. M. *Energy transfer processes along a supramolecular chain of π-conjugated molecules*, 2012; Vol. 370.

(15)   Blankenship, R. E. *Proceedings of the National Academy of Sciences* **2015**, *112*, 13751.

(16)   Zuber, H. *Trends in Biochemical Sciences* **1986**, *11*, 414.

(17)   Barber, J.; Tran, P. D. *Journal of the Royal Society Interface* **2013**, *10*, 20120984.

(18)   Hui, J. K. H.; Yu, Z.; MacLachlan, M. J. *Angewandte Chemie International Edition* **2007**, *46*, 7980.

(19)   Taherimehr, M.; Decortes, A.; Al-Amsyar, S. M.; Lueangchaichaweng, W.; Whiteoak, C. J.; Escudero-Adan, E. C.; Kleij, A. W.; Pescarmona, P. P. *Catalysis Science & Technology* **2012**, *2*, 2231.

(20)   Bhattacharjee, C. R.; Chakraborty, S.; Das, G.; Mondal, P. *Liquid Crystals* **2012**, *39*, 1435.

(21)   Sakakibara, K.; Hill, J. P.; Ariga, K. *Small* **2011**, *7*, 1288.

(22)   Etheridge, F. S.; Fernando, R.; Golen, J. A.; Rheingold, A. L.; Sauve, G. *RSC Advances* **2015**, *5*, 46534.

(23)   Scholes, G. D.; Fleming, G. R.; Olaya-Castro, A.; van Grondelle, R. *Nat Chem* **2011**, *3*, 763.

(24)   Paudel, K.; Johnson, B.; Thieme, M.; Haley, M. M.; Payne, M. M.; Anthony, J. E.; Ostroverkhova, O. *Applied Physics Letters* **2014**, *105*, 043301.

(25)   Whiteoak, C. J.; Salassa, G.; Kleij, A. W. *Chemical Society Reviews* **2012**, *41*, 622.

(26)   Şener, M.; Strümpfer, J.; Timney, J. A.; Freiberg, A.; Hunter, C. N.; Schulten, K. *Biophysical Journal* **2010**, *99*, 67.

(27)   Haferkamp, S.; Haase, W.; Pascal, A. A.; van Amerongen, H.; Kirchhoff, H. *The Journal of Biological Chemistry* **2010**, *285*, 17020.

(28)   Unver, E. K.; Tarkuc, S.; Udum, Y. A.; Tanyeli, C.; Toppare, L. *Journal of Polymer Science Part A: Polymer Chemistry* **2010**, *48*, 1714.

(29)   Hoffmann, M.; Wilson, C. J.; Odell, B.; Anderson, H. L. *Angewandte Chemie International Edition* **2007**, *46*, 3122.

(30)   Uetomo, A.; Kozaki, M.; Suzuki, S.; Yamanaka, K.-i.; Ito, O.; Okada, K. *Journal of the American Chemical Society* **2011**, *133*, 13276.

(31)   Wang, C.-L.; Hu, J.-Y.; Wu, C.-H.; Kuo, H.-H.; Chang, Y.-C.; Lan, Z.-J.; Wu, H.-P.; Wei-Guang Diau, E.; Lin, C.-Y. *Energy & Environmental Science* **2014**, *7*, 1392.

(32)   Son, H.-J.; Jin, S.; Patwardhan, S.; Wezenberg, S. J.; Jeong, N. C.; So, M.; Wilmer, C. E.; Sarjeant, A. A.; Schatz, G. C.; Snurr, R. Q.; Farha, O. K.; Wiederrecht, G. P.; Hupp, J. T. *Journal of the American Chemical Society* **2013**, *135*, 862.

(33)   Lambert, N.; Chen, Y.-N.; Cheng, Y.-C.; Li, C.-M.; Chen, G.-Y.; Nori, F. *Nat Phys* **2013**, *9*, 10.

(34)   Zhang, L.; Silva, D.-A.; Zhang, H.; Yue, A.; Yan, Y.; Huang, X. *Nat Commun* **2014**, *5*.

(35)   Traub, M. C.; DuBay, K. H.; Ingle, S. E.; Zhu, X.; Plunkett, K. N.; Reichman, D. R.; Vanden Bout, D. A. *The Journal of Physical Chemistry Letters* **2013**, *4*, 2520.

(36)   Kato, M.; Kosuge, C.; Yano, S.; Kimura, M. *Acta Crystallographica Section C %@ 0108-2701* **1998**, *54*, 621.

(37)   Vagin, S. I.; Reichardt, R.; Klaus, S.; Rieger, B. *Journal of the American Chemical Society* **2010**, *132*, 14367.

(38)   Salassa, G.; Coenen, M. J. J.; Wezenberg, S. J.; Hendriksen, B. L. M.; Speller, S.; Elemans, J. A. A. W.; Kleij, A. W. *Journal of the American Chemical Society* **2012**, *134*, 7186.

(39)   Ganapathy, S.; Sengupta, S.; Wawrzyniak, P. K.; Huber, V.; Buda, F.; Baumeister, U.; Würthner, F.; de Groot, H. J. M. *Proceedings of the National Academy of Sciences* **2009**, *106*, 11472.

(40)   Van Rossum, B. J.; Förster, H.; De Groot, H. J. M. *Journal of Magnetic Resonance* **1997**, *124*, 516.

(41)   Polander, L. E.; Pandey, L.; Romanov, A.; Fonari, A.; Barlow, S.; Seifried, B. M.; Timofeeva, T. V.; Brédas, J.-L.; Marder, S. R. *The Journal of Organic Chemistry* **2012**, *77*, 5544.

(42)   Schafer, B.; Gorls, H.; Presselt, M.; Schmitt, M.; Popp, J.; Henry, W.; Vos, J. G.; Rau, S. *Dalton Transactions* **2006**, 2225.

(43)   Wozniak, K.; Kariuki, B.; Jones, W. *Acta Crystallographica Section C* **1991**, *47*, 1113.

(44)   Rombouts, J. A.; Ravensbergen, J.; Frese, R. N.; Kennis, J. T. M.; Ehlers, A. W.; Slootweg, J. C.; Ruijter, E.; Lammertsma, K.; Orru, R. V. A. *Chemistry – A European Journal* **2014**, *20*, 10285.
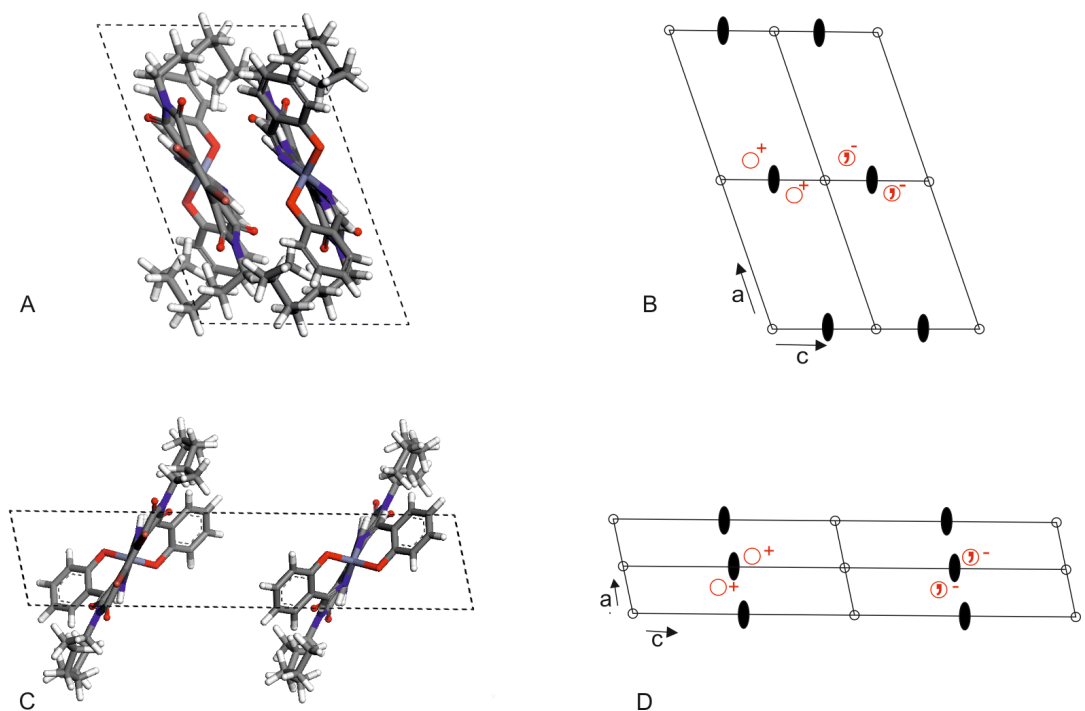
Supporting information to chapter 4

Figure S4.1 1D ^{13}C CP/MAS spectrum of DATZnS(4H) recorded at 750 MHz.

Figure S4.2 HETCOR spectra of the DATZnS(4H) at a short mixing time of 0.256 ms.

Figure S4.3 ● indicates the two fold axis, ○ indicates the inversion point, ○⁺and ⊙⁻indicates enantiomers running in mutually opposite direction. The parallel stacking (A) an antiparallel stacking (C) molecules in the unit cell observed along the 'b' axis with their respective space group diagram (B and D).
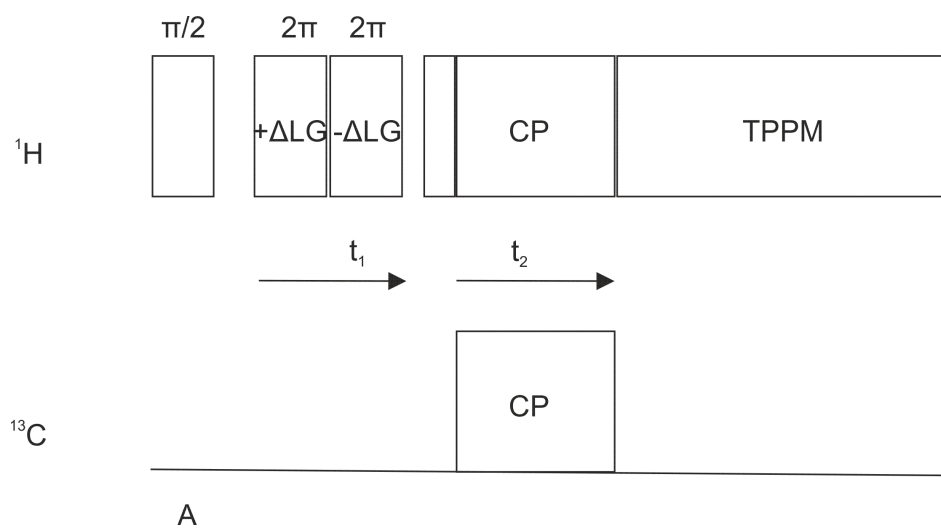

Figure S4.4 Pulse sequence used for the HETCOR experiment.

Chapter 5

Conclusions and outlook

5.1 Discussion

The primary source of energy in the universe is the sun and to harvest it for the production of clean fuel requires artificial antenna complexes. Structural analyses of chromophores that are compatible for light harvesting were performed. At a later stage, such chromophores could be integrated into to the artificial light harvesting antenna modules of a solar fuel cell device. For the three different supramolecular self-assemblies, building blocks in each packing are derived from one of the most frequently occuring space groups in the 230 crystal classes. For moderately sized organic molecules the packing generally involves screw axes and glide planes that have a translational component to accommodate the steric hindrance of functional motifs to achieve low energy and high density. Here however glide planes account for the steric hindrance in DATZnS(3′-NMe) and DATZnS(4H) using $P2/c$ space group and an inverse symmetry that results in the centerosymmetric dimers with P-1 space group for D1A2. Knowledge about the packing is essential for the design of solar fuel cells since it plays a crucial role in bridging a photo electrode comprising artificial light harvesters to a catalyst motif. In this thesis, a methodology is developed involving the integration of electron microscopy and solid state NMR spectroscopy, in addition to molecular modelling with force fields to converge on reasonable packing. This methodology is used to understand the packing in self-assembled supramolecular light harvesters DATZnS(3'-NMe) - chapter 2, D1A2 - chapter 3 and DATZnS(4H) - chapter 4.

Symmetry constraints obtained from CP/MAS NMR, systematic absences obtained from the Fourier transformation of the diffraction patterns and density of the sample helps to converge on the $P2/c$ space group for describing the packing of DATZnS(3′-NMe).[1] The supramolecular scaffold is stabilized by sheets of dipoles running in mutually opposite directions. Parallel stacking of NDI and the alignment of electric dipole moments perpendicular to each other in layers of DATZnS(3'-NMe) forms a grid, which may have future application in the design of a solar fuel cell device (Figure 2.5 and 5.1). Packing of DATZnS(3′-NMe) in parallel molecular

stacks in an antiparallel lamellar framework is validated, by comparing the strength of the heteronuclear dipolar coupling from an LGCP build up curve experiment and simulation, for selected ^{1}H-^{13}C pairs. Simulation of a DATZnS(3′-NMe) diffraction pattern using CrystalMaker generates the same systematic absence as observed in the Fourier transformation of the TEM image, which validated the proposed packing (Figure 2.4). Moreover, simulation with CrystalMaker is successfully used to generate the preferred orientation of the material on the surface, though there is a possibility to have the existence of polymorph forms. Recognition motif formed between the salphen and NDI is the driving force for the aggregation along the principal axis of the molecule. Intermolecular correlation peaks from ^{1}H-^{13}C HETCOR at the higher mixing time of 4 ms confirms the recoginition motif and the folding of tails in between the stacks along the phenazine moiety. This supramolecular recognition motif is a characteristic of the packing of DATZnS(3′-NMe). The Lewis acid character of the Zn^{2+} can be used to attach a catalyst to this scaffold.
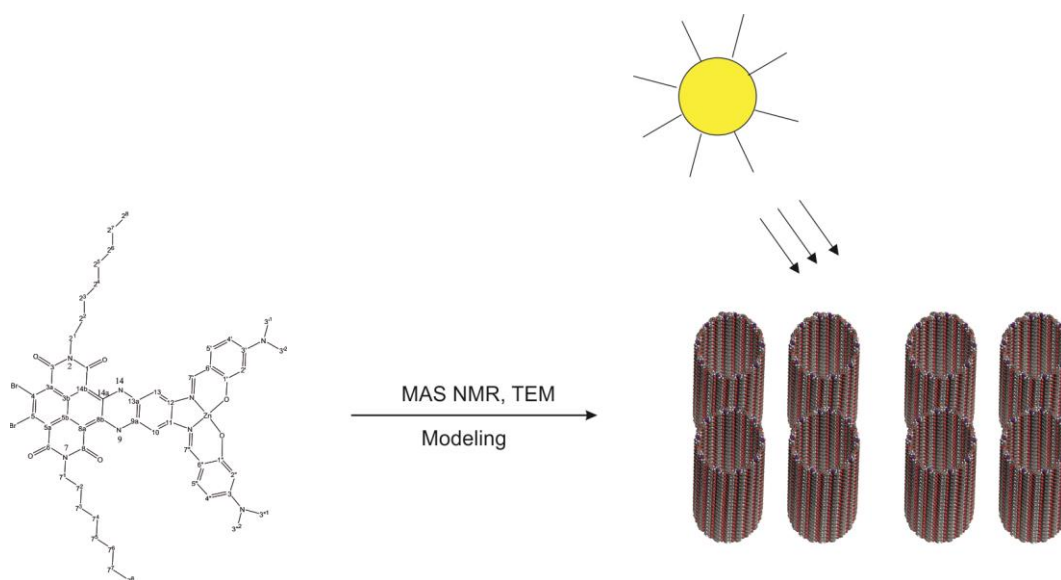

Figure 5.1 Schematic representation of how CP/MAS NMR in conjunction with TEM and molecular modelling allows to converge on a *P*2/*c* space group which could be modified into nanorods for attaching to a photo electrode surface. Dipole moments are aligned along the surface of the rods.
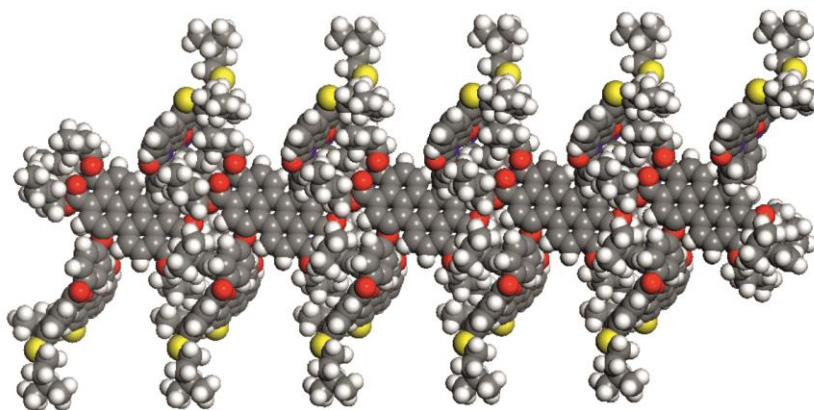
Figure 5.2 The stacking of D1A2 in one dimension showing the formation of rod type packing for perylene core and naphthalene monoimides projecting outwards.

In the case of D1A2 specific heteronuclear correlations point to centrosymmetric dimer formation, from P and M enantiomers. Computational integration of ENC and MAS NMR with a biased molecular replacement approach is performed to determine the packing of D1A2. Unit cell parameters obtained from ENC with density and HETCOR analysis converges up on *P*-1 packing with antiparallel stacking. The rod type structure of D1A2 in the solid state leads to the formation of rows of dimers, with naphthalene monoimide antennas projecting out (Figure 5.2). This will serve as an antenna system in which light energy is harvested by naphthalene monoimide and fed into the system with nano rods of perylene through FRET. D1A2 molecules exhibit good overlap between the donor's emission and the acceptor's absorption, which is a prerequisite for an efficient excited energy transfer (EET) by the Forster mechanism.[2,3]

A homology approach is proposed in chapter 4 for the DATZnS(4H) molecule based on the DATZnS(3′-NMe) parent compound in chapter 2. Distance constraints obtained from CP/MAS NMR data with limited data from TEM are used to put forth packing in the same *P*2/*c* space group but with a different positioning of the molecules in the unit cell where the axes were changed accordingly. Since the structure of DATZnS(4H) is a homologue of the DATZnS(3′-NMe), this implies that the NCH_3 functional group can be used to steer the packing from a parallel sheet in DATZnS(3′-NMe) to an antiparallel sheet in DATZnS(4H). Thus, chemical
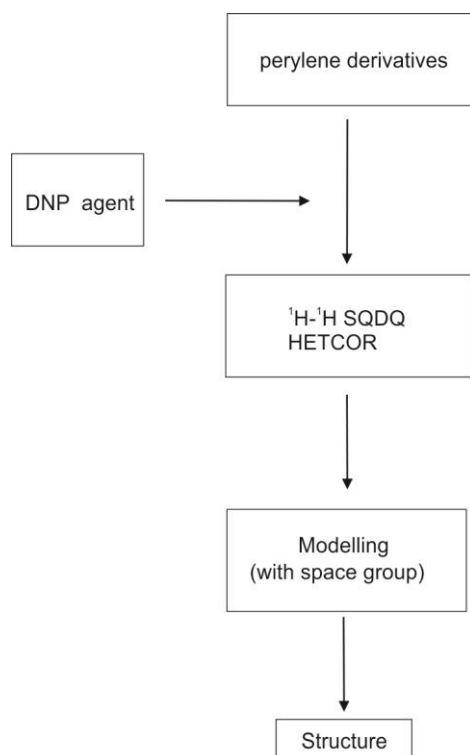
104

Figure 5.3 Schematic representation of DNP enhanced structure determination. It involves incorporating DNP agents into perylene derivatives by wet impregnation or glassy formation. Once it is successfully fused with the sample, a ^{1}H-^{1}H SQDQ could be employed, which helps to get highly resolved intermolecular correlation peaks. DNP could enhance the signal intensity up to 100 times.

substituents can be utilized to steer the alignment of the dipole between parallel and antiparallel in a sheet. We anticipate that this understanding is key to the chemical design of supramolecular scaffolds as an artificial antenna complex for the organic solar fuel cell device concepts.[4-7]

5.2 Future experiments

5.2.1. DNP enhancement

MAS NMR spectroscopy with Dynamic nuclear polarization (DNP) has the potential to enhance NMR signals by several orders of magnitude. High speed spinning Single Quantum Double Quantum (SQDQ) ^{1}H-^{1}H spectroscopy with DNP will help to get highly resolved intermolecular correlations.[8-11] DNP as explained by Overhauser in 1953 and demonstrated by Carver and Slichter involves the transfer of electron polarisation from a radical to neighbouring nuclei of interest resulting in enhancement of intensity.[12,13] DNP is usually achieved by a suitable polarising agent, which is excited by the irradiation of a sample with microwaves from a
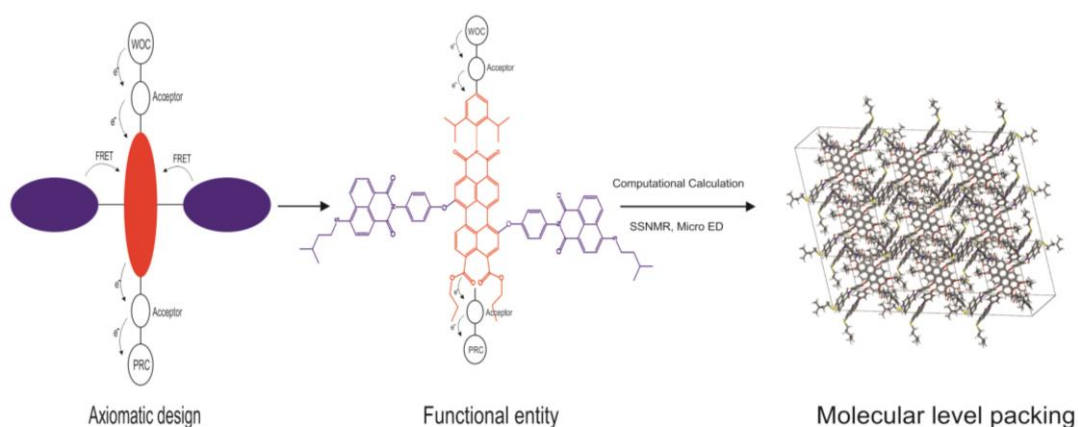
Figure 5.4 Axiomatic design of a solar fuel cell device using the D1A2 molecule. Packing studies give an insight in to the molecular level arrangement of the perylene derivative and its associated naphthalene monoimide functional motifs. This insight can be used in the design of modular photo electro chemical device concepts.

gyrotron source followed by the acquisition of the spectra. A combination of radical, polarising agent 4-hydroxy-TEMPO (TEMPOL) and ortho-Terphenyl (OTP) could be the best DNP agent as described in the work of Ong *et al*.[8] Researchers tried to incorporate DNP on the surface studies and structural analysis of proteins.[14] For unlabelled materials, DNP enhancement is so strong that you can incorporate DNP agents to SQDQ experiments, which lead to a much better resolution. This kind of methodology development will help to increase the accuracy and to resolve the packing of heterogeneous structures, which are inaccessible with the current state of the art. Since although these experiments are emerging, I foresee that they will be more powerful when combined with diffraction methods that discussed in this thesis (Figure 5.3). At a later stage, this could be extended to understand the mechanism on the electrode surfaces.

5.2.2 Design of a solar fuel cell device

Axiomatic design is a well-known concept in engineering, which is able to produce highly complex devices. I foresee the development of structure based strategies, involving bioinspired design concepts for crystal engineering to guide the fabrication of chromophores with structure determination facilitating the
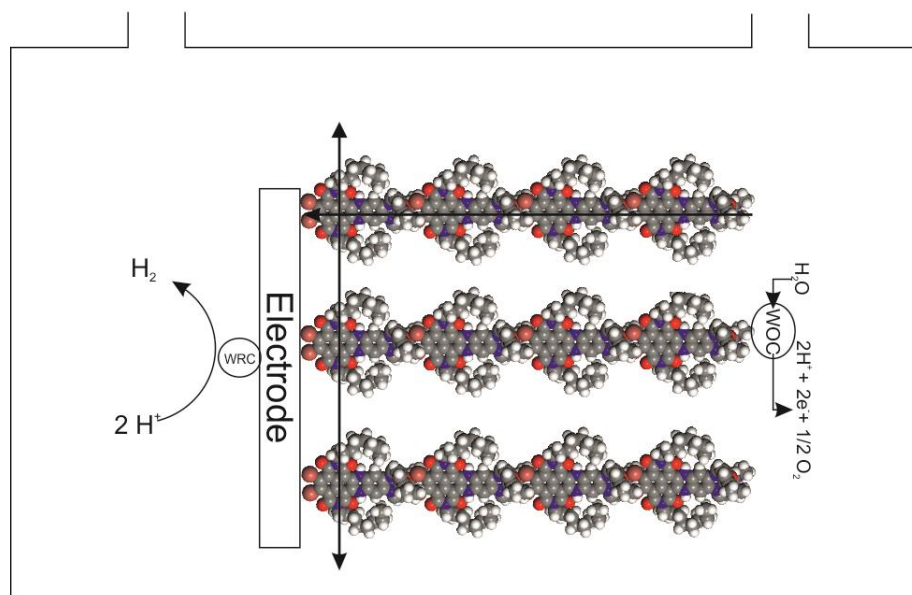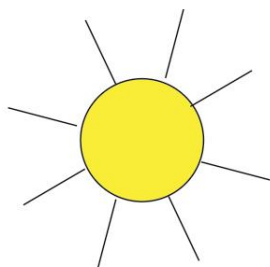
Figure 5.5 Schematic design of a solar fuel cell device. The fused DATZnS chromophore derivatives could be modified to attach to the electrode surface. A water oxidation catalyst could be grafted to the antenna complex by using the Lewis acid property of salphen.

fabrication of chromophores that can be synthetically modified for coherent transfer of electrons. It is important that D1A2 dimer operates in synergy for transfer of energy and can be optimized further. In the design matrix, we have to find the components analogous to a protein that lowers the transition state and energy barrier for optimal energy conversion. Axiomatic design helps to tune the J-aggregate overlap, engineering the barrier less mixing of a charge transfer state into the exciton state and finally stabilize the charge separation against the back reaction(Figure 5.4).[15-17] On a conceptual level, the strategy behind the design is to choose a specific building block, which has a typical stacking to generate the topology   of   a

specific target *i.e.* reaction center or it could be a retro synthetic approach in which a specific target is reduced to functional entities which can self-assemble. Bichromophoric D1A2, light harvesting antenna with centrosymmetric dimers of perylene motif, could be further optimised as an antenna but also can be considered as the first step on the way to a reaction centre using the axiomatic design strategy. This approach is similar to how nature has done through evolution. These results enable a direct molecular level approach to axiomatic design and improvement of light harvesting antenna systems D1A2 with D1 and A2 as molecular entities. This will allow the designer to choose materials with predetermined structures to develop a nano-architecture of interest. Transfer of energy from donor to acceptor is achieved through FRET.[18] A water oxidation catalyst could be attached to perylene to design it as a half-cell for solar fuel device. Rich functionalities will help to tune the energy gap for optimum water oxidation and to harvest an extensive range of photons(Figure 5.5).

For the self-assembled structures of DATZnS(3'-NMe), the challenge is to guide the design of planar two-dimensional salphen-NDI based supramolecular frameworks containing chromophores with a recognition motif to establish a device capable of doing effective charge separation with PCET for driving water oxidation catalysts.[19] Knowledge about the orientation of the DATZnS(3'-NMe) on the surface of the grid helps to design the electrode for solar fuel cell device. The catalyst could be attached at the zinc salphen, which has Lewis acid character.[1] A grid formed from the alignment of the electric dipole and NDI stacks gives a strong scaffold to attach the catalyst. The supramolecular scaffold with well-defined building units opens the possibility of modifying it as a nanorod. Electronegative bromine on the 4, 5 carbon atoms make it suitable for a selective nucleophilic substitution of anchoring groups like carboxyl, to attach to the electrode surface. It could be possible to modify the terminal methyl group of the alkyl chain to attach to the electrode surface. The flexibility of the molecule is the added advantage to modify it according to the need of a solar fuel cell device.

References

(1)   Rombouts, J. A.; Ravensbergen, J.; Frese, R. N.; Kennis, J. T. M.; Ehlers, A. W.; Slootweg, J. C.; Ruijter, E.; Lammertsma, K.; Orru, R. V. A. *Chemistry – A European Journal* **2014**, *20*, 10285.

(2)   Dubey, R. K.; Inan, D.; Sengupta, S.; Sudholter, E. J. R.; Grozema, F. C.; Jager, W. F. *Chemical Science* **2016**, *7*, 3517.

(3)   Dubey, R. K.; Niemi, M.; Kaunisto, K.; Efimov, A.; Tkachenko, N. V.; Lemmetyinen, H. *Chemistry – A European Journal* **2013**, *19*, 6791.

(4)   Kongkanand, A.; Martínez Domínguez, R.; Kamat, P. V. *Nano Letters* **2007**, *7*, 676.

(5)   Joya, K. S.; Joya, Y. F.; Ocakoglu, K.; van de Krol, R. *Angewandte Chemie International Edition* **2013**, *52*, 10426.

(6)   Lewis, N. S.; Nocera, D. G. *Proceedings of the National Academy of Sciences* **2006**, *103*, 15729.

(7)   Walter, M. G.; Warren, E. L.; McKone, J. R.; Boettcher, S. W.; Mi, Q.; Santori, E. A.; Lewis, N. S. *Chemical Reviews* **2010**, *110*, 6446.

(8)   Ong, T.-C.; Mak-Jurkauskas, M. L.; Walish, J. J.; Michaelis, V. K.; Corzilius, B.; Smith, A. A.; Clausen, A. M.; Cheetham, J. C.; Swager, T. M.; Griffin, R. G. *The Journal of Physical Chemistry B* **2013**, *117*, 3040.

(9)   Corzilius, B.; Michaelis, V. K.; Penzel, S. A.; Ravera, E.; Smith, A. A.; Luchinat, C.; Griffin, R. G. *Journal of the American Chemical Society* **2014**, *136*, 11716.

(10)   Michaelis, V. K.; Ong, T.-C.; Kiesewetter, M. K.; Frantz, D. K.; Walish, J. J.; Ravera, E.; Luchinat, C.; Swager, T. M.; Griffin, R. G. *Israel Journal of Chemistry* **2014**, *54*, 207.

(11)   Ni, Q. Z.; Daviso, E.; Can, T. V.; Markhasin, E.; Jawla, S. K.; Swager, T. M.; Temkin, R. J.; Herzfeld, J.; Griffin, R. G. *Accounts of Chemical Research* **2013**, *46*, 1933.

(12)   Overhauser, A. W. *Physical Review* **1953**, *92*, 411.

(13)   Carver, T. R.; Slichter, C. P. *Physical Review* **1953**, *92*, 212.

(14)   Zagdoun, A.; Rossini, A. J.; Conley, M. P.; Grüning, W. R.; Schwarzwälder, M.; Lelli, M.; Franks, W. T.; Oschkinat, H.; Copéret, C.; Emsley, L.; Lesage, A. *Angewandte Chemie International Edition* **2013**, *52*, 1222.

(15)   Kulak, O.; Cebi, S.; Kahraman, C. *Expert Systems with Applications* **2010**, *37*, 6705.

(16)   Thompson, M. K.; Giorgetti, A.; Citti, P.; Matt, D.; Suh, N. P.; Thomas, J.; Mantri, P. *Procedia CIRP* **2015**, *34*, 269.

(17)   Gebala, D. A.; Suh, N. P. *Research in Engineering Design* **1992**, *3*, 149.

(18)   Dubey, R. K.; Inan, D.; Sengupta, S.; Sudholter, E. J. R.; Grozema, F. C.; Jager, W. F. *Chemical Science* **2016**.

(19)   Joya, K. S.; de Groot, H. J. M. *International Journal of Hydrogen Energy* **2012**, *37*, 8787.

Summary

Photosynthesis is a highly cross linked process. However, we can distinguish a set of fundamental building blocks like chlorophylls, which interact to form photosystem, which performs the complex function of water splitting. The key challenge in artificial photosynthesis is to learn how to design systems that can adapt and optimize their topologies in line with self-assembly of natural photosystem. In this thesis I combine different techniques of cross polarization Magic angle spinning Nuclear Magnetic Resonance and Transmission Electron Microscopy with simulation and modeling, to resolve the global packing of molecules which are potential candidates for efficient solar fuel cell devices. This thesis focuses on the packing analysis of three-dimensional structures, which are heterogeneous in nature. I demonstrate a new and general structure determination approach that, in combination with first-principles quantum chemical calculations, establishes the structures of molecularly ordered antenna complexes that lack long-range 3D atomic crystalline order. This is possible despite the absence of a priori information on the space group or atomic coordinates.

Chapter 2 describes DATZnS($3'$-NMe) parallel stacking in an antiparallel framework with the $P2/c$ space group. ^{13}C CP/MAS NMR yields number of asymmetric sites in the structure and recognition motif. This in conjunction with unit cell parameters and diffraction spots from the Fourier transformation of a TEM image is used to resolve the structure. Supramolecular recognition motif is a characteristic of the packing of the DATZnS($3'$-NMe) molecule. The molecular recognition and molecular symmetry steer the packing into a racemic mixture with a c-glide plane and inversion symmetry to release the steric hindrance. Simulation of the LGCP build up curve between specific pairs and electron diffraction were used to validate the proposed packing.

Chapter 3 describes the centerosymmetric dimer formation with NMI extending outwards to capture the solar energy. MAS NMR chemical shifts were used to generate a truncated 1,7-perylene-3,4,9,10-tetracarboxylic monoimide dibutylester motif. This motif is further optimized and used for molecular replacement approach to generate a partial 3D electron density approach. The P-1 symmetry obtained from Electron Nano Crystallography is used to graft the

naphathelene monoimide substituents. The alkyl chains are modeled using the intermolecular correlation observed in HETCOR. Naphthalene monoimide antennas projecting out from the rows of dimers formed out of rod type D1A2 could capture the light energy and transfer to dimers through FRET.

Finally, in chapter 4 C_2 molecular symmetry obtained from MAS NMR and DFT modeling is used as the core motif to propose the packing of the DATZnS(4H). Intermolecular correlations obtained from the HETCOR shows the folding of the tails along the phenazine moiety. The analogous modeling showed how the packing could be steered by the NCH3 functional group between antiparallel and parallel dipoles. This understanding opens the way for the evidence based design of light harvesting antenna.

In summary, a novel methodology to resolve the structure of chromophore antenna from a structural background with static and dynamic heterogeneity that strongly limits the diffraction response is shown. Furthermore, I anticipate that the insights into packing of the antenna are key to the design of the organic solar fuel cell device in the future.

Samenvatting

Fotosynthese is een sterk verknoopt proces. Maar, we kunnen een fundamentele set van bouwstenen onderscheiden zoals chlorofyl, die interactie met elkaar hebben om een fotosysteem te vormen dat de complexe functie water splitsen uitvoert. De hoofd uitdaging in artificiële fotosynthese is om te leren hoe een systeem ontworpen kan worden dat zijn topologie kan aanpassen en optimaliseren in lijn met de zelf-assemblage van het natuurlijke fotosystem. In deze thesis combineer ik de verschillende technieken cross polarisatie Magische hoek spin Nucleair Magnetische Resonantie en Transmissie Elektron Microscopie met simulatie en modeleren, om de globale pakking van moleculen die potentiele kandidaten zijn voor efficiënte biobrandstof cellen op te helderen. Deze thesis focust op de analyse van de pakking van drie dimensionale structuren, die heterogeen in natuur zijn. Ik laat een nieuwe en algemene structuur bepalingsmethode zien die, in combinatie met eerste-principe kwantum chemische berekeningen, de structuren van moleculair geordende antenne complexen die geen lange afstand 3D atomische kristal orde hebben kan vaststellen. Dit is mogelijk ondanks de afwezigheid van a priori informatie over de ruimtelijke groep of atoom coördinaten.

Hoofdstuk 2 beschrijft DATZnS(3'-NMe) parallel stapelen in een antiparallel raamwerk met de P2/c ruimtelijke groep. ^{13}C CP/MAS NMR levert een aantal asymmetrische locaties in het structuur- en herkenningsmotief op. Dit in conjunctie met eenheidscel parameters en diffractie stippen van de Fourier transformatie van een TEM beeld is gebruikt om de structuur op te helderen. Een supramoleculair herkenningsmotief is een eigenschap van de pakking van de van het DATZnS(3`-NMe) molecuul. De moleculaire herkenning en moleculaire symmetrie sturen de pakking naar een racemisch mengsel met een c-glij vlak en inversie symmetrie om de sterische hindering te verminderen. Simulatie van de LGCP opbouw curve tussen specifieke paren en elektron diffractie werden gebruikt om de voorgestelde pakking te bevestigen.

Hoofdstuk 3 beschrijft de center symmetrische dimeer formatie met NMI naar buiten uitstekend om zonne-energie te vangen. MAS NMR chemische verschuiving werden gebruikt om een afgevlakt 1.7-perylene-3,4,9,10-tetracarboxylische mono-imide dibutylester motief te genereren. Dit motief is verder geoptimiseerd en gebruikt voor een moleculaire vervangingsbenadering om een partiele 3D elektron dichtheidsbenadering te genereren. De P-1 symmetrie verkregen van Elektron Nano Kristallografie is gebruikt om de naftaleen mono-imide substituties te enten. De alkyl ketens zijn gemodelleerd gebruik makende van de intermoleculaire correlatie geobserveerd in HETCOR. Naftaleen mono-imide antennes die uit de rijen van dimeren bestaande uit staaf type D1A2 steken zouden light kunnen opvangen en overdragen aan dimeren door FRET.

Tenslotte, in hoofdstuk 4 wordt C_2 moleculaire symmetrie verkregen uit MAS NMR en is DFT modulatie gebruikt als het kern motief om de pakking van de DATZnS(4H) voor te stellen. Intermoleculaire correlaties verkregen uit de HETCOR laten de vouwing van de staarten langs de phenazine eenheid zien. De analoge modeleren liet zien hoe de pakking gestuurd kon worden door de NCH3 functionele groep tussen anti-parallelle en parallelle dipolen. Dit begrip opent de deur voor het op bewijs gebaseerde ontwerp van de light oogstende antenne.

Samenvattend, een nieuwe methode om de structuur van chromofoor antennes op te helderen vanuit een structurele achtergrond met statische en dynamische heterogeniteit die sterk de diffractie reactie limiteert wordt weergegeven. Bovendien, ik anticipeer dat de inzichten in de pakking van de antenne de sleutel zijn tot het ontwerp van de organische biobrandstofcellen van de toekomst.

Publications

Sundaram Ganesh Babu, Brijith Thomas, Abdulrahiman Nijamudheen, Ayan Datta and Ramaswamy Karvembu "Cu/AlO(OH)-catalyzed formation of β-enamino ketones / esters under solvent, ligand and base free conditions - experimental and computational studies" *Catal. Sci. Technol.* 2(9), 1872-1878 (2012).

Khurram Saleem Joya, Jose L. Vallés-Pardo, Yasir F. Joya, Thomas Eisenmayer, Brijith Thomas, Francesco Buda, Huub J. M. de Groot" Molecular Catalytic Assemblies for Electrodriven Water Splitting." *ChemPlusChem.*78, 35–47(2013).

Brijith Thomas, Jeroen Rombouts, Gert T. Oostergetel, Karthick Babu Sai Sankar Gupta, Francesco Buda, Koop Lammertsma, Romano Orru, Huub J. M. de Groot "DATZnS(3′-NMe) chromophore light harvesting antennae form parallel molecular stacks in an antiparallel lamellar packing framework" Chapter 2 of this thesis. *Submitted.*

Brijith Thomas, Max Clabbers, Rajeev K. Dubey, Karthick Babu Sai Sankar Gupta, W. T. Fu, Wolter F. Jager, Jan Pieter Abrahams, Ernst J.R. Sudholter, Huub J. M. de Groot "De novo structure determination of an artificial bichromophoric light-harvesting antenna system by integrating MAS NMR and Electron Nano Crystallography" Chapter 3 of this thesis. *Submitted.*

Brijith Thomas, Jeroen Rombouts, Igor Nederlof, Karthick Babu Sai Sankar Gupta, Romano V.A. Orru, Jan Pieter Abrahams, Huub J. M. de Groot "Structural analysis of DATZnS(4H) using homology modelling" Chapter 4 of this thesis. *Manuscript in preparation.*

Yuliya Milsolvania, Brijtih Thomas, Michel Reus, Xinmeng Li, Agur Sevnik, Swapna Ganapathy, Karthick Babu Sai Sankar Gupta, Alfred Holzwarth, Huub J. M. de Groot. "A low complexity 3D model for heterogeneous wild type *Chlorobaculum tepidium* chlorosomes." *Manuscript in preparation.*

Brijith Thomas, Rajeev K. Dubey, Karthick Babu Sai Sankar Gupta, Wolter F. Jager, Ernst J.R. Sudholter, Huub J. M. de Groot "Structural analysis of perylene antenna: Combining CPMAS NMR spectroscopy and GIPAW Chemical-Shift Calculations" *Manuscript in preparation.*

Curriculum vitae

I was born in Thiruvalla, Kerala, India, on March 19, 1988. I joined the Mahatma Gandhi University, Kottayam for my Bachelors Degree in Chemistry in June 2005. I started my Masters Degree program in July 2009 at the Department of Chemistry, National Institute of Technology, Tiruchirappalli. In March 2010, I was selected as a summer fellow at the Indian Institute of Science, Banglore where I worked under the guidance of S Umapathy, E Arunan and K L Sebastian in the project "*Theoretical investigation into the rearrangement of orthocarborane to metacarborane.*" In 2011, I submitted my Masters dissertation entitled "*Copper on Boehmite: Efficient nano catalyst for the synthesis of beta ketoenamines*" under the guidance of R Karvembu in collaboration with K L Sebastian (Indian Institute of Science) and Ayan Datta (Indian Institute of Education and Research, Thiruvananthapuram). In January 2012, I started my doctoral studies in the solid-state NMR group at the Leiden University under the supervision of Prof. dr. H. J. M de Groot. In the course of Ph.D., my work got selected for oral presentation at *ISMAR Conference,* Shangha*i* (2015), *Rocky Mountain Conference,* Colorado (2016), *SMARTER5,* Bayreuth (2016), *Developments and Applications of Solid State NMR to Materials Science, Chemistry and Engineering Conference,* Varna (2016), *International Conference and Exhibition on Materials Chemistry,* Valencia (2016), *EuroSolarFuel Meeting,* Torun (2013). My research work was presented as posters at the *Experimental Nuclear Magnetic Resonance Conference,* Boston (2014), *Alpine Conference on Solid-State NMR,* Chamonix *(*2013, 2015), *Solar Fuel Cell Meeting,* Passau (2014), *SMARTER4 Conference,* Durham (2014), and *EUROMAR,* Prague (2015).